Repair of Corrosion-Damaged Columns using FRP Wraps

by

Ronald S. Harichandran
Professor and Chairperson

and

M. Imad Baiyasi
Graduate Student

Department of Civil and Environmental Engineering
Michigan State University
East Lansing, MI 48824-1226

Phone: (517) 355-5107
Fax: (517) 432-1827
E-Mail: harichan@egr.msu.edu
http://www.egr.msu.edu/~harichan

December 2000

Technical Report Documentation Page

1. Report No. Research Report RC-1386	2. Government Accession No.	3. Recipient's Catalog No.
4. Title and Subtitle Repair of Corrosion-Damaged Columns using FRP Wraps		5. Report Date December 21, 2000
7. Author(s) Ronald S. Harichandran, Ph.D., P.E. M. Imad Baiyasi, Ph.D.		6. Performing Organization Code
9. Performing Organization Name and Address Michigan State University Department of Civil and Environmental Engineering East Lansing, MI 48824-1226		8. Performing Org Report No. RC-1386
12. Sponsoring Agency Name and Address Michigan Department of Transportation Construction and Technology Division P.O. Box 30049 Lansing, MI 48909		10. Work Unit No. (TRAIS) 11. Contract/Grant No.
15. Supplementary Notes		13. Type of Report & Period Covered 1/15/97 – 7/15/00 14. Sponsoring Agency Code

16. Abstract

Experiments were conducted to assess the effects of using fiber reinforced polymer (FRP) wraps with fibers oriented in the hoop direction for rehabilitating corrosion-damaged columns. Issues that were explored are: (1) freeze-thaw durability of concrete square and cylindrical specimens wrapped with glass and carbon FRP and subjected to an internal expansive force; (2) effect of wrapping on the rate of corrosion in an accelerated corrosion test; (3) effect of freeze-thaw and wet-dry cycles on the properties of FRP panels; (4) impact resistant of FRP panels supported on a concrete substrate; (5) effect of high temperature on wraps; and (6) field installation of wraps on corrosion-damaged bridge columns.

The results of the freeze-thaw experiment indicate that freeze-thaw cycles have no statistically significant effect on the compressive strength of glass and carbon wrapped specimens. For round specimens, glass and carbon wraps increased the strength by a factor of about 2.3 and 2.6, respectively. For square specimens, glass and carbon wraps increased the strength by a factor of 1.4-1.5. Freeze-thaw conditioning generally reduced the longitudinal failure strain of wrapped specimens.

The results of the accelerated corrosion experiment indicate that wrapping reduced the corrosion depth in the reinforcing bars by 46% to 59% after 190 days of testing. Both glass and carbon wraps are equally effective in slowing down corrosion.

Freeze-thaw and wet-dry conditioning had no detrimental effect on carbon FRP panels other than a 28% and 36% reduction, respectively, in the ultimate strain. Glass FRP panels showed 21% and 20% reductions in ultimate strength and ultimate strain due to freeze-thaw conditioning, and 18% and 20% reductions in ultimate strength and ultimate strain due to wet-dry conditioning. The results of tension tests on carbon panels were somewhat unreliable. Better grip fixtures should be used for future testing.

Both glass and carbon FRP panels did not display any significant damage due to the impact test.

At temperatures in excess of 200°C the epoxy in the FRPs burn and evaporate and the individual plies of wraps unravel. Hence the wraps become ineffective at such high temperatures unless effective insulation is provided.

It is evident from the experimental study conducted that both carbon and glass wrap systems are sufficiently resistant to freeze-thaw cycles and reduce the corrosion rate by about the same rate. Therefore, three layers of glass wrap or two layers of carbon wrap may be used to repair Michigan bridge columns.

17. Key Words	18. Distribution Statement No restrictions. This document is available to the public through the Michigan Department of Transportation.		
19. Security Classification (report) Unclassified	20. Security Classification (Page) Unclassified	21. No of Pages	22. Price

Form DOT F 1700.7 (8-72)

Executive Summary

Repair of Corrosion-Damaged Columns Using FRP Wraps

Many bridge columns in Michigan are damaged by chloride contamination resulting in the corrosion of the steel reinforcement, and swelling and spalling of the concrete and use of the bridges is typically continued. This in itself may not be a serious problem since most columns in Michigan are over-designed and the loss of strength is not a significant issue. However, the lack of any method to minimize or prevent corrosion of the steel results in continued deterioration and unsightly columns. Polymer composite (also known as fiber-reinforced polymer or FRP) jackets offer a possible remedy to this problem. They offer a rapid repair technique with the potential to enhance the long-term durability and compression strength of damaged columns due to the confinement that is provided when fibers are oriented in the hoop direction. Fibers oriented in the vertical direction can enhance the bending strength.

Experiments were conducted to assess the effects of using FRP wraps with fibers oriented in the hoop direction for rehabilitating corrosion-damaged columns. Issues that were explored are: (1) freeze-thaw durability of concrete square and cylindrical specimens wrapped with glass and carbon FRP and subjected to an internal expansive force; (2) effect of wrapping on the rate of corrosion in an accelerated corrosion test; (3) effect of freeze-thaw and wet-dry cycles on the properties of FRP panels; (4) impact resistant of FRP panels supported on a concrete substrate; (5) effect of high temperature on wraps; and (6) field installation of wraps on corrosion-damaged bridge columns.

The results of the freeze-thaw experiment indicate that freeze-thaw cycles have no statistically significant effect on the compressive strength of glass and carbon wrapped specimens. For round specimens, glass and carbon wraps increased the strength by a factor of about 2.3 and 2.6, respectively. For square specimens, glass and carbon wraps increased the strength by a factor of 1.4-1.5. Freeze-thaw conditioning generally reduced the longitudinal failure strain of wrapped specimens.

The square wrapped specimens had lower compressive strength compared to the round specimens, even though the cross sectional area of the square prisms is higher than that of the round cylinders. This is due to the reduced confinement provided by the wraps for square cross sections and stress concentrations that develop at the corners. Wrapped square prisms always failed by rupture of the wrap at a corner. A reduction of approximately 30% to 40% in failure stress was noted between round and square wrapped specimens.

The results of the accelerated corrosion experiment indicate that wrapping reduced the corrosion depth in the reinforcing bars by 46% to 59% after 190 days of testing. Both glass and carbon wraps are equally effective in slowing down corrosion. Although unbonded wraps do reduce stress concentrations in the FRP, they are less effective in reducing the corrosion rate than the bonded wraps. It is postulated that this is due to the ingress of water along the unbonded FRP-concrete interface.

Wrap strains for bonded specimens with both types of wraps tend to level off with time indicating that corrosion slows down significantly after some time. One explanation could be that the stress concentration near the anodes in the bonded wraps is more effective in containing the corrosion-induced crack and reducing the corrosion rate. The slip of unbonded wraps and the

resulting redistribution of strain along the entire wrap may be less effective at containing the large corrosion-induced crack near the anodes.

Freeze-thaw conditioning had little effect on the effective stiffness (modulus × thickness) of glass FRP panels. Although the effective stiffness of carbon panels showed an apparent increase due to freeze-thaw conditioning, re-testing indicated that this observation was unreliable. The ultimate strength per unit width per layer of glass FRP decreased by 21% and the decrease was significant at the 95% level. The change in the ultimate strength of carbon was not significant at the 95% level. Ultimate strains decreased by 20% and 28% for glass and carbon panels, respectively, and these decreases were significant at the 95% level.

Wet-dry conditioning had no effect on the effective stiffness of glass panels. As with freeze-thaw conditioning, the effective stiffness of carbon panels showed an apparent increase due to wet-dry conditioning, but re-testing indicated that this observation was unreliable. The ultimate strength per unit width per layer of glass FRP decreased by 18% and the decrease was significant at the 95% level. The change in the strength of carbon was not significant at the 95% level. Ultimate strains decreased by 20% and 36% for glass and carbon panels, respectively, and these decreases were significant at the 95% level.

The panel test results are somewhat unreliable for the very thin carbon specimens. Also, many of the specimens broke at the grips. Better grip fixtures should be used for future tests.

Both glass and carbon FRP panels did not display any significant damage due to the impact test. Minor interlaminar debonding was visible on the glass panels, which are somewhat transparent, at the point of impact. Interlaminar debonding could not be observed on the carbon FRP panels because they are opaque.

At temperatures in excess of 200°C the epoxy in the FRPs burn and evaporate and the individual plies of wraps unravel. Hence the wraps become ineffective at such high temperatures unless effective insulation is provided.

It is evident from the experimental study conducted that both carbon and glass wrap systems are sufficiently resistant to freeze-thaw cycles and reduce the corrosion rate by about the same rate. Therefore, three layers of glass wrap or two layers of carbon wrap may be used to repair Michigan bridge columns. Reducing the number of layers may also be feasible, but it is not possible to provide any recommendation about this without additional studies.

The preferred wrap system will most likely depend on the material and installation cost rather than performance issues. However, it should be noted that many studies indicate strength degradation of glass FRP in an alkaline and/or humid environment under elevated temperature. Thus in regions with long periods of hot and humid conditions, carbon FRP may be preferable to glass FRP.

It is also recommended that a non-destructive technique or coring be used every ten years to monitor the condition of the concrete inside the wrap.

TABLE OF CONTENTS

CHAPTER 1: INTRODUCTION AND LITERATURE REVIEW

CHAPTER 2: DESCRIPTION OF EXPERIMENTS

CHAPTER 3: DATA COLLECTION AND ANALYSIS OF RESULTS

CHAPTER 4: SUMMARY, CONCLUSIONS, AND RECOMMENDATIONS

CHAPTER 5: FIELD INSTALLATION AND FUTURE STUDIES

APPENDIXES

LIST OF TABLES

LIST OF FIGURES

Chapter 1
Introduction and Literature Review

1.1 Introduction

Retrofitting bridge columns with jackets encasing the concrete has been undertaken extensively in the West Coast, primarily for seismic rehabilitation. Steel jackets have been used for the most part, but are expensive to install and require several days for each column. The use of fiber reinforced polymers (FRP) wraps also has been developed and numerous columns have been retrofitted with different kinds of wraps. FRP wraps can be installed quickly (four to six columns per day), with minimal interruption to traffic flow. FRP wraps can be made of low-cost glass fiber, medium-cost aramid (also known as Kevlar) fiber, or high-cost high- performance carbon fiber, and polyester, vinyl ester or epoxy resins can be used as a matrix. Hexcel Fyfe Co. (Del Mar, Calif.) is the first composite fabricator to install a field demonstration with the California Department of Transportation, but other suppliers such as XXsys Technologies Inc., C. C. Myers Inc., Master Builders Inc., Mitsubishi Corporation, and Hardcore DuPont Composites L.L.C. also are performing field installations now.

The Pennsylvania Department of Transportation selected the Tyfo-S fiber wrap system (by Fyfe Company) for a concrete-column repair project on Interstate 84 in Scranton (Tarricone 1995). The New York State Department of Transportation used FRP wraps on six severely deteriorated concrete columns of the Court Street Bridge (Tioga County) in the summer of 1998 to protect against failures and to improve their durability in a cost effective manner. Six suppliers of FRP column wraps participated in this project (Alampalli et al. 1999). In California numerous columns have been wrapped with the Tyfo-S fiber wrap system, and XXsys

Technologies'filament winding for the bridges under the jurisdiction of the California Department of Transportation. This was done mainly for seismic strengthening. XXsys Technologies in conjunction with the Utah Department of Transportation used its composite wrapping system in 1996 to strengthen and extend the useful life of an existing bridge. The bridge had deteriorated from the effects of more than thirty years of corrosion of the steel reinforcing bars. Structural Preservation Systems of Baltimore, Maryland has used carbon wraps in 1997 to strengthen parking garage columns in Charleston, South Carolina.

While advanced composite materials are relatively expensive, labor costs are approximately 30% less than for conventional strengthening methods primarily because of the light weight of the materials. The quick turnaround and the reduced labor costs associated with FRP have reduced the overall cost making its use attractive for rehabilitation and strengthening of concrete infrastructure.

Four types of FRP jackets are currently available:

- Composite fabrics: The fabrics must be thoroughly saturated usually with two-part resin during installation and are cured at room temperature. The mechanical properties of the final product are somewhat variable. The Tyfo™ S Fiberwrap System by Fyfe Company is of this type.
- Prepregnated composite fabrics (Prepregs): Prepregs are pre-impregnated, usually with an epoxy resin, which results in good control over the mechanical properties of the final product. However, most prepregs must be stored in cold storage before installation, and need to be thermally cured after installation. For column applications, thermal curing can be achieved using heating blankets. There are few commercial carbon fiber prepregs, such as MBrace and REPLARK marketed by Master Builders and Mitsubishi respectively, that may be air cured.

- Filament winding: Jackets are produced by winding a continuous composite fiber onto the resin coated column. Typically automated winding equipment is used and the jacket is heat cured. XXsys Technolgies has retrofitted several columns in the West Coast using this technology.
- Precured shells: Precured jackets are formed around a mandrel of the diameter matching the column to be jacketed, typically using a multi-axial, stitched, nonwoven E-glass fiber fabric. The jackets have an axial slit that allows them to be opened and placed around a column for installation. Field crews install the jacket by first spraying a urethane adhesive onto the column. Two workers can then snap on a 132 kg, 1.2 m tall by 1.2 m diameter jacket segment. The adhesive and jacket installations are repeated to obtain three to five plies of composite, with the axial slit in each additional ply being staggered from that of the previous ply to avoid overlap. The whole multi-layer jacket system is bound to the column while the adhesive cures, creating an efficient, labor-saving system. As an alternative to the 360^0 bands, smaller arc segments can be installed by gluing each segment around the column with sufficient overlap. The smaller arc segments are easier to package and ship.

All of the jacketing systems described above are acceptable, and the advantage of one over another would depend on their performance in Michigan's harsh climate, their cost and their availability. Precured shells are presently available only for circular columns.

1.2 Project Objectives

The main objective of this project was to investigate the suitability of using glass and carbon FRP wraps to repair concrete columns damaged by corrosion in Michigan. The following issues were investigated:

- Strength loss of wrapped columns subjected to expansive forces, due to freezing and thawing.
- Strains in FRP wraps during freeze-thaw conditioning.
- Increased strength of concrete due to confinement provided by wraps.
- Magnitude of confining pressure generated by wraps due to corrosion.
- Localization of strains in wraps bonded to the concrete near reinforcing bars and the merit of using unbonded wraps.
- Reduction in corrosion rate due to the use of FRP wraps.

1.3 Literature Review

1.3.1 Fiber Reinforced Polymers (FRP) for Infrastructure

Newly developed composite materials have been used recently in civil engineering structures because of their superior mechanical properties as well as their resistance to aggressive environmental conditions. In general composites can be defined as a combination of two or more materials, that are insoluble into one another, without chemical interaction such that the properties of the combination is better than the individual constituents (De Wilde 1988). Fiber reinforced polymers are made of two constituent materials: polymer fibers and polymer matrices.

1.3.1.1 Fibers

Fibers have the largest volume and are the load-carrying element of FRP composites. Proper selection of the amount, type and orientation results in a composite with the desired mechanical properties.

- Glass fibers: These are widely used. Molten glass can be drawn into fine continuous filaments. These can be fabricated into continuous fibers, chopped strands, woven fabrics

and milled fibers. The strength of glass fiber is highly dependent on the form in which the fibers are used. Continuous fibers have the highest strength and chopped fibers have the lowest strength. The average tensile strength for freshly drawn glass fibers may exceed 3500 MPa. Surface flaws tend to reduce this value to between 1750-2100 MPa. The internal structure of a glass fiber is a three dimensional network of different atoms. They behave in a linearly elastic manner until failure (Mallik 1993). Glass fibers are available in a variety of forms suited for different applications. The most common type is E-glass (which was initially developed for use in electrical applications). Other types of glass fibers that are used include S-glass (which has approximately 25% greater tensile strength than E-glass but is more expensive), C-glass (which was developed for application in corrosive environments), D-glass (which has lower density and dielectric constant than the other types of glass fibers), AR-glass (alkali resistant), and ECR-glass (modified E-glass which provides improved acid resistance).

- Carbon and graphite fibers: The difference between carbon and graphite is in the molecular structure. In carbon, the bonding between layers is weak, so it has two-dimensional ordering. Graphite is formed from carbon atoms, which are arranged in crystallographical parallel planes of regular hexagons. Carbon fibers are commercially available in three basic forms: long and continuous tow, chopped (6-50 mm long), and milled (30-300mm long). Carbon fiber can also be woven into two-dimensional fabrics of various styles. Graphite fibers are mainly considered in high strength composite applications. They show very high specific strength and stiffness. Graphite has a higher tensile modulus than carbon. Generally, as the modulus of elasticity increases, ultimate load and elongation decreases. Therefore, high modulus graphite fibers exhibit a lower strain at failure than high strength carbon. The tensile

strength and the modulus of elasticity of graphite and carbon are not temperature dependent. These fibers behave elastically to failure and are highly resistant to aggressive environment. Their diameter is in the range of 5 to 10 microns.

- Aramid fibers: Made from aromatic polyamides, these have the lowest specific gravity and highest specific tensile strength among all type of fibers (Mallik 1993). Due to its high tensile strength and modulus of elasticity, aramid was the first organic fiber to be used as a reinforcing fiber.

1.3.1.2 Matrices

The matrix is considered the secondary material in FRPs. Its major roles are transferring stresses between the fibers and protecting fibers against the environmental and mechanical conditions. The importance of the matrix in a composite is its effect on interlaminar and in-plane shear strengths. It also provides support against buckling of the fibers under compressive loads. Polymer matrices are divided into two categories:

- Thermoplastic Polymers: Individual molecules are in a linear structural form. Weak secondary bond holds these molecules together. Heat or pressure temporarily breaks the bonds, which causes movement between the molecules. After cooling, the molecules set into their new position. Thermoplastics have higher impact strength, fracture and microcracking resistance compared to thermosetting polymers. Examples of thermoplastic polymers include nylon and polyethylene.
- Thermosetting Polymers: Also known as resin. The molecules are joined together by cross-links, which leads to a more stable three-dimensional form that can not be reshaped by heat

or pressure. Epoxy, polyester, and vinyl ester are the most common types of thermosetting polymers (Malek and Saadatmanesh 1996).

1.3.2 Durability of Concrete

Concrete is a porous material consisting of cement, water, fine and coarse aggregates and, possibly, admixtures. Cement and water react to form a hardened paste binding together the coarse and the fine aggregates. Voids are left in the originally water-filled space between the cement grains, which are not filled with the hydration products of the chemical reactions. These voids are known as capillary pores. They range in size from approximately 5 nm to 1 mm. Capillary forces in such small volumes play an important role in the durability characteristics of concrete.

The capillary pore volume is a function of two parameters: the water/cement ratio of the paste, and degree of hydration of the cement (Pigeon and Pleau 1988). Table 1.1 gives the approximate capillary porosity of Portland cement paste as a function of the water/cement ratio and the degree of hydration. The water/cement ratio and the degree of hydration also have an influence on the average size of capillary pores. The average size decreases significantly with the degree of hydration, and the number of very large pores decreases significantly with lower water/cement ratios.

Table 1.1. Capillary porosity of Portland cement paste as a function of the water/cement ratio and the degree of hydration

Water/cement ratio (by mass)	Capillary Porosity (% volume)	
	At 50% hydration	At 75% hydration
0.4	31	18
0.5	39	28
0.6	46	36

Cement paste also contains a significant volume of smaller pores that are called gel pores. The hydrants have a very large specific surface area, which is covered with a few layers of absorbed water. The gel pores correspond to the surface occupied by this absorbed water. Unless the temperature is high or the relative humidity is very low, the gel pores are always filled with water because the forces that bind water to the surfaces of the hydrates are strong.

When ice forms in the pores, a 9% increase in the volume of water takes place when water changes from liquid to solid. This volume expansion and the flow of water, as it is forced out of the pores, cause tensile stress to be generated in the paste. This is the basic cause of damage to concrete due to freezing.

When concrete is **air entrained**, which is achieved by adding admixtures to the mix, a very large number of closely spaced air voids develop. If these air voids are sufficiently close, the pressure generated by the flow of water out of the pores does not cause any damage and water can freeze in these voids without generating internal pressures in the concrete (Pigeon and Pleau 1988).

1.3.3 Environmental Effects on FRP Composites

Environmental factors such as extreme temperature fluctuation and water absorption can adversely affect the behavior of some polymer composite material. Water absorption reduces the strength and stiffness of some polymeric composites by as much as 30%, compared to dry material. Water absorption breaks down the interface between the reinforcing fiber and resin matrix leading to loss of strength and rigidity. Cycles of freezing and thawing tend to magnify

the effect of water absorption (Gomez and Casto 1996). The strength loss in glass FRP due to 300 cycles of freezing and thawing is depicted in Figure 1.1

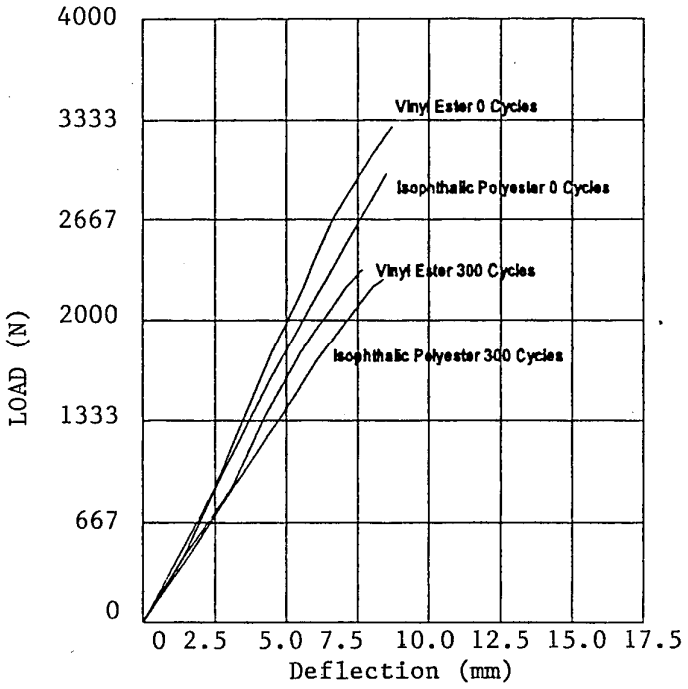

Figure 1.1 Load vs. deflection curve for glass FRP composite specimens subjected to 300 cycles of freezing and thawing (reproduced from Gomez and Casto 1996)

While several studies have been conducted on the strength of columns wrapped with FRPs, studies on durability under harsh environmental conditions such as freeze-thaw, exposure to chloride, and degradation from exposure to ultraviolet light are much fewer. Questions related to durability under harsh environmental conditions are extremely important in Michigan, and it is important to provide answers to these questions based on laboratory research prior to field installation.

Chajes et al. (1994) investigated the durability of several composite systems externally attached to concrete beams. One set of beams was exposed to cycles of freezing and thawing, the second set was exposed to cycles of wetting and drying, while the third set was unconditioned.

Their results indicated that flexural strength was lost due to a degradation of the bond between the concrete and the external reinforcement. Degradation of the composite material was not reported.

Sen et al. (1993) investigated the durability concrete beams pretensioned with glass/epoxy FRP subjected to cycles of wetting and drying. Several specimens were initially cracked to simulate pile-driving damage. Their results indicated extensive damage in the glass FRP, leading to an unacceptable level of strength loss.

Gomez and Casto (1996) studied the effect of chloride and freeze-thaw on two pultruded fiberglass all-composite systems. Both systems used glass fibers, but one used a vinyl ester resin while the other used a polyester resin. Samples were exposed to freeze-thaw cycles while immersed in a 2% sodium chloride and water solution. Their results indicated a loss of 22-32% in the flexural strength and stiffness of the composite materials.

Fyfe et al. (1996) studied the effect of prolonged (1000 hours) exposure of the Tyfo™ S System to ozone, salt water immersion, fresh water immersion, alkaline soil burial, high temperature, low temperature, and Weatherometer aging. All tests were performed according to ASTM standards, but only on the composite material, not on wrapped concrete specimens. In general, no serious degradation was observed due to prolonged exposure. However, a fundamental limitation of this study is that the environmental conditions were not cycled, and hence durability against cyclic freeze-thaw and chloride immersion cannot be assessed.

Toutanji and Balaguru (1998) studied the effect of wet-dry and freeze-thaw conditions on the performance of concrete columns wrapped with two layers of carbon and two layers of glass FRP composites. Three types of FRP wraps were used; two types of carbon and one glass. Twenty four concrete specimens (76 mm diameter and 305 mm long cylinders) were divided into

three groups. Each goup consisted of eight specimens: six confined (two with each type of the FRP sheets) and two unconfined. The first group was used as virgin samples and the second was exposed to wet-dry cycling and the third group was exposed to freeze-thaw cycling. Three hundred wet-dry and freeze-thaw cycles were performed in a salt water solution. CFRP experienced no reduction in strength or ductility due to wet-dry exposure, whereas samples with GFRP experienced reduction of 10% and 20% in strength and ductility, respectively. In the case of freeze-thaw exposure, both CFRP and GFRP wrapped specimens experienced reductions in strength and ductility. Strength losses were 28% and 19% for glass and carbon, respectively. Ductility losses were 65% and 30% for glass and carbon, respectively. The specimens subjected to freeze-thaw cycling also exihibited more catastrophic brittle failure as compared with the unconditioned and the wet-dry conditioned specimens.

Rivera and Karbhari (1999) conducted tests on concrete cylinders wrapped with glass and carbon FRP after subjecting them to 201 freeze-thaw cycles (between 22.5^{o} C and -20^{o} C). Three layers of carbon fabric and seven layers of glass fabric were used. Wrapped specimens subjected to freeze-thaw cycling showed increased stiffness and strength and more catastrophic failure compared to control specimens under ambient temperature. In order to isolate the effects of temperature from those of excessive moisture absorption, thawing was in air.

Murphy et al. (1999) investigated the effects of alkali exposure on the performance of glass fiber reinforced composites. Glass fiber reinforced vinylester coupons (two, four and six layers) were placed in solutions with pH and salt content predicted by leaching out the concrete itself, new concrete (28 days) and old concrete (ten years). In addition, a cementitious extract was prepared by collecting the solution that formed after settling of the aggregates (while preparing the new concrete). The starting pH level was approximately 12 and dropped to 8.5 in

about 60-80 days for the new and old concrete solutions. For the cementitious extract solution, the pH dropped to 8.5 in about 250 days. The strength was degraded by 17 to 32% over a period of one year. The coupons placed in the cementitious extract was degraded the most (32%) indicating that reduction in strength cannot be attributed to pH levels alone, but rather to a combination of alkaline salts from concrete and the pH levels present.

Almusallam et al. (2000) conducted tests on concrete specimens wrapped with three layers of bi-directional glass FRP. Each group of specimens contained three GFRP wrapped specimens and three unwrapped specimens. It was concluded that the compressive strength of wrapped cylinders subjected to alkaline solution and alkaline solution at elevated temperature (60 ^{o}C) exhibited lower increase in strength than the other groups. The increase in strength was about 23% compared to 54% for wrapped specimens at room temperature.

The Aerospace Corporation (Los Angeles, California) conducted extensive FRP panel durability testing on various wrap systems (Steckel 2000). For the glass and carbon systems used in this research study, they concluded that carbon panels are not affected by conditioning while glass panels showed strength and strain reduction of up to 35% and 15% - 20% under 10,000 hours of humidity and salt water (or alkaline solution) exposures, respectively. It should be noted that these conditions were not cycled. Only 20 freeze-thaw cycles were conducted and those had no effect on the FRP panels was noted. Appendix A shows the results obtained by of the Aerospace Corporation for glass and carbon FRP panels, respectively.

1.3.4 Corrosion of Reinforcing Steel

Corrosion is a natural process and is a result of the inherent tendency of metals to revert to their more stable compounds, usually oxides. Most metals are found in nature in the form of

various chemical compounds called ores. In the refining process, energy is added to the ore, to produce the metal. It is this same energy that provides the driving force causing the metal to revert back to the more stable compound.

Corrosion of the reinforcement reduces strength, durability, and service life of the reinforced concrete structure. As the reinforcement corrodes, it expands causing cracking of concrete and spalling.

An ASTM-sponsored study (Guttman and Sereda 1968) found the corrosion rate in steel exposed to air at various locations varied from 0.033 to 0.058 mm per year in Cleveland to 0.030 to 0.043 mm per year in Ottawa. For a #25 bar, these translate to 5.3% to 9.1% in Cleveland and 5.0% to 6.7% in Ottawa in 10 years. Similar rates have been observed in Michigan steel bridges (McCrum 1994).

1.3.4.1 Factors Affecting Corrosion

The presence of chlorides, temperature, relative humidity, cover depth, and concrete quality are the major factors affecting the rate of corrosion.

Chlorides can come from several sources. They can be cast into the concrete to promote rapid hardening or they can diffuse from the outside. Chlorides can diffuse into concrete as a result of sea salt spray and deicing salt. Chloride contamination of bridge columns resulting from winter maintenance chloride (deicing salt) applications results in the continuing deterioration of the steel reinforcement, which in turn causes bursting forces emanating from the steel location outward to the periphery of the columns.

Minimum concrete cover and low quality of concrete (high water/cement ratio) decrease the time needed for chlorides to reach the reinforcement. The time for corrosion to start will therefore be decreased and the rate of corrosion will increase (Allen 1995).

Environmental conditions such as ambient temperature and relative humidity also affect corrosion. The concentration of free chloride ions in the pore water increases with temperature. In addition, corrosion reactions occur at a much faster rate with an increase in temperature. The corrosion rate of steel was found to vary linearly with temperature. The corrosion rates at 40^{o} C was found to be almost double that at 0^{o} C (Lopez et al 1993).

Concrete is alkaline. It contains microscopic pores with high concentrations of soluble calcium, sodium and potassium oxides. These oxides form hydroxides, which are highly alkaline when water is added. This alkaline condition leads to a passive layer forming on the steel surface in the form of a dense, impenetrable film, which if fully established and maintained, prevents further corrosion of the steel. Chlorides act as catalysts to promote corrosion. When there is sufficent chloride concentration at the reinforcing bar surface to break down the passive layer of oxide on the steel, the corrosion process proceeds quickly.

Brockenbrough et al. (1985) conducted tests on stacks of Cor-Ten A steel and carbon steel compressed together with spring washers and exposed (to the atmosphere) at Monroeville, Pennsylvania and Kure Beach, North Carolina. The stacks clamped at low pressures (21.5 and 43.5 kPa) showed large increase in thickness because of corrosion product pressure after five and a half years of exposure. In addition, it was concluded that there is an initial pressure threshold of about 1035 to 1380 kPa above which the rate of corrosion is extremely small and no significant expansion due to corrosion product pressure takes place.

1.3.4.2 Volume Expansion Due to Corrosion of Steel

Corrosion of steel is an electrochemical process. The electrochemical potentials to form the corrosion cells may be generated when cells are formed due to differences in concentration of dissolved ion in the vicinity of steel, such as alkalies, chlorides, and oxygen. As a result, some parts of the metal become anodic and the others cathodic. The fundamental chemical changes occurring at the anodic and cathodic areas are as follows (see Fig. 1.2-a).

Anode: $Fe \rightarrow 2e^{-} + Fe^{2+}$

Cathode: $\frac{1}{2} O_2 + H_2O + 2e^{-} \rightarrow 2(OH)^{-}$

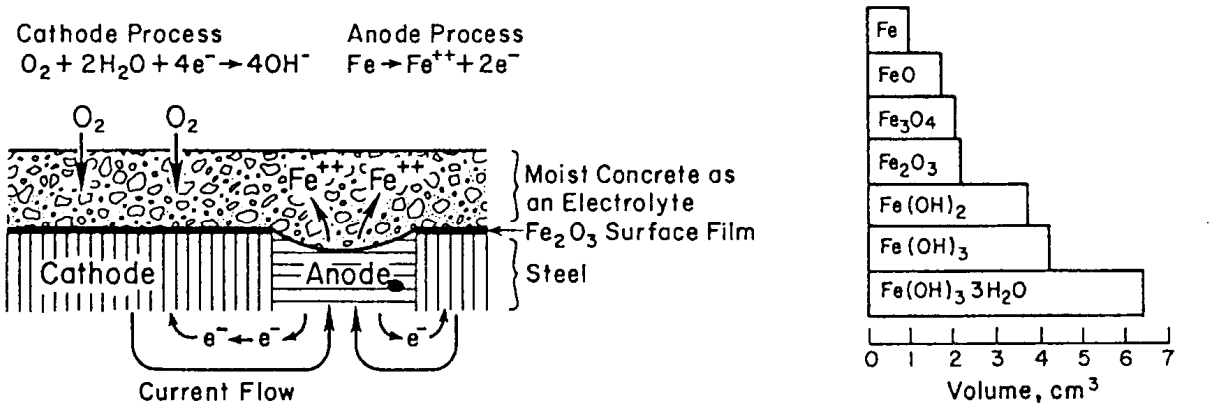

(a) (b)

Figure 1.2. Expansion and cracking of concrete due to corrosion of the embedded steel (reproduced from Mehta 1996)

The transformation of metallic iron to rust can result in increases in volume of up to 600% (Mehta 1996), depending on the final rust form (see Fig. 1.2-b). Since the presence of

both air and water is required for the corrosion activity to continue, column wrapping may provide adequate confinement that would minimize the entry of air and water, thereby slowing down the continuation of corrosion.

1.3.4.3 Localized Corrosion

Corrosion of steel reinforcement inside bridge columns is not uniform. It is dependent on the location of cracks and surface exposure (i.e. salt contact due to deicing of roads). Further, the volume expansion due to corrosion is localized near the reinforcement bars. This may exert strains on the wrap at localized areas. All or most of the metal loss occurs at discrete areas (Fontana 1986).

Pitting corrosion is highly localized corrosion occurring on a metal surface. Pitting is commonly observed on surfaces with little or no general corrosion. Pitting typically occurs as a process of local anodic dissolution where metal loss is exacerbated by the presence of a small anode and a large cathode.

Crevice corrosion is another form of localized corrosion which may occur in small areas of stagnant solution in crevices, joints and under corrosion deposits. Crevice corrosion is the localized corrosive attack that occurs as a result of the occluded cell that forms under a crevice on the metal surface. To prevent this type of corrosion, it is recommended that crevices be closed with non-absorbent materials or a barrier to prevent moisture penetration into the crevice be incorporated.

1.3.5 Mechanical Properties of FRPs

Many FRPs have tensile strengths that exceed the strength of steel, but their stiffness is generally lower than that of steel. When loaded along the fiber direction they behave essentially linearly until fracture, and are therefore brittle by nature.

1.3.5.1 Stress Corrosion and Stress Rupture

The average ultimate tensile strength of freshly drawn glass fibers may exceed 3500 MPa. However, surface flaws tend to reduce the tensile strength to values in the range of 1750 to 2100 MPa. Strength degradation is increased as the surface flaws grow under cyclic loads. This is one of the major disadvantages of using glass fibers in applications where fatigue may be an issue. Sustained loads also cause surface flaws to grow, resulting in reduced tensile strength. Figure 1.3 shows reduction of strength with time for E-glass fiber under different temperatures.

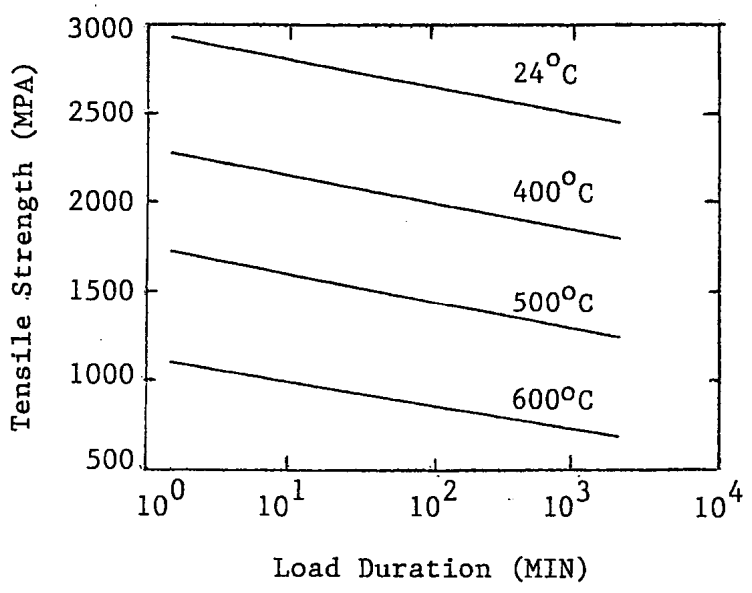

Figure 1.3 Reduction of tensile strength of E-glass fibers under sustained loads (taken from Mallick 1993)

Stress corrosion refers to the characteristic property of FRPs in which the failure strength under long term sustained loads in a chemical environment is lower than its short term tensile strength. In air, this phenomenon is referred to as "stress rupture" (Sen et al. 1993). Stress rupture tests are usually performed by applying a constant tensile stress to a specimen until it fractures completely. The time at which fracture occurs is termed the "lifetime". Creep, on the other hand, is defined as the increase in strain with time at a constant load level (Mallick 1993).

Glass, Aramid, and Boron fibers and their composites exhibit failure by stress rupture. Carbon fibers, on the other hand, are relatively less prone to stress rupture failure. In order to prevent stress rupture in glass FRP for a period of 10, 30, and 50 years, the sustained strains in the GFRP should be less than about 0.35 ε_u, 0.32 ε_u, 0.30 ε_u, respectively (Sen et al.1993, ACI 2000).

The relationship between the sustained stress (or strain) and the logarithm of time is approximately linear as shown in Figure 1.3. ACI Committee 440R recommends the use of a safety factor of 1.67 and hence a safe level of sustained strain to prevent stress rupture in glass is about 0.2 ε_u.

1.3.6 Effect of Confinement

Lateral confining pressure increases the strength and ductility of concrete in the axial direction. The stress-strain curves of confined concrete show a remarkable energy dissipation characteristic. Such behavior is of great importance as it can prevent catastrophic failure of highway bridges or high-rise buildings under overload conditions. Figure 1.4 shows stress-strain curves for confined and unconfined concrete.

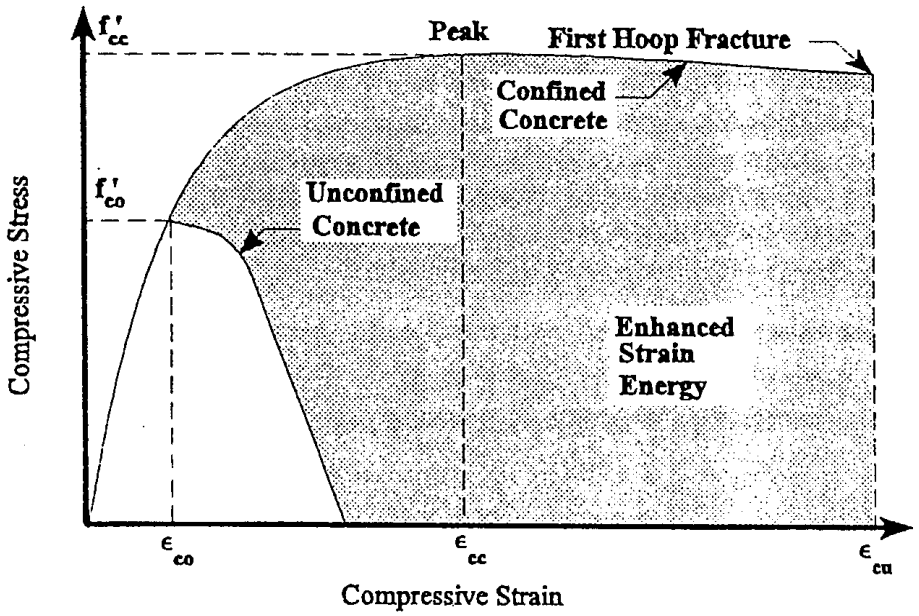

Figure 1.4 Stress/strain curves for confined and unconfined concrete (Mander, et al.1988)

The relationship between confined compressive strength (f_{cc}'), unconfined compressive strength (f_c'), and the lateral stress in core concrete produced by confining pressure (f_r) is

$$f_{cc}' = f_c' + k f_r \tag{1.1}$$

The average value of the confinement effectiveness coefficient k was found to be equal to 4.1 (Richart, et al. 1928).

For circular column with spiral steel, the confining pressure f_r is given by (Nilson and Winter 1991)

$$f_r = \frac{2A_{sp} f_y}{d_c S} \tag{1.2}$$

where

A_{sp} = the cross-sectional area of the spiral steel

d_c = the outside diameter of the spiral

S = the pitch of the spiral.

f_y = spiral steel yield stress

Eq. (1.2) is calculated assuming that the spiral steel reaches its yield stress f_y before the column eventually fails.

FRP materials are essentially linear elastic up to the point of fracture, while steel shows an elastic-plastic behavior. The stress-strain curve of the confining materials affects the failure mode of the confined core. Figure 1.5 shows stress-strain curves for A36 steel, E-glass and carbon fibers.

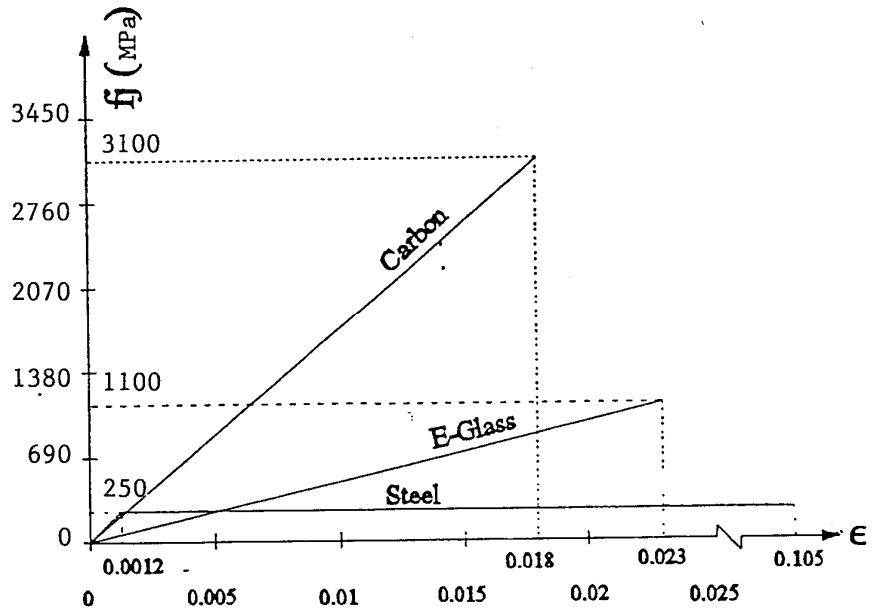

Figure 1.5 Stress-strain curves for A36 steel, E-glass and carbon fibers

Confinement of concrete columns with FRP wraps offers many advantages in comparison to other confinement methods. Composite material with their high strength and high stiffness to

density ratios allow for field installation with minimal workforce and disruptions to traffic. Preliminary testing of concrete columns wrapped with FRPs has shown that the confinement provided results in improved compressive strength and ductility. Picher at el. (1996) conducted a series of tests on confined circular, square and rectangular concrete specimens. Axial loads were applied to concrete specimens wrapped with different orientation of carbon FRP wraps. It was concluded that confinement of concrete cylinders with CFRP wraps improves their compressive strength and ductility (up to 41% axial strength increase and about 500% axial strain increase for cylinders confined with three layers of carbon sheets with fibers oriented in the hoop direction) compared to unconfined specimens. Although axial stiffness decreases with the increase of fiber angle orientation, ductility and modes of failure remain the same. Wrapping of square and rectangular specimens improves ductility but to a lesser degree than that observed for cylindrical specimens. In the case of square and rectangular specimens, it was found that rounding the corners greatly improved the compressive strength.

Tests on round and rectangular specimens and full scale columns wrapped with glass and carbon FRPs was conducted by Kestner at el. (1997). They found that enhancement in axial strength and deformation are proportional to jacket strength and stiffness. It was found that due to the ineffectively confined concrete region in the square cross sections, the jackets provided to square cross sections were not as effective as those provided to circular cross sections. A shape factor, κ_s, was used to account for the ineffectively confined regions of concrete within the rectangular and square cross sections.

From mechanics of thin walled cylinders, the confining pressure in a confined column can be determined to be

$$f_r = 2\,(f_t\, t\, n) / D \qquad (1.3)$$

where

t = the thickness of the wrap per layer

f_t = the circumferential stress of wrap

n = number of wrap layers

D = the diameter of the concrete cylindrical column

The maximum confining pressure, f_{ru} is determined by the ultimate tensile strength of the wrap f_{tu} given by

$$f_{ru} = 2\,(f_{tu}\,t\,n) / D = 2\,(E\varepsilon_{tu}\,t\,n) / D \qquad (1.4)$$

where

E = modulus of elasticity of the wrap

ε_{tu} = wrap ultimate strain

Substituting f_{ru} from Eq. (1.4) into Eq. (1.1) yields the maximum compressive strength due to confinement with FRP wraps.

More generally, for round and rectangular cross sections, the maximum confining pressure may be expressed as (Restrepol and DeVino 1996)

$$f_{ru} = 0.5\,\kappa_s\,\rho_j\,E\varepsilon_{tu}\,t \qquad (1.5)$$

where

$\rho_j = 4n/D$ for circular columns

$\rho_j = 2n(d+b)/db$ for rectangular columns

n = number of layers of wrap

D = overall diameter of circular column

b = overall width of rectangular column

d = overall depth of rectangular column

κ_s = shape factor determined as the ratio of effectively confined concrete to the gross area of the section

The shape factors for circular and rectangular are

Circular: $\kappa_s = 1$

Rectangular: $\kappa_s = \dfrac{1-\left[(b-2r)^2+(d-2r)^2\right]-\rho}{1-\rho}$

where

r = radius of rounded corners

ρ = longitudinal reinforcement ratio of cross section

Fig. 1.6 shows the effectively confined area of a rectangular cross section.

For circular columns, substituting $\kappa_s = 1$ in Eq. (1.5) will yield Equation (1.4), while for rectangular columns

$$f_{ru} = \kappa_s \, n \, E\varepsilon_{tu} \, t \, (d+b)/db \qquad (1.6)$$

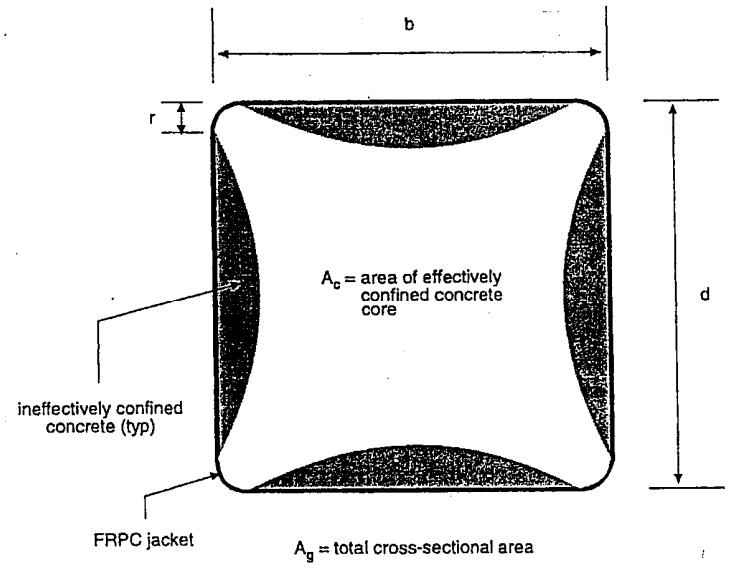

Fig. 1.6 Illustration of effectively confined area of a rectangular cross section

1.3.7 Repair of Corrosion-Damaged Columns Using FRP

A review of research conducted to study the effectiveness of FRP wraps in repairing corrosion-damaged columns indicates that FRP wraps have the following advantages:

- They provide a barrier to oxygen, moisture and chlorides.
- They have high strength and stiffness and provide confinement and ductility to the concrete structure.

Debaiky and Green (1999) are investigating the suitability of using FRP wrap to rehabilitate corroded concrete structures. The focus of the experiment is to assess what happens to the corrosion process after the structure has been rehabilitated with FRP wraps. The experiment consists of 12 reinforced concrete columns (300x 1200 mm) with chlorides cast in the concrete cover. The columns are placed in a water bath to initiate corrosion. After the initial corrosion phase, the columns will be wrapped with FRP sheets. The "natural" accelerated corrosion environment will then be continued. Monitoring corrosion will be through the use of a half-cell potential. This project is still underway.

Pantazopoulou et al. (1996), Michniewicz (1996), and Lee (1998) from the University of Toronto conducted several projects using FRP for repair of corrosion damaged columns since 1993.

Two concrete mixes were used to construct the 150x300 mm cylinders. High density concrete was used for the end caps, and high porosity concrete contaminated with 2.6% NaCl by weight of cement was used for the middle 210 mm of the cylinder height. The corrosion was electrically accelerated using a 6 volt potential while the cylinders were placed in 50 mm of 2% chloride solution. Damage was significant after 150 days. Several repair techniques were

considered such as conventional patching, epoxy coating and wrapping with plastic foil. In addition, glass FRP wrap also was used. The most effective repair method was the use of a conventional patch with two layers of glass FRP (GFRP) wrap. The strength was fully restored and ductility was doubled compared with an undamaged specimen.

Ten large-scale circular columns also were built and corrosion was accelerated in a similar manner (voltage ranged from 3 to 15V). The columns were repaired using different methods ranging from:

- Surface cleaning, non shrinkage grout, epoxy coat, and 2 layers of GFRP wrap to
- Epoxy coat and 2 layers of GFRP wrap only.

Compression tests results showed only columns that were repaired using the first method, surface cleaning, non shrinkage grout, epoxy coat, and 2 layers of GFRP wrap, had the capacity of an undamaged column.

Another project was also conducted at the University of Toronto. Seven large scale columns were corroded using a 12 V fixed potential and wet-dry cycles consisting of one day wet and 2.5 days dry. After significant corrosion, they were wrapped with one layer of carbon FRP (CFRP) sheet. The results showed that using the CFRP wrap increased the strength of the corroded specimens by 28% compared to the unwrapped specimens. The axial deformation at failure was six times that of corroded unrepaired specimens.

It should mentioned that the above research projects conducted at the University of Toronto did not investigate the effect of continuing corrosion on the FRP rehabilitation.

At the University of Sherbrooke, the following field applications have been conducted (Rochette et al. 1996, Demers et al. 1996, and Kenneth et al. 1998):

- Corrosion-damaged circular building columns were repaired with GFRP after the column section was restored with cement grout. The repair took place in November 1995, the resin cured properly despite the cold temperature.
- Eighteen (18) circular bridge columns were repaired in August 1996. Five columns were wrapped with GFRP, four with CFRP, and three were repaired using conventional material. Axial deformation and circumferential expansion were monitored.
- The concrete pier on the Champlain bridge in Montreal was repaired in 1997. The pier received nine layers of GRFP wrap in the four meters above its base.

The University of Minnesota is currently monitoring the rehabilitation of corrosion-damaged columns for a bridge near Minneapolis (Debaiky and Green 1999). The set up is as follows:

- Electrochemical chloride extraction (ECE) was used on three columns and then one column was wrapped with CFRP sheets (supplied by Hexcel-Fyfe Company), the second was wrapped with CFRP sheets (supplied by Tonen Corporation), and the third was wrapped with chopped glass sheets.
- ECE was used on three columns and were then sealed without wrapping.
- Three columns were wrapped similar to the first group without the ECE.
- Three columns were left as control specimens.

Corrosion will be monitored for five years. Chloride sampling will be conducted once a year. This project started in 1997 and is still underway.

In order to study the deterioration and evaluate different repair techniques, an FRP column wrap project was initiated by the New York State Department of Transportation in 1998 (Halstead et al. 2000). Six severely deteriorated concrete columns of the Court Street Bridge

(Tioga County) were wrapped using six different wrap systems (by different suppliers). A comprehensive testing program to evaluate the effectiveness of FRP column wrapping was implemented. Prior to installation of the FRP wraps, three corrosion probes were embedded in each column. Additional monitoring equipment was installed on each column and data collection started in September 1998. Strain sensors were installed on the surface to measure the effect of continued corrosion on the wraps. Concrete humidity and temperature are also being monitored. The corrosion probes use linear polarization to monitor instantaneous corrosion rates. Data is being collected at three month intervals. This non-destructive testing is scheduled to continue for five years.

1.3.8 Effect of Fire and High Temperature on FRPs

Few studies have been performed on the effect of fire and high temperatures on carbon and glass FRPs. Swiss researchers performed a series of bending tests on beams strengthened with pultruded carbon FRP plates and steel plates, positioned in a large testing oven (Meier 1996). Four beam were strengthened by bonding carbon FRP plates (74 mm wide, 1mm thick), and one beam was strengthened with steel plates (75 mm wide, 8 mm thick). The beams were placed in the oven and the temperature was raised to 652°C. The steel plates debonded from the beam in 8 minutes. The carbon FRP began to burn at the surface of the laminates and their cross sections slowly decreased. The carbon FRP debonded from the beam after one hour.

The Aerospace Corporation subjected carbon and glass FRP panels constructed by the wet lay-up method to dry heat at 60°C for 1000 and 3000 hours (Steckel 2000). The effect of these exposures on modulus, ultimate strength and ultimate strain are given in Appendix A. There was no significant effect on either carbon or glass FRP.

No studies appear to have been done on the fire resistance of conventional FRP panels constructed by the wet lay-up method and not treated with fire retardents.

Chapter 2
Description of Experiments

2.1 Stiffness and Strength of Glass and Carbon FRPs

A 4-ply composite Tyfo-S fiber glass/epoxy sheet and a 2-ply Tonen carbon/epoxy sheet were fabricated at MSU on 9/30/97 and 10/21/97 under the supervision of the respective composite vendors. After the vendor-recommended curing periods of five to seven days, these specimens were tested under direct tension at the MSU Composite Material and Structures Center to check the moduli against the vendor-recommended values. The width of the test specimens varied from 13 to 19 mm and their length varied from 190 to 230 mm, depending on the test. Gage length over which strains were measured was 89 mm. The test machine was equipped with hydraulically actuated wedge grips with serrated face. Table 2.1 shows a comparison between actual tested and vendor-recommended moduli, thickness, effective axial stiffness per unit width (equal to modulus × thickness), ultimate strength, ultimate strength per unit width (equal to ultimate strength × thickness), and ultimate strain (FYFE 2000, Master Builders 1998). Because the effective stiffness and ultimate strength per unit width are not dependent on the thickness of sheets, these properties should be used in comparisons. Although the properties varied from the vender recommended values, especially for carbon, the effective axial stiffness which controls confinement and behavior was almost identical to and about 88% of the vendor-recommended design values for glass and carbon FRPs, respectively. Master Builders specify the thickness, modulus, and ultimate strength of their carbon FRP based on the fiber properties only, which is why their values differ significantly from the measured values. The design ultimate strengths per unit width recommended by the vendors, however, are 13%

and 22% higher than the measured values. The properties of each individual test specimen are given in Appendix B.

Table 2.1 Vendor recommended and measured wrap properties for a single layer

Wrap Type	Thickness (mm)	Modulus (MPa)	Effective Stiffness (N/mm)	Ultimate Strength (MPa)	Ult. Str. per Unit Width (N/mm)	Ultimate Strain
	Test Properties Published by Vendors					
Glass	1.3	26100	33930	575	747	.022
Carbon	0.165	228000	37620	4275	705	.0175
	Design Values Recommended by Vendors					
Glass	1.3	20684	26889	448	582	.020
Carbon	0.165	228000	37620	3790	625	.015
	As Measured					
Glass	1.227	22011	26967	421	516	.019
Carbon	0.625	53061	33191	821	513	.015

2.2 Strain Expected in Wraps Due to Corrosion

The transformation of metallic iron to rust can result in increases in volume of up to 600% (Mehta 1996), depending on the final rust form. (Table 2.2 shows sample calculations for the volume expansion for some rust products.)

Rust Forms: FeO, Fe_3O_4, Fe_2O_3, $Fe(OH)_2$, $Fe(OH)_3$, $Fe(OH)_3$ $3H_2O$

Table 2.2. Volume expansion for some rust products

Rust Form	Density (D)	Mol.Wt.	Volume(MW/D)	Vol.Rust/Vol.Fe
Fe	7.86	56	7.12	
FeO	5.7	71.85	12.6	12.6/7.12=1.7
Fe_3O_4	5.18	231.54	44.70	44.7/(3x7.12) =2
$Fe(OH)_2$	3.4	89.86	26.43	26.43/7.12=3.71

Table 2.3 shows the strain developed in the wrap due to corrosion in a 915 mm diameter column with longitudinal steel ratios of 3%, 2%, and 1%, and ties spaced at 152 mm and 305

mm. Corrosion rates by cross section of 5% in the longitudinal reinforcement and 20% in the lateral reinforcement over a 10 year period are assumed (Martin and Schieles 1969). For cases one and two it is assumed that the volume of rust is three times and six times, respectively, the volume of the corroded steel. The table shows that the strain in the wrap is within 0.30 ε_u = 0.6% for GFRP (which is the sustained strain limit in order to prevent stress rupture in glass FRP for a period of 50 years) for all situations considered, indicating that stress rupture should not be a problem. If carbon FRP is used, then stress rupture is not an issue and the strains in Table 2.3 are below the rupture strain of ε_u = 1.5%. Hence the use of CFRP is also feasible.

Table 2.3 Strain in column wrap due to steel corrosion after 10 years

Column dia. (mm)	Spacing of tie (mm)	Steel ratio of cross section	Strain in wrap	
			Case 1	Case 2
#13 tie				
915	305	3%	0.394%	0.450%
		2%	0.260%	0.327%*
		1%	0.145%	0.203%
	152	3%	0.414%	0.530%
		2%	0.290%	0.410%
		1%	0.160%	0.284%

* Sample calculation for this row is shown in Appendix C.1.

2.3 Freeze-Thaw Test

Strength and durability tests were carried out on circular (diameter of 152 mm by 305 mm high) and square cylinders (152 mm by152 mm by 305 mm high) wrapped with three layers of glass FRP or two layers of carbon FRP. The primary purpose of the tests was to determine the endurance of the jackets under simulated cyclic environmental conditions, with strength considerations being secondary. An internal bursting force similar to that produced by corroding steel was induced. This was done by fabricating cylinders with a hole in the longitudinal

direction and filling it with an expanding cement known as Bristar (used for silent demolition). Chloride was impregnated into the cylinders during casting in order to simulate deteriorated concrete (11 kg of $NaCl/m^3$ was used). Strength tests were carried out on plain control cylinders as well as wrapped test specimens before and after freeze-thaw conditioning.

Climate data for Lansing, Michigan indicates that there were 58 days in the 1993/1994 year when the temperature cycled above and below 32° F and 78 days for the 1992/1993 year. Based on this and ASTM C666 specifications, 150 and 300 freeze/thaw cycles were used in the freeze-thaw conditioning. Subsequent to freeze/thaw cycles, the compressive strengths were compared against those of wrapped control specimens that were not subjected to freeze-thaw cycles. In addition, unwrapped plain concrete specimens also were exposed to freeze-thaw cycles to establish loss of strength in concrete alone due to freeze/thaw conditioning.

Table 2.4 shows the test matrix used for the freeze/thaw laboratory testing. A total of 60 specimens were involved in the testing, of which 30 were subjected to freeze/thaw. Specimen and gage numbering is shown in Table D.1 in Appendix D. A water/cement ratio of 0.4 was used. Table E in Appendix E provides the concrete mix ratios and the 28 day strength for the freeze-thaw specimens.

A half bridge configuration was used for reading the strain gages, and temperature correction was done by using dummy gages mounted on glass and carbon FRP panels which also were located in the freeze-thaw machine. However, thermal contraction and expansion of the FRP panels on which the dummy gages were mounted had to be determined and compensated for. The dummy gages also were used when reading strains on control specimens not subjected to freeze-thaw.

Table 2.4 Freeze-thaw laboratory testing matrix

Specimen Type	Conditioning	No. of Specimens		
		Unwrapped	Glass Wrap	Carbon Wrap
Round	None	3	3	3
Square	None		3	3
Round	None	3	3	3
Square	None		3	3
Round	150 cycles of freeze-thaw	3	3	3
Square	150 cycles of freeze-thaw		3	3
Round	300 cycles of freeze-thaw	3	3	3
Square	300 cycles of freeze-thaw		3	3

2.3.1 Mold Fabrication

Prism molds

Nine 152 mm x 152 mm x 305 mm PVC molds were fabricated. Each is composed of five panels (four sides and one bottom). The short side panels were fabricated with a center hole that was 38 mm in diameter. A 38 mm steel rod was placed in the hole during casting. Dow Corning release agent was applied to the steel rod and a plastic sheet was then wrapped around it to aid removal after the concrete sets. The center hole was later filled with Bristar (a form of an expanding grout). Fig. 2.1 provides a picture of the prism mold.

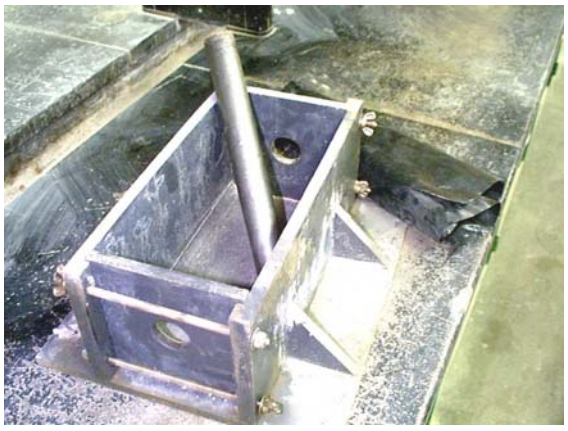

Fig. 2.1 Prism mold used for freeze-thaw test specimens

Cylindrical Molds

Nine 152 mm x 305 mm steel cylindrical molds were fabricated. Steel base plates and wooden top plates with a 38 mm diameter center hole were used. As with the prism molds, a steel rod was inserted at the middle of each cylinder to create a hole in which Bristar was later inserted. Fig. 2.2 provides a picture of the cylindrical mold.

Fig. 2.2 Cylindrical mold used for freeze-thaw test specimens

2.3.2 Bristar Calibration

The Bristar mix used to create an internal bursting force in cylinders had to be calibrated to yield the appropriate pressure when set. Nine 152 mm x 305 mm steel tubes were filled with concrete and a 38 mm diameter hole was fabricated in the center of each. Each steel tube was mounted with two strain gages located diametrically opposite each other at mid-height on the exterior surface.

After the concrete was allowed to set, Bristar mixes with different water/Bristar ratios were poured into the center hole. The intent was to calibrate the water/Bristar ratio so that a

confining pressure in the steel tube similar to that developed by corrosion-induced expansion could be generated. The desired confining pressure was based on the strains in composite wraps due to the expected volume expansion in a bridge column caused by corrosion (see Table 2.3).

Table 2.5 shows the strains that would be induced in the steel tube used for calibration by confining pressures expected to be generated by corrosion in composite wrapped columns (for a wrap strain of 0.531%). This strain, selected from Table 2.3, corresponds to a wrap strain that would be generated in a 915 mm diameter column due to steel corrosion after 10 years when the steel ratio by cross section and tie spacing are 3% and 152 mm, respectively. A steel ratio of 3% and tie spacing of 152 mm are conservative. Sample calculations on how the values in Table 2.5 were obtained are shown in Appendix C.2.

Table 2.5 Internal pressure generated by corrosion for wrap strain of 0.531%

Wrap	Number of layers	Pressure (kPa)	Strain in steel jacket
Glass	2	3763.6	0.029%
	3	5644.9*	0.045%*
	4	7527.2	0.060%
Carbon	1	2310.4	0.018%
	2	4620.8	0.037%
	3	6931.2	0.055%

* Sample calculation for this row is shown in Appendix C.2.

Figs. 2.3 and 2.4 show the strain generated in the steel jacket when the water/Bristar weight ratio was 400g/1000g and 500g/1000g, respectively. The maximum strain of over 0.062% generated in the steel calibration jacket by the 400g/1000g water/Bristar ratio corresponds to an internal pressure of over 7600 kPa, which is larger than all the pressures shown in Table 2.5. However, the maximum strain of about 0.038% generated in the steel calibration jacket by the 500g/1000g water/Bristar ratio corresponds to an internal pressure of about 4830 kPa. This is

closer to the pressures expected due to corrosion in columns (with wrap strain of 0.531%) wrapped with 3 layers of fiberglass and 2 layers of carbon. The 500g/1000g water/Bristar ratio is quite dilute and a higher water content is not feasible. Therefore, a water/Bristar ratio of 500g/1000g was used for all specimens requiring Bristar.

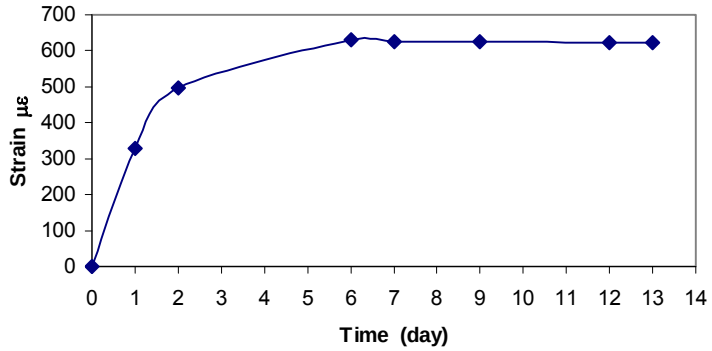

Fig.2.3 Strain in steel tube for water/Bristar ratio of 400g/1000g

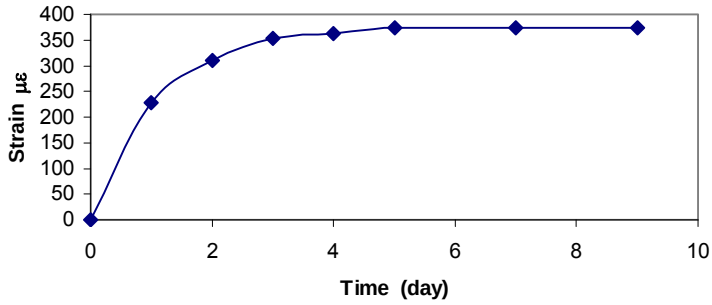

Fig.2.4 Strain in steel tube for water/Bristar ratio of 500g/1000g

It was decided that three layers of glass and two layers of carbon would be used in the freeze/thaw tests, and that the Bristar would be prepared to generate a pressure of about 4830 kPa. The strain in the glass wrap would then be about 0.45% while that in the carbon wrap would be about 0.55%. Variations in these values occurred because it was not possible to control

the Bristar pressure precisely. It was felt that using more than three layers of glass and two layers of carbon would unnecessarily increase the cost of the wraps.

Since Bristar is highly porous, and water absorption with subsequent freezing and thawing within the hole containing Bristar was undesirable, the ends of the specimens were coated with epoxy prior to the freeze/thaw tests.

2.3.3 Chloride Content

Sodium chloride (NaCl) was used exclusively in freeze/thaw and accelerated corrosion tests to contaminate concrete with chloride ions. Some examples of NaCl concentrations found in the literature are:

1. Arya and Sa'id-Shawaqi (1996) conducted tests on concrete prisms. Concrete was dosed throughout by either 2%, 3% or 4% Cl^- ions by weight of cement.

   For concrete mix data used by the Michigan Department of Transportation (MDOT) and 4% Cl^- ions by weight, this translates to 22.12 kg NaCl/m^3 of concrete:

   - 336 kg cement/m^3 of concrete × 0.04 = 13.44 kg Cl^-/m^3 of concrete
   - 13.44 kg Cl^-/ m^3 of concrete × (58.5 NaCl/35.5 Cl^-) = 22.12 kg NaCl/m^3 of concrete.

   For 3%Cl^- and 2%Cl^- this translates to 16.59 and 11.06 kg NaCl/m^3 of concrete respectively.
2. Yamato, et al. (1987) found that the chloride content investigated in an off-shore concrete bridge was about 3.0% Cl^- by weight of cement at a point 2 cm in from the vertical sides of a girder. Following calculations as in item 1, this translates to 22.69 kg NaCl/m^3 of concrete.

A 2% Cl^- ion by weight of cement was used in the freeze/thaw and accelerated corrosion tests. This translates to 11 kg NaCl/m^3 of concrete.

2.3.4 Strain Gage Placement

Strain gages were used to monitor wrap hoop strains during freeze/thaw tests on six round specimens and six square specimens (three specimens for each type of wrap), and four control specimens (one for each type of wrap and specimen shape). Each specimen was fitted with two strain gages oriented in the circumferential direction and placed opposite each other at mid-height.

Half of the specimens were wrapped with three layers of Tyfo-SEH Glass composite and the other half were wrapped with two layers of MBrace (Tonen) Carbon composite. A total of 16 specimens (eight with each type of wrap system) that were to undergo 300 cycles of freeze-thaw were fitted with strain gages (two strain gages per specimen). The gages were coated with wax and silicon for moisture and mechanical protection.

The expansive nature of Bristar caused the specimens to expand in the hoop direction as desired. An undesirable side effect was simultaneous expansion in the longitudinal direction. This caused the specimens with the carbon wrap to split across the cross sectional area since the carbon wrap contained no longitudinal fibers. The glass wrap had Kevlar strands embedded in the longitudinal direction, which prevents these specimens from splitting.

Considerable effort was devoted to devising a system for releasing the vertical expansion of Bristar using a greased aluminum tube. However, after several unsuccessful trials it was determined that the vertical stresses caused by Bristar could not be totally eliminated. In order not to risk having the carbon-wrapped specimens fail while in the freeze-thaw machine, additional longitudinal reinforcement was provided to the carbon-wrapped specimens. This was done by strengthening with strips of carbon in the longitudinal direction. The strain gage reading should not be affected since the strips are placed adjacent to the gages but not above them, and

the longitudinal strips should not provide any additional confinement. Carbon-wrapped specimens subjected to freeze-thaw as well as carbon-wrapped control specimens were fitted with vertical strips.

Initial strain gage readings were taken prior to pouring Bristar in the center hole of each specimen. After the initial expansion period of the Bristar, which is about one week, an epoxy compound was used to cap the top and the bottom of the center hole. It was not possible to control the Bristar pressure precisely. The average strain in the wraps after the addition of Bristar to the specimens measured before starting the freeze/thaw testing varied from:

- 0.31% to 0.60% for Glass with an average of 0.47%
- 0.24% to 0.68% for Carbon with an average of 0.48%

The freeze/thaw machine was set to subject the specimens to freeze/thaw cycles according to ASTM C666 Procedure B, with freezing in air and thawing in water. Strains were monitored during the freeze/thaw tests. A half bridge configuration was used for strain measurements, with dummy gages mounted on FRP panels located inside the freeze/thaw machine so that strains due to temperature variations were eliminated.

Considerable effort was required to properly adjust the freeze/thaw machine. Since some of the specimens were wrapped with composite wrap systems and others were not, careful and precise calibration was needed to control the freeze and thaw temperatures. The wrapped specimens took longer to reach -17.8^{o}C (end set point for the freeze cycle) and 4.4^{o}C (end set point for the thaw cycle) than the unwrapped specimens. A plus or minus 1.7^{o}C tolerance is allowed at the upper and lower set points by ASTM C666. After a few trials, it was established that an ideal sump water temperature of 7.2°C would ensure that all specimens attain temperatures of −17.78±1.7°C at the end of the freeze cycle and 4.4±1.7°C at the end of the thaw

cycle according to ASTM C666. Temperatures at the center of control specimens were monitored for both unwrapped and wrapped specimens.

Specimens prepared as mentioned above were then placed in the freeze/thaw chamber for 150 and 300 freeze-thaw cycles. The strains were measured throughout this period. Two switch boxes were fabricated to facilitate reading of the strain gages during the freeze/thaw and accelerated corrosion tests. A switch box is shown in Fig. 2.5.

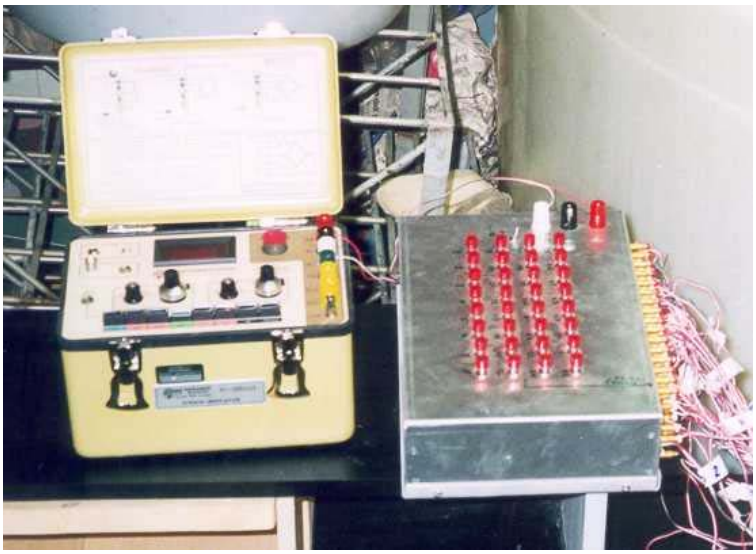

Fig. 2.5 Strain measurement instrument (left) and switch box (right) used for strain gage reading

2.3.5 Compression Testing

Considerable preparation was required prior to compression testing of the freeze-thaw specimens. Two special fixtures were manufactured to facilitate the testing.

Both end surfaces of each specimen had to be capped in order to provide two perfectly parallel contact surfaces for load application. Sulphur is commonly used for capping. The standard fixture used to align specimens vertically and cap the ends is not effective for wrapped specimens. The standard fixture requires specimens with smooth sides, but FRP wraps make the sides of wrapped specimens uneven. The standard fixture, therefore, does not assure parallel end surfaces after capping. A special fixture was fabricated to enable capping of wrapped specimens. The new fixture could be used with cylinders and square prisms, and minimized the physical labor required to lift up a specimen, pour melted sulphur on a plate, and lower the specimen onto the plate to install the end cap. This fixture is shown in Fig. 2.6.

The standard ASTM compressometer (fixture used to measure the axial strain during compression testing) cannot be used with square prisms. A new compressometer was fabricated for use with the square prisms. This new compressometer is shown in Fig. 2.7.

Fig. 2.6 Capping Fixture

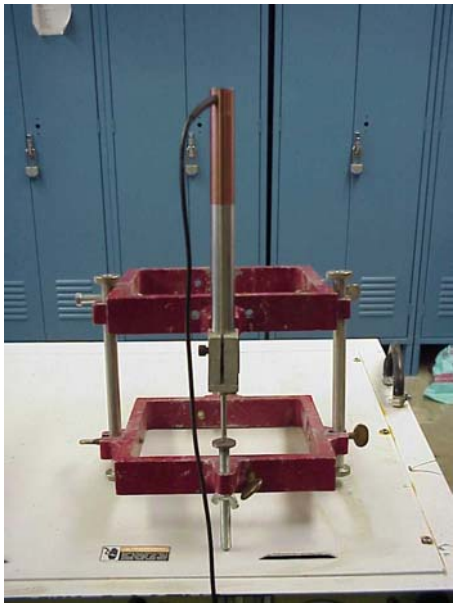

Fig. 2.7 New Compressometer

The following data was gathered every six seconds using a data acquisition system:

- The compressive load and axial strain on all specimens using a load cell and a compressometer fitted with an LVDT, respectively.
- The hoop strain in wraps for specimens fitted with strain gages

2.4 Accelerated Corrosion

Accelerated corrosion tests using an electrochemical cell were conducted to study the effect of confinment on the progression of corrosion in the reinforcing steel within a reasonable time frame. In addition, the hypothesis that FRP wraps slow down corrosion by reducing permeability of water and oxygen or that they inhibit corrosion by developing sufficient confining pressure (Brockenbrough at el. 1985) was to be evaluated. The confining pressure was monitored using the strain readings of the wraps during the accelerated corrosion tests. In addition, the rate of corrosion was indirectly measured to determine if confinement had any effect on corrosion activity.

The test used by Detwiler (1991) on lollipop specimens was adopted for use with four #13 steel reinforcing bars cast in 152 mm diameter by 305 mm high concrete cylinders. The specimens were initially immersed in salt water (with 3% NaCl) at room temperature (approximately 20 °C) and connected to a power source so that two of the steel rods became anodic and the other two became cathodic. Figure 2.8 shows the wiring diagram used for connecting specimens to the power supply in order to accelerate corrosion of the reinforcement. The exposed ends of the steel bars were protected against crevice corrosion by using a Teflon tube tightened with a nut and by covering the exposed end with silicon rubber. This forms a

barrier to prevent moisture penetration into the crevice (the interface between the steel bars and the concrete surface).

Two bars were used as anodes and two bars were used as cathodes to keep the corrosion products within the specimens as in natural corrosion. When an external cathode is used, the corrosion products tend to migrate out of the cylinder. In addition, since a conductive medium must be provided during accelerated corrosion testing, the cathodes must be placed inside the wraps, because the specimens were not continually immersed in water. Corrosion was induced on only two of the four bars in each specimen (i.e., at the anodes). Table 2.6 shows the corrosion level required in two bars for various volume ratios (i.e., vol. of rust/vol. of corroded steel) to induce a hoop strain of 0.531%, which is the anticipated strain in the wrap due to steel corrosion after 10 years (see Table 2.3). Two layers of carbon and three layers of glass were used for the accelerated corrosion test. This was the same number used for the freeze-thaw test.

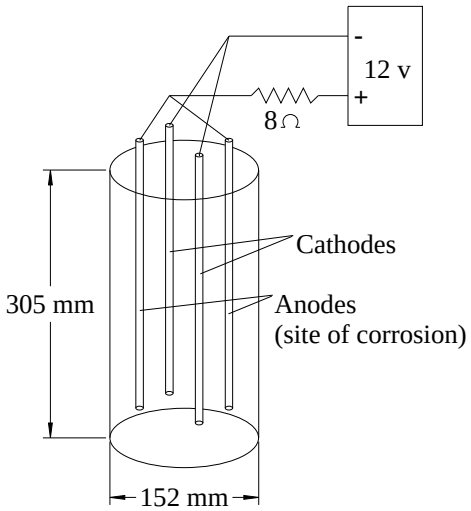

Figure 2.8 Wiring diagram for accelerated corrosion specimens

Table 2.6 Corrosion level required in two bars to induce a strain of 0.531% in the wrap*

Wrap	Strain %	Volume Ratio	Percent Corrosion
Any number of layers of carbon or glass	0.531	3	38.1
		4	25.4
		5	19.1
		6	15.3

*Two #13 bars in 6" (152 mm) diameter cylinder

In order to simulate road column exposure to rain and water spray due to passing traffic, the concrete specimens were subjected to cycles of wetting and drying. The specimens were soaked in salt water for one hour each day and the water was then drained.

The rate of corrosion was measured to determine if confinement has any effect on corrosion activity. The corrosion rate was measured using the ASTM G1 (ASTM 1990) test. The hoop strain generated in the wraps due to corrosion induced expansion was monitored using strain gages oriented in the circumferential direction. ASTM G1 test specifications is provided in Appendix F.

A water/cement ratio of 0.6 was used for the accelerated corrosion specimens to promote capillary porosity, which in turn would aid the corrosion process (see Table 1.1). Table E in Appendix E provides the concrete mix ratios and the 28-day strength for the corrosion specimens. The proportion of NaCl added to the mix to promote corrosion also is shown in the table.

Four unwrapped dummy specimens were subjected to accelerated corrosion using different resistors to vary the current intensities. These specimens were closely monitored to determine when cracking initiated. Based on these trials, resistors of 8 Ω were used with a 12 V power supply.

2.4.1 Corrosion Prior to Wrapping

Samples were exposed to accelerated corrosion while submerged in salt water prior to applying the composite wrap. This simulated initial corrosion in field columns before wrapping is applied. The initial corrosion period was closely monitored. When cracking started to develop, the specimens were taken out of the water and dried thoroughly before wrapping them with the two types of wrap systems (glass and carbon).

One approach to prevent stress concentrations on FRP wraps due to localized volume expansion is not to bond the wrap directly on the column but only provide bond between the different layers of the wrap. Thus localized volume expansion is contained by the entire wrap system. As with bonded wraps, volume expansion due to corrosion will strain the wrap inducing confining pressure. About half of the wrapped specimens contained a plastic sheet between the concrete and the wrap in order to prevent the wrap from bonding to the concrete.

A total of 24 specimens were subjected to the initial phase of accelerated corrosion for 13 days. Although subjected to the same conditions, the specimens had significant variation in corrosion level as observed from concrete cracking. The specimens were divided into three groups based on the severity of cracking — severe, moderate and light.

A total of five severely corroded specimens, in which some concrete had spalled off, were patched. Patching was done using a sand/cement mortar that was contaminated with 2% Cl^- ion by weight of cement. Specimens for which spalls occurred at an edge were placed in a mold and mortar was placed within the mold. These severely corroded specimens before and after patching are shown in Figs. 2.9 and 2.10, respectively. Specimens were selected systematically from the three groups for wrapping as shown in Table 2.7. Three layers of glass wrap and two layers of carbon wrap were used to be consistent with the number of layers used in the freeze-

thaw test. A total of 16 specimens were fitted with strain gages oriented in the circumferential direction (two gages per specimen located diametrically opposite each other at mid-height). All specimens were then ready for the next phase of accelerated corrosion.

Table 2.7 Number of wrapped and unwrapped specimens in corrosion groups

Corrosion Group	Wrap Adhesion	Number Wrapped with		
		Glass	Carbon	Nothing
Severe	Bonded	1	1	1
	Unbonded	1	1	
Moderate	Bonded	1	1	1
	Unbonded	1	1	
Light	Bonded	2+2	2	2+2
	Unbonded	2	2	

Fig. 2.9 Severely corroded specimens prior to patching

Fig. 2.10 Patching of the severely corroded speciemns

2.4.2 Construction of the Corrosion Tank and Appurtenances

A special wood tank coated with fiberglass to accommodate the corrosion specimens was constructed. The tank was fitted with a marine pump, a float shut-off mechanism, ball valves, and a timer control. In automatic mode, the pump was activated once a day to fill the tank with salt water (3% NaCl) from a holding tank located below the fiberglass tank. The float shut-off mechanism would turn the pump off when the water level covered the top of the specimens. After one hour of soaking, the timer opened the ball valve and the water was drained into the holding tank. Photographs of the corrosion tank and the corrosion specimens placed in the tank are shown in Figs. 2.11 and 2.12, respectively.

2.4.3 Monitoring Progress of Corrosion During Test

Monitoring corrosion levels during the accelerated corrosion test was important in order to know when to remove specimens. Unwrapped specimens were expected to corrode faster than

Fig. 2.11 Corrosion tank

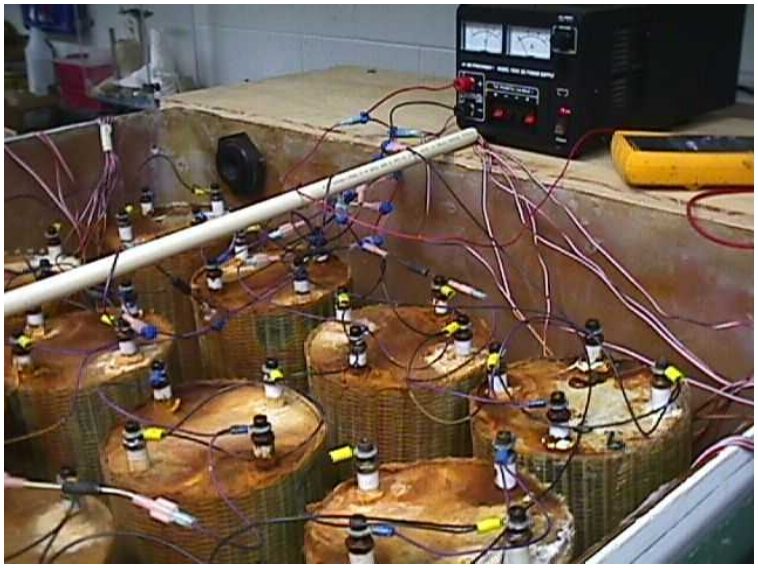

Fig. 2.12 Corrosion specimens in the tank

wrapped specimens. Also, some specimens were to be removed approximately mid-way through testing when the anodic reinforcement in unwrapped specimens lost about half their cross sectional area. The total length of time for the corrosion test could not be predicted in advance. A method was needed to monitor corrosion levels during the test.

Two dummy specimens were originally fabricated to monitor corrosion levels through destructive means. The plan was to cut off sections of the dummy specimens at regular intervals and visually examine the cross section of corroded bars. This approach was error prone because corrosion occurs unevenly and the dummy specimen size would be altered each time a section was sliced off.

A non-destructive method of monitoring corrosion levels was sought, and an approach utilizing X-rays was identified. Some unwrapped and wrapped pre-corroded specimens were subjected to X-rays in a standard radiology laboratory. The X-ray negatives clearly show the uncorroded parts of the anodic steel reinforcement.

Prior to beginning the accelerated corrosion process after specimens were wrapped, representative specimens were subjected to X-rays to ascertain the level of corrosion during the pre-corrosion phase. The X-ray images showed the reinforcing bars inside the specimen and the approximate level of corrosion in them. This was necessary to establish a reference point and assess the progress of corrosion.

Periodically, the specimens selected for observation were transported to the radiology laboratory and subjected to X-rays. By comparing the state of corrosion in the wrapped and unwrapped specimens, it was evident that the corrosion rate in wrapped specimens was significantly lower than that in unwrapped specimens. Fig. 2.13, 2.14, and 2.15 show views of the X-rays of a typical unwrapped specimen taken after 0, 90 and 105 days of accelerated

corrosion after the precorrosion stage, respectively. To facilitate reproduction, the X-ray images were outlined to clearly show the edges of the reinforcing bars and the specimen, and the photographic image was reduced to create the line drawings shown in the figures. Fig. 2.16 shows typical reinforcing bars removed from a specimen. The middle two bars are the cathodes while the outer two bars are the anodes (the site of corrosion).

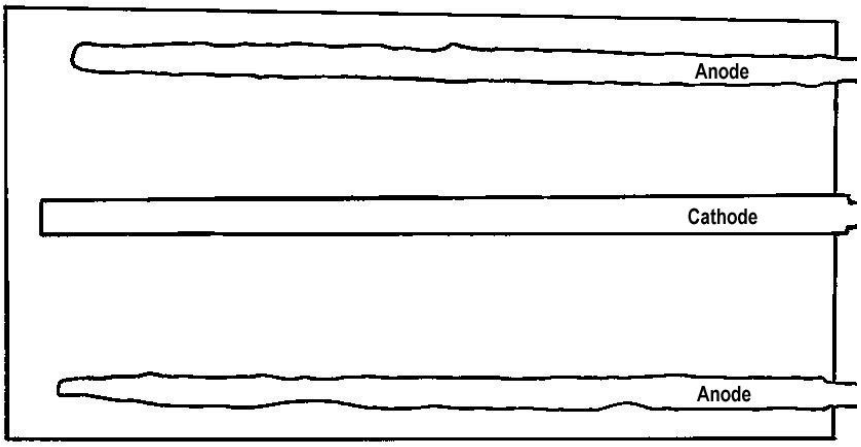

Figs. 2.13 Sample X-ray taken in the beginning of the accelerated corrosion test

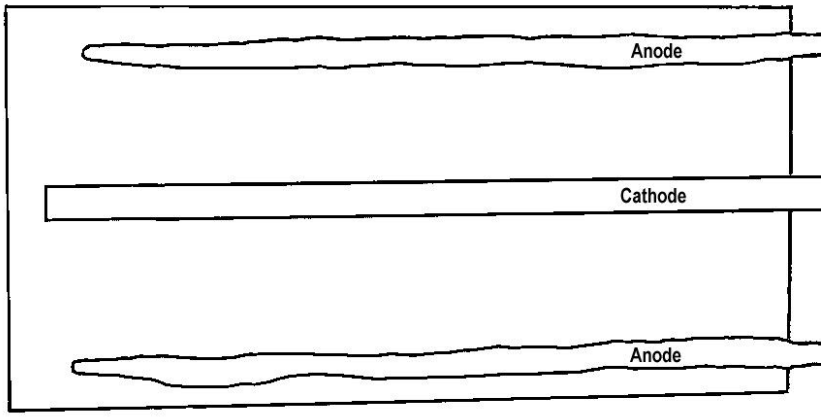

Figs. 2.14 Sample X-ray taken after 90 days of accelerated corrosion test

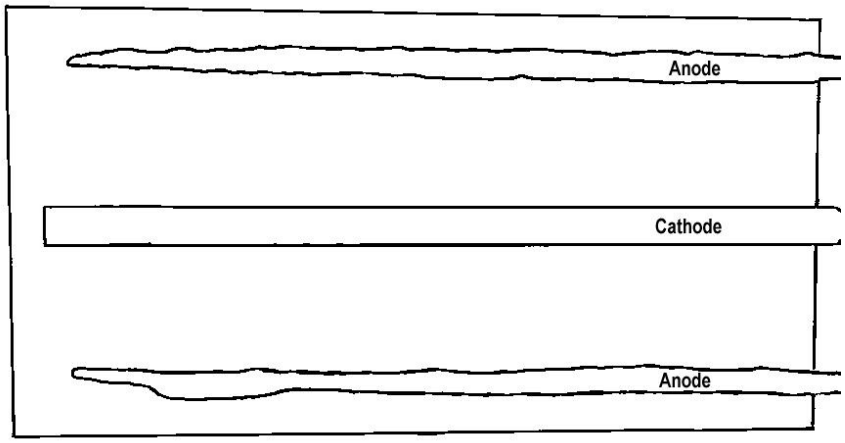

Figs. 2.15 Sample X-ray taken after 105 days of accelerated corrosion test

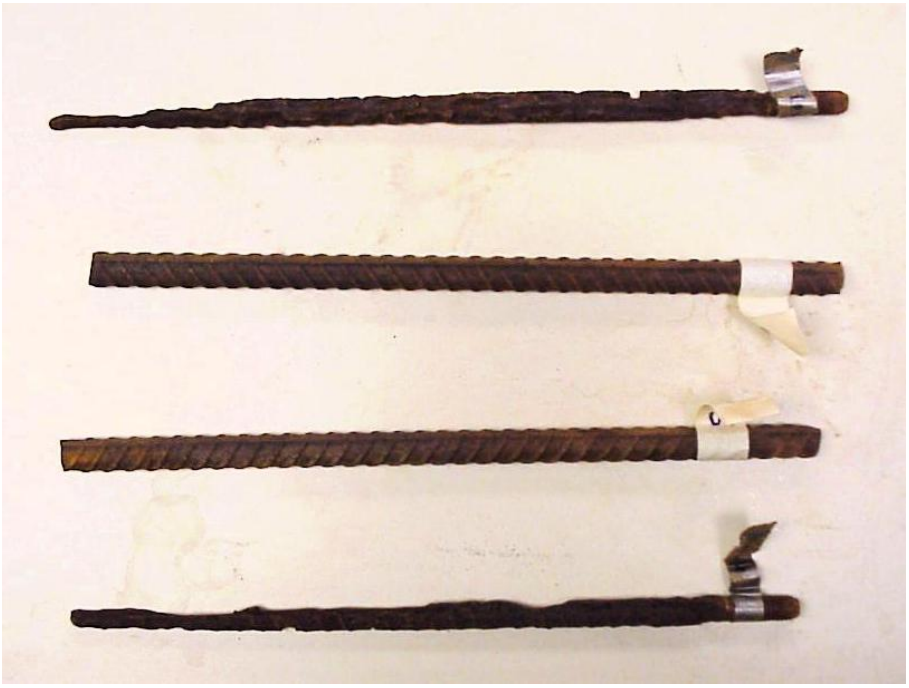

Fig. 2.16 Reinforcing bars after removal from a corrosion specimen. The middle two bars are the cathodes while the outer two bars are the anodes (the site of corrosion)

Specimens were removed for X-ray exposure when there was no water in the tank. The current used to accelerate corrosion was shut-off while the specimens were removed and transported to the radiology laboratory, and turned back on when the specimens were returned to the corrosion tank approximately two hours later.

2.4.4 Corrosion Test Matrix

The total number of specimens was 24, including the two extra specimens originally planned for corrosion monitoring through destructive means. The numbers of samples of the various types of specimens used are given in Table 2.8. Specimen, bar and strain gage numbering is shown in Table D.2 in Appendix D. Specimens were removed from the corrosion process and the amount of corrosion was measured as follows:

1. Four unwrapped, four carbon wrapped (two bonded, two unbonded), and five glass wrapped (three bonded, two unbonded) specimens were removed when the X-ray technique indicated that the diameter of corroded bars in unwrapped specimens was reduced to about 70% of the initial diameter (which corresponds to about 50% reduction in the cross sectional area). This corresponded to 130 days of accelerated corrosion.
2. Two unwrapped, four carbon wrapped (two bonded, two unbonded), and five glass wrapped (three bonded, two unbonded) specimens were removed when the accelerated corrosion test could not be effectively continued for the unwrapped specimens. This was due to the upper tips of the anodes breaking off and occurred after 190 days of accelerated corrosion.

Comparisons of corrosion levels at each of the two stages mentioned above was used evaluate the effectiveness of the different wrapping systems in reducing corrosion.

Wrap strains were monitored until specimens were removed from the corrosion process. These strains were used to estimate the amount of confining pressure built up due to corrosion.

Table 2.8 Accelerated corrosion laboratory test matrix

Wrap	No. of Specimens Tested for 130 days	No. of Specimens Tested for 190 days
None (control)	4	2
Carbon bonded Glass bonded	2 3	2 3
Carbon unbonded Glass unbonded	2 2	2 2

2.5 Freeze-Thaw and Wet-Dry Cycling of FRP Panels

The dummy carbon and glass FRP panels used in the freeze-thaw and corrosion tests for temperature correction were later used to assess the effect of freeze-thaw and wet-dry cycles on the properties of the panels. The FRP panels in the freeze-thaw test were exposed to 300 freeze-thaw cycles, with freezing in air and thawing in water. The FRP panels in the corrosion test were exposed to 190 wet-dry cycles with 3% NaCl solution.

2.6 Impact Test

Impact testing was conducted on glass and carbon FRP panels. Three layers of glass and two layers of carbon were used to make the panels. This number of layers was chosen to be consistent with the number of glass and carbon layers for both the freeze-thaw test and the corrosion test.

The impact machine is made of a 75 mm diameter semi-spherical aluminum head which is dropped from a 0.79 m height. The impact force can be increased by adding more weight. (This was a modified ASTM D1037 test.) In order to simulate impact of a wrapped column, the FRP panel was placed on top of a 150 × 150 × 150 mm concrete block and the impact head was dropped on it. The impact head was repeatedly dropped on the FRP panel while the weight was gradually increased after each impact. The panel was examined after each impact and replaced so that the subsequent impact would be at the same location. The starting weight used was 8.12 kg and the capacity of the machine was 16.5 kg. Figure 2.17 shows the impact test machine.

2.7 High Temperature Test

One glass-wrapped and one carbon-wrapped specimens was sawed into three slices each, and each slice was exposed to temperatures of 100°C, 150°C and 200°C for four hours. The specimens were visually examined each half hour.

Fig. 2.17 Machine used for impact test of FRP panels

Note: Intentionally left blank

Chapter 3
Data Collection and Analysis of Results

3.1 Freeze-Thaw Test

3.1.1 Strain Gage Readings

Specimens subjected to 300 freeze-thaw cycles were equipped with strain gages, while those subjected to 150 freeze-thaw cycles were not equipped with strain gages. The FRP hoop strains were monitored about once a day during the entire testing period for specimens fitted with strain gages. Two readings were made each day, one during the freeze phase and the other during the thaw phase. All strain gages survived the freeze-thaw test.

Dummy gages mounted on FRP panels were used for monitoring the strain using a half bridge configuration so that temperature compensation was performed. The same dummy gages were used both for specimens subjected to freeze-thaw as well as for control specimens not subjected to freeze-thaw. The FRP panels containing the dummy gages were located in the freeze-thaw machine. By observing the difference in the strain reading of the control specimens (wrapped, no freeze-thaw conditioning) between freeze and thaw cycles, the thermal contraction of the FRP panels from thaw to freeze cycles could be determined. Figures 3.1-3.4 show the uncorrected strain readings on round and square control specimens that were not subjected to freeze-thaw. On any given day, the reading of a gage during a freeze or thaw cycle should be approximately the same, since the control specimens were not subjected to freeze-thaw. The difference in gage readings from the thaw to freeze curves observed in Figures 3.1-3.4 is therefore due to contraction of the dummy FRP panel. The compensation strains for glass and carbon were determined by the average difference between the thaw and freeze readings for

control specimens from day 15 onward, when the strains were stable. Note that for carbon (Figures 3.3-3.4), there is only a slight difference between thaw and freeze readings since its coefficient of thermal expansion is close to zero. The compensation strains computed in this manner are 372 micro-strain for glass FRP and –37 micro-strain for carbon FRP. Figures 3.7, 3.11, 3.15 and 3.19 show the compensated strains on the same four control specimens, respectively. The strains during the thaw and freeze cycles are now approximately the same for the control specimens without freeze-thaw conditioning from day 10 onward as expected.

The compensated FRP strains on round and square specimens wrapped with glass and subjected to freeze-thaw are shown in Figures 3.5. 3.6, 3.8, 3.9, 3.10 and 3.12. In general, the strain during the freeze cycle is 100-200 micro-strain higher than that during the thaw cycle. This is most likely due to the thermal contraction of the glass wrap during freezing. Since the concrete specimens prevent the contraction, the tensile strain in the glass wraps increase. An exception is Figure 3.6, in which the strains during the thaw cycle is slightly but consistently higher than that during the freeze cycle.

The compensated FRP strains on round and square specimens wrapped with carbon and subjected to freeze-thaw are shown in Figures 3.13, 3.14, 3.16-3.18 and 3.20. The results are less consistent for carbon than for glass. In Figures 3.13, 3.16 and 3.17 the thaw strains are higher than the freeze strains, while the reverse is true in Figures 3.14 and 3.20.

A reason for some of the variability in the wrap strains could be the ingestion of water into the Bristar. Although epoxy caps were used on both ends of each specimen to prevent water penetration, during freeze-thaw cycling the caps of several specimens ruptured due to expansive pressure from Bristar. The loss of strain with time in Figure 3.17 also is likely to be due to the loss of pressure in the Bristar.

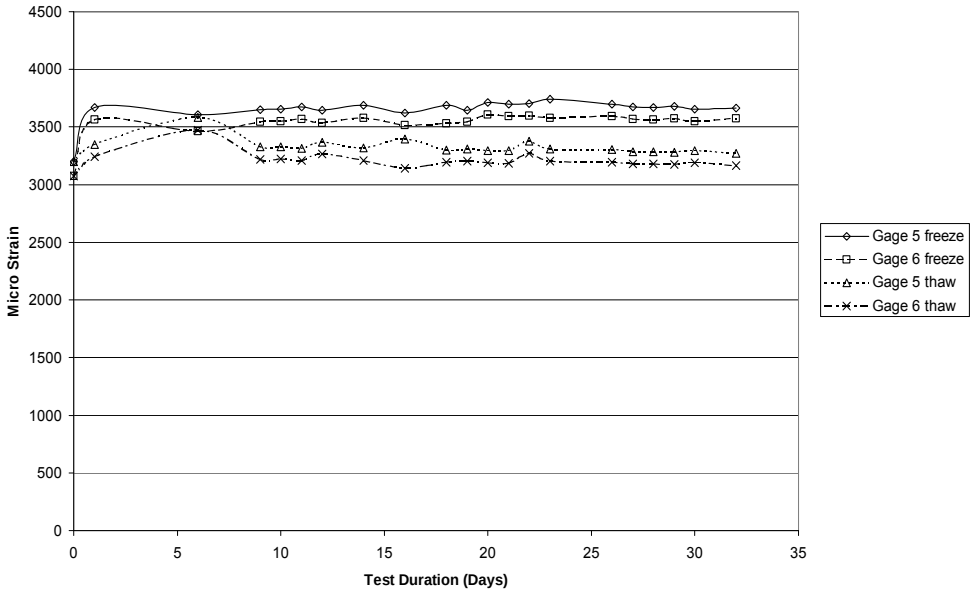

Fig. 3.1 Hoop strains in glass wrap of round control specimen #3 before correcting for thermal contraction of dummy FRP panel

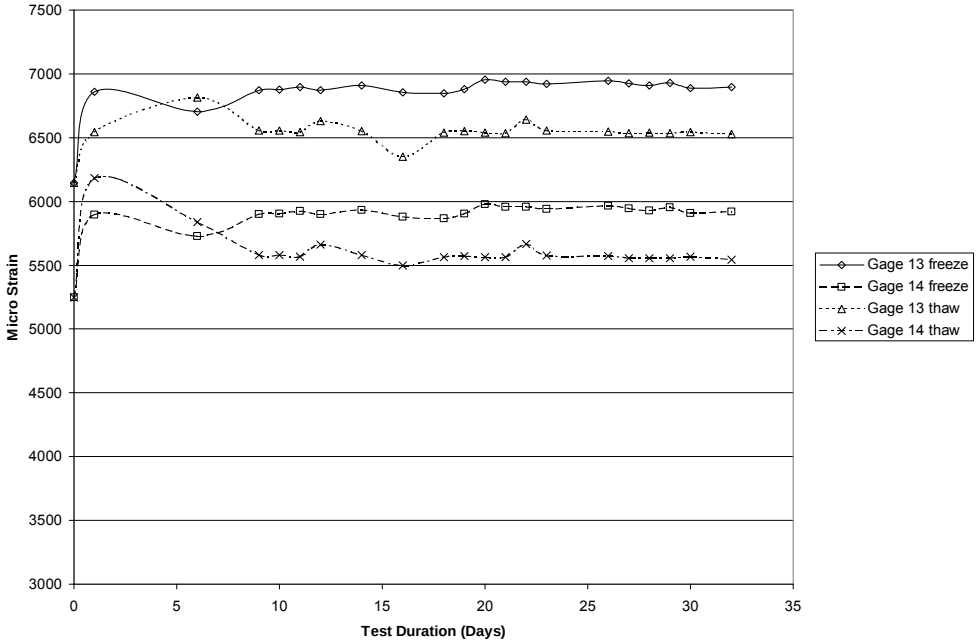

Fig. 3.2 Hoop strains in glass wrap of square control specimen #7 before correcting for thermal contraction of dummy FRP panel

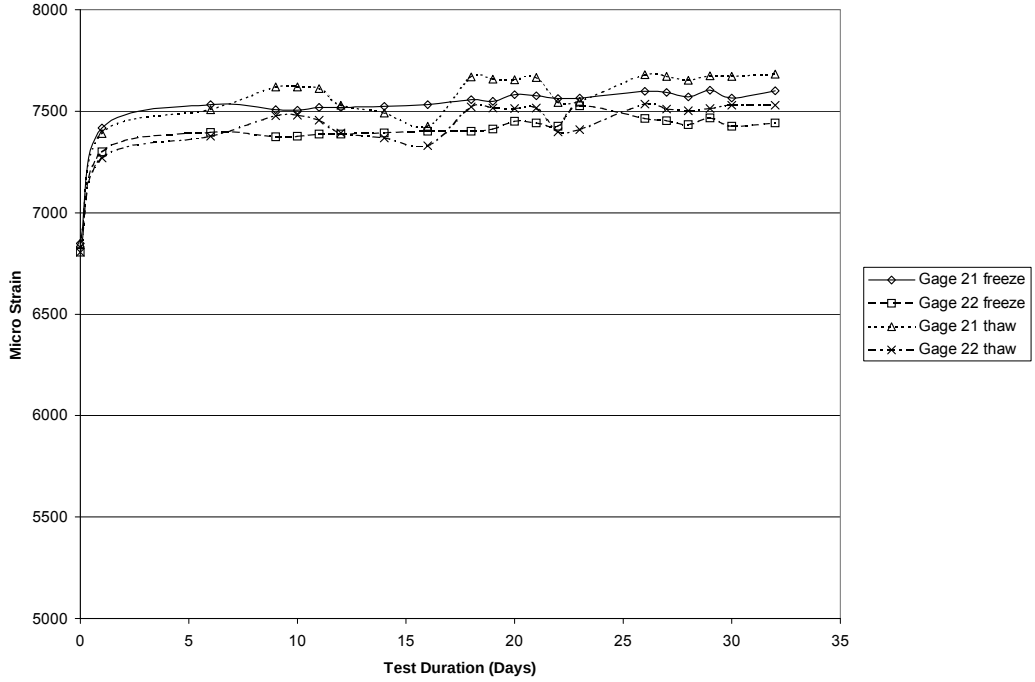

Fig. 3.3 Hoop strains in carbon wrap of round control specimen #11 before correcting for thermal contraction of dummy FRP panel

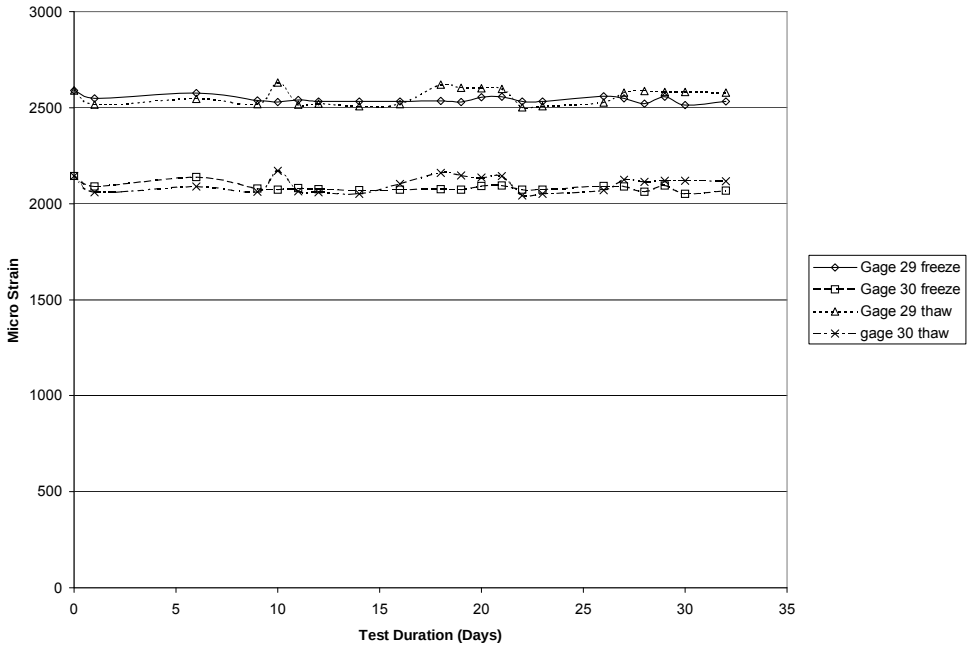

Fig. 3.4 Hoop strains in carbon wrap of square control specimen #15 before correcting for thermal contraction of dummy FRP panel

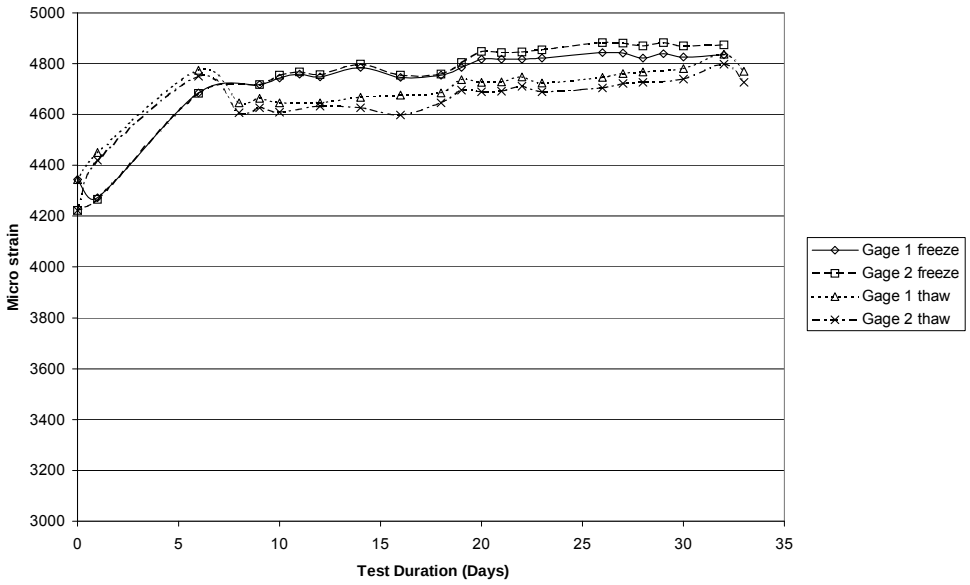

Fig. 3.5 Hoop strains in glass wrap of round specimen #1 during freeze-thaw cycles

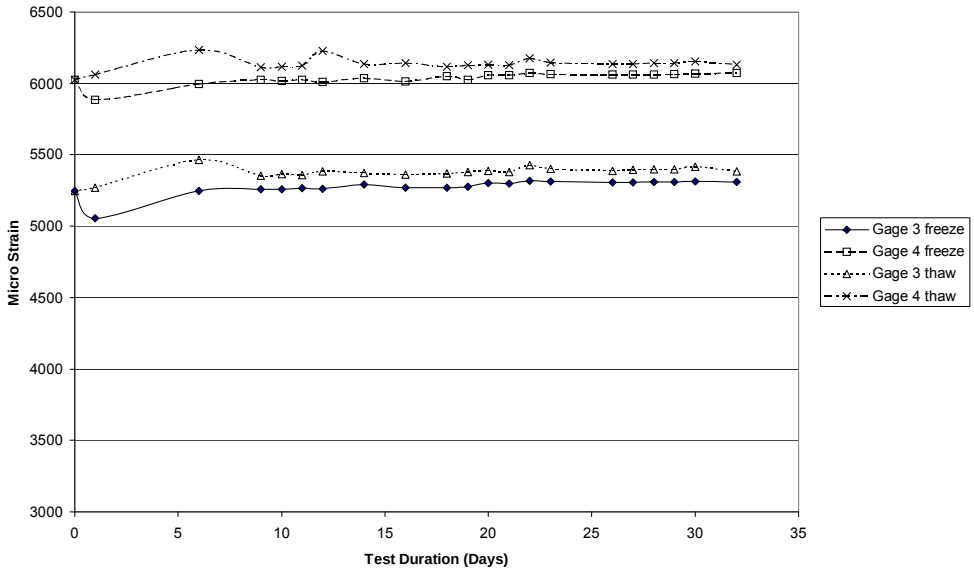

Fig. 3.6 Hoop strains in glass wrap of round specimen #2 during freeze-thaw cycles

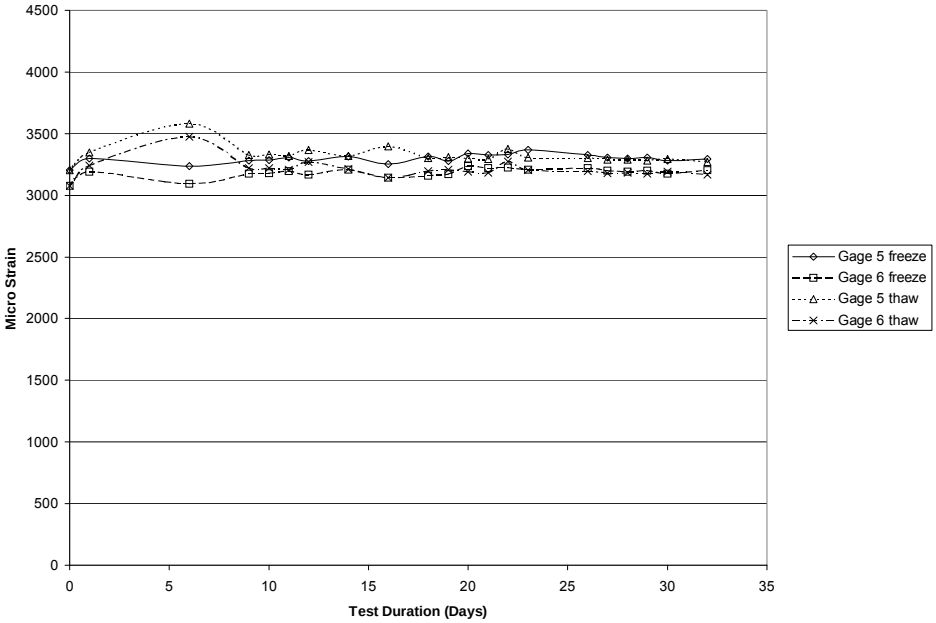

Fig. 3.7 Hoop strains in glass wrap of control round specimen #3

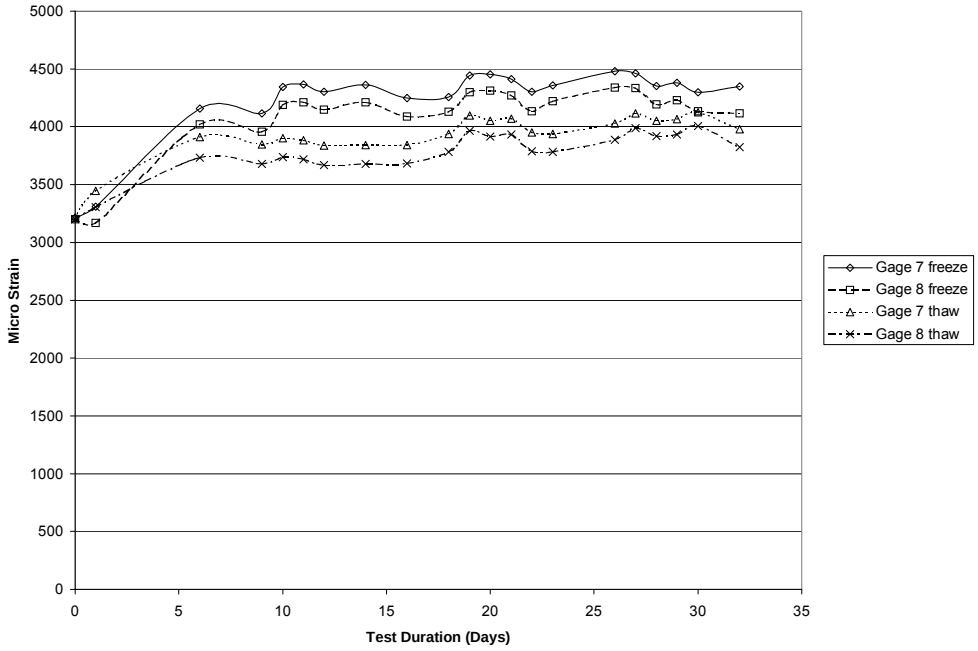

Fig. 3.8 Hoop strains in glass wrap, round specimen #4 during freeze-thaw cycles

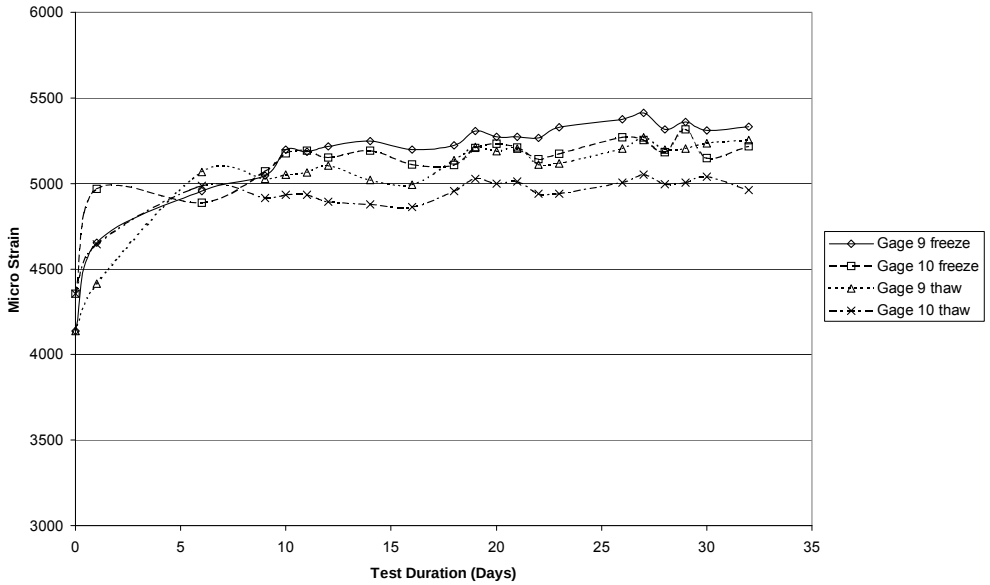

Fig. 3.9 Hoop strains in glass wrap, square specimen #5 during freeze-thaw cycles

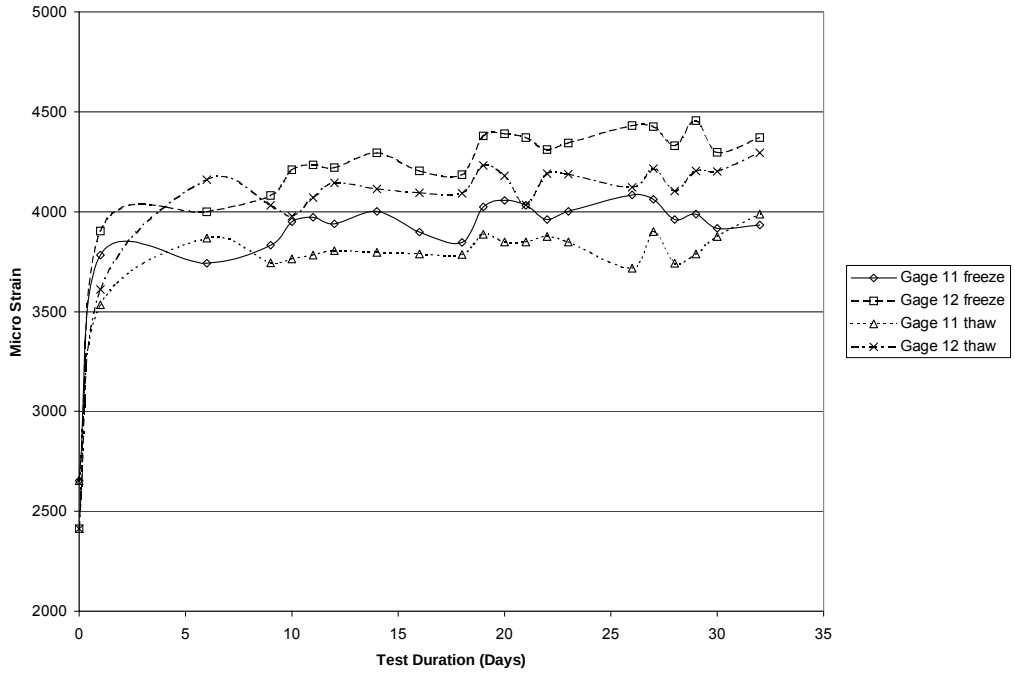

Fig. 3.10 Hoop strains in glass wrap, square specimen #6 during freeze-thaw cycles

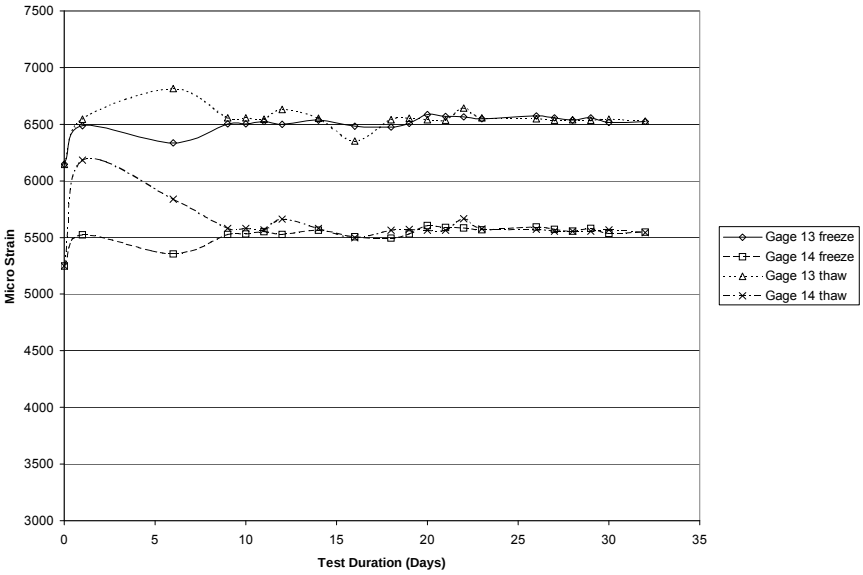

Fig. 3.11 Hoop strains in glass wrap of control square specimen #7

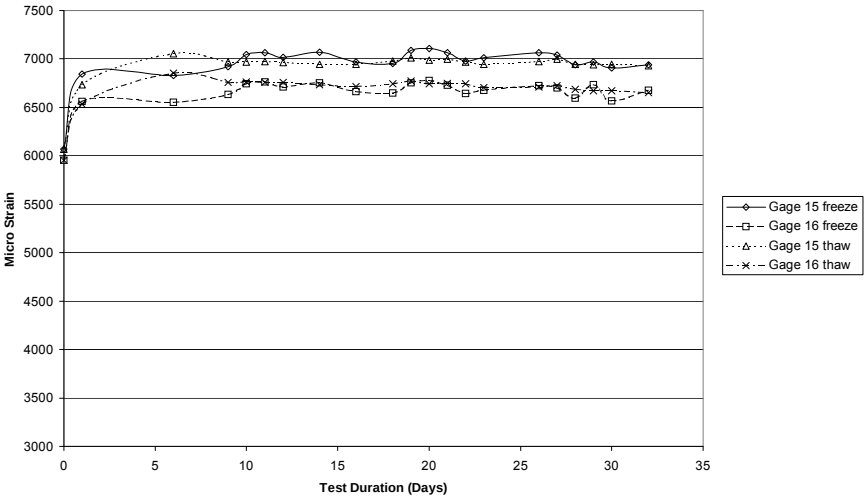

Fig. 3.12 Hoop strains in glass wrap of square specimen #8 during freeze-thaw cycles

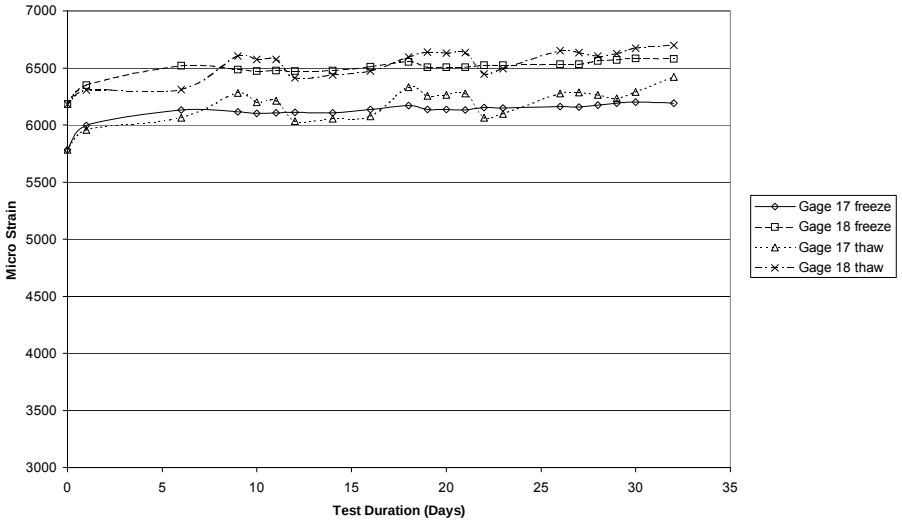

Fig. 3.13 Hoop strains in carbon wrap of round specimen #9 during freeze-thaw cycles

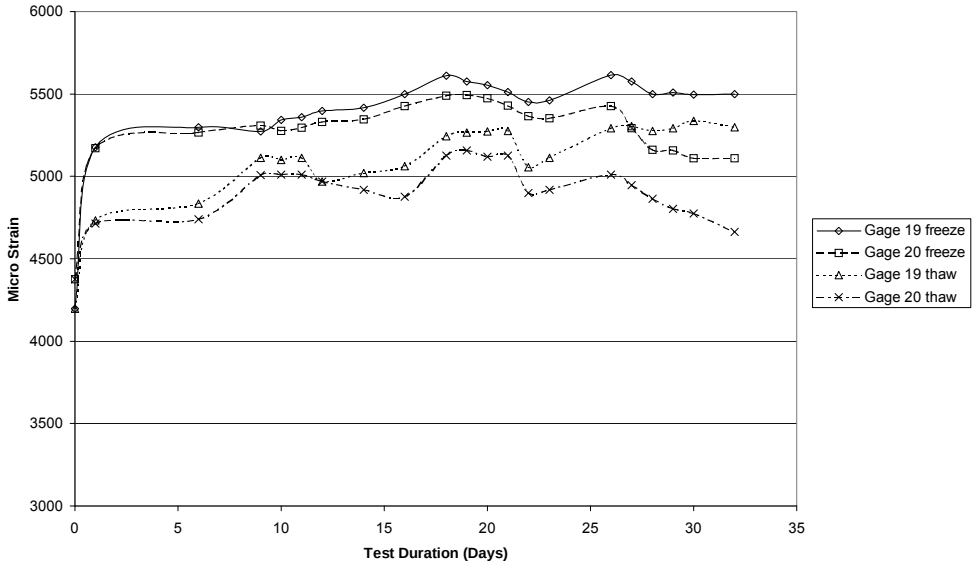

Fig. 3.14 Hoop strains in carbon wrap of round specimen #10 during freeze-thaw cycles

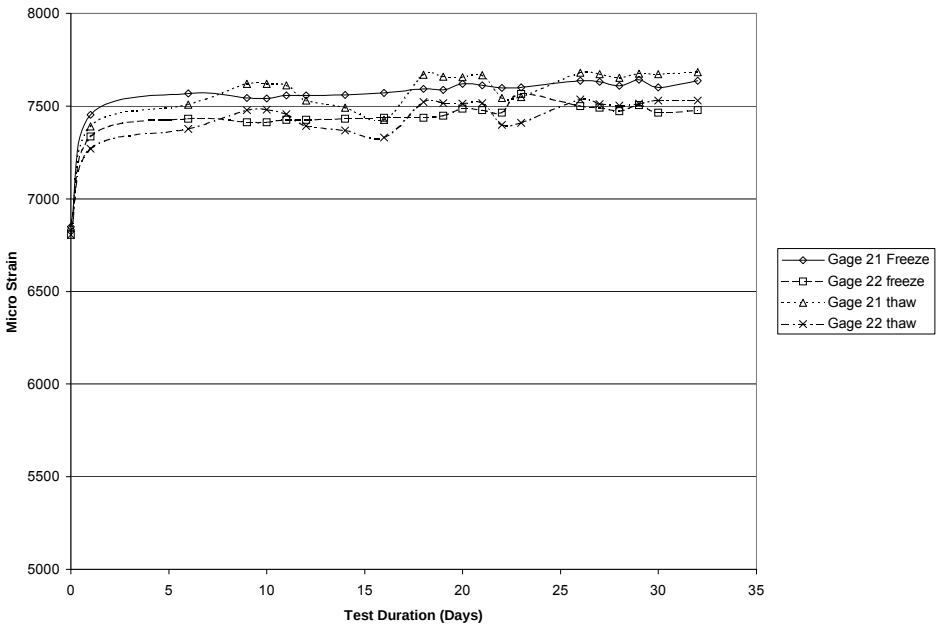

Fig. 3.15 Hoop strains in carbon wrap of control round specimen #11

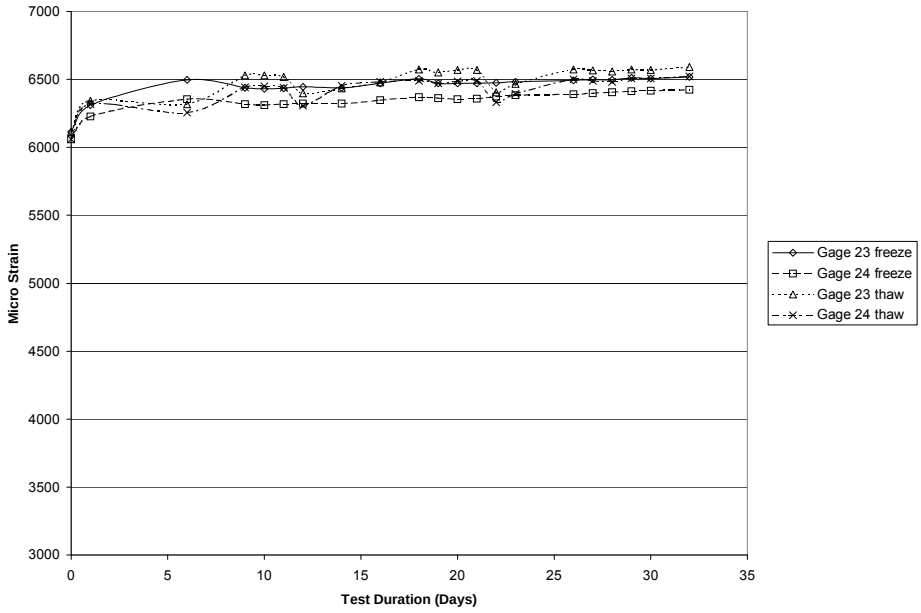

Fig. 3.16 Hoop strains in carbon wrap of round specimen #12 during freeze-thaw cycles

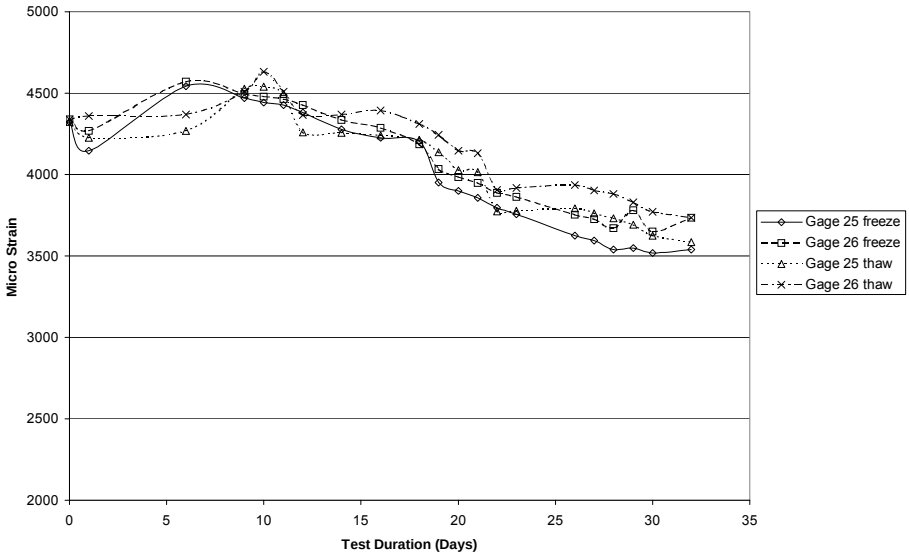

Fig. 3.17 Hoop strains in carbon wrap of square specimen #13 during freeze-thaw cycles

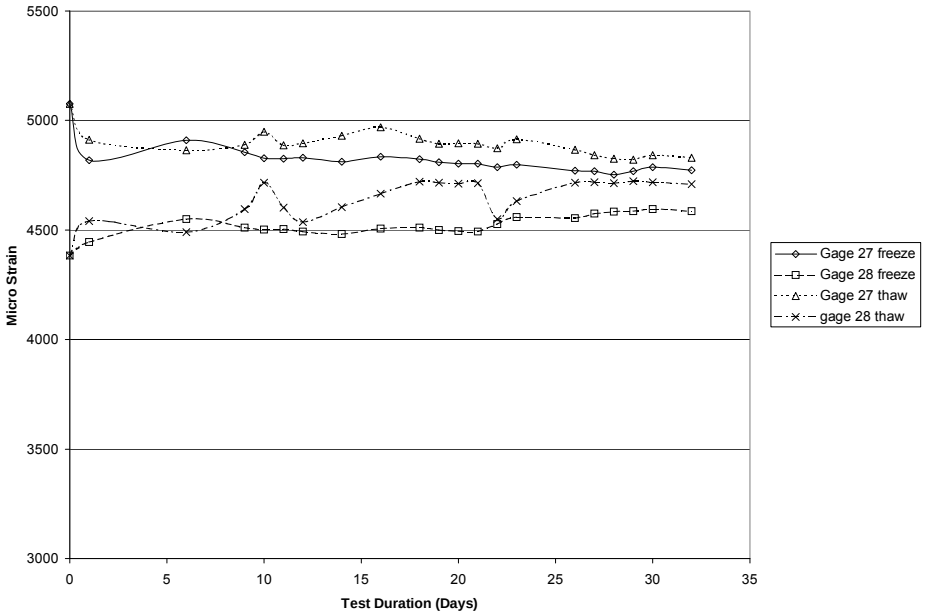

Fig. 3.18 Hoop strains in carbon wrap of square specimen #14 during freeze-thaw cycles

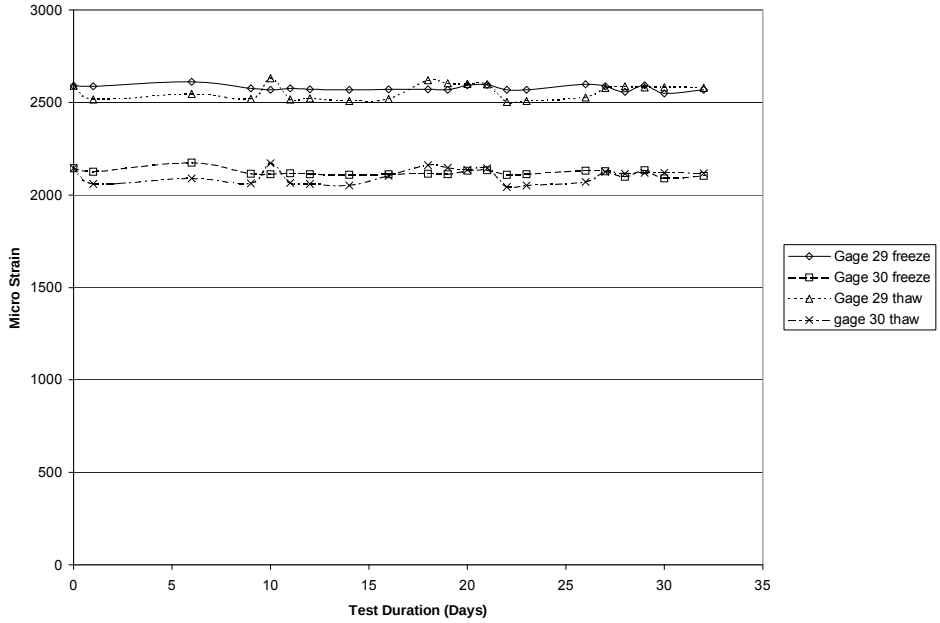

Fig. 3.19 Hoop strains in carbon wrap of control square specimen #15

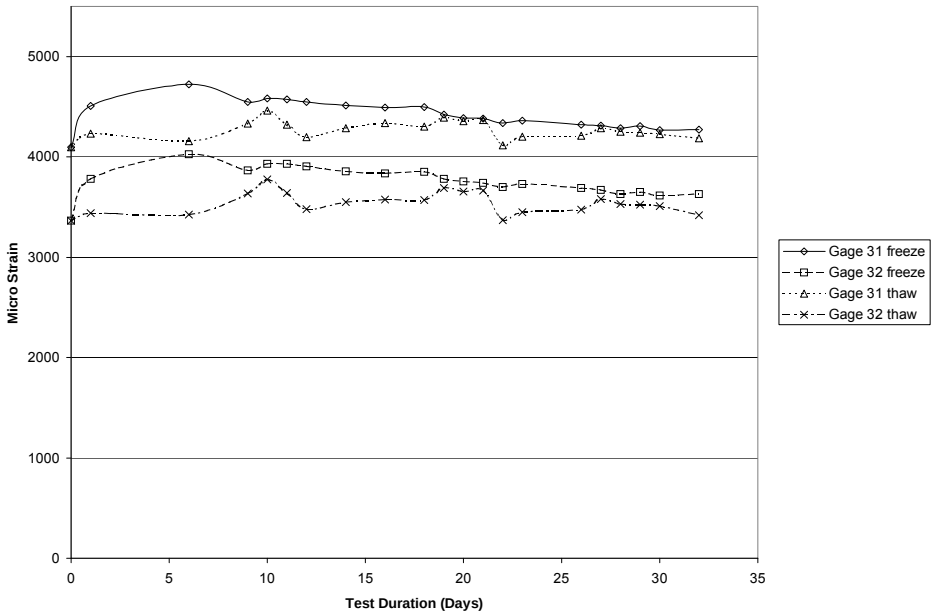

Fig. 3.20 Hoop strains in carbon wrap of square specimen #16 during freeze-thaw cycles

3.1.2 Results of Compression Testing

Figures 3.21 to 3.35 show results of the compression tests for plain and wrapped control specimens and those subjected to 150 and 300 cycles of freeze-thaw. For wrapped specimens fitted with strain gages in the hoop direction, longitudinal compression strains are given along the positive x-axis while the average tensile hoop strain is shown along the negative x-axis. The compression stress for wrapped specimens was computed by excluding the concrete cross sectional area lost due to the presence of the hole in which Bristar was inserted. The following observations are made:

- **Plain round specimens (Figures 3.21-3.23):** Only one of three specimens survived freeze-thaw conditioning for 300 cycles. This specimen had approximately the same compression strength as the control specimens (~35000-45000 kPa). One of the specimens subjected to 150 freeze-thaw cycles displayed low stiffness and strength, and a progressively hardening behavior— it is not apparent what contributed to this behavior. There is no significant reduction in strength due to freeze-thaw conditioning except for the anomalous specimen.
- **Round glass-wrapped specimens (Figures 3.24-3.26):** The ultimate strength values for two of the six control specimens were unreliable because these specimens could not be crushed in the MSU compression testing machine and were retested at MDOT. In general, conditioning had little effect and compression strength and failure strains were approximately the same for control and conditioned specimens. Strength of wrapped specimens (~105000-114000 kPa) was approximately 2.6 times larger than the strength of unwrapped specimens.
- **Square glass-wrapped specimens (Figures 3.27-3.29):** Again conditioning had little effect on the compressive strength (~62000-66000 kPa), but it reduced the longitudinal strain at

failure from about 0.01-0.017 to ~0.007. Strength of wrapped specimens was approximately 1.5 times larger than the strength of unwrapped specimens.

- **Round carbon-wrapped specimens (Figures 3.30-3.32):** Conditioning reduced compression strengths from about 92000 kPa (unconditioned) to about 80000 kPa (300 cycles) representing about a 15% strength loss. One specimen each in the 150 and 300 cycle batches had unusually high strengths, indicating that one batch of specimens prepared might have had a different strength level. Longitudinal failure strains reduced from about 0.015 to 0.01 (~33%). Strength of wrapped specimens (~95000 kPa) is approximately 2.3 times larger than the strength of unwrapped specimens.
- **Square carbon-wrapped specimens (Figures 3.33-3.35):** Conditioning reduced compression strengths slightly from about 58000-65000 kPa to about 55000-63000 kPa. Longitudinal failure strains reduced from about 0.007-0.01 to about 0.005. Strength of wrapped specimens (~60000 kPa) is approximately 1.4 times larger than the strength of unwrapped specimens. Note that for square specimens, glass and carbon wraps increased the strength by about the same amount.

The square wrapped specimens had lower compressive strength compared to the round specimens, even though the cross sectional area of the square prisms is higher than that of the round cylinders. This is due to the reduced confinement provided by the wraps for square cross sections and stress concentrations that develop at the corners. Wrapped square prisms always failed by rupture of the wrap at a corner (see Figure 3.36). Note that a reduction of approximately 30% to 40% in failure stress exists between the round and the square specimens. Figures 3.36–3.37 show the failure modes under compression testing.

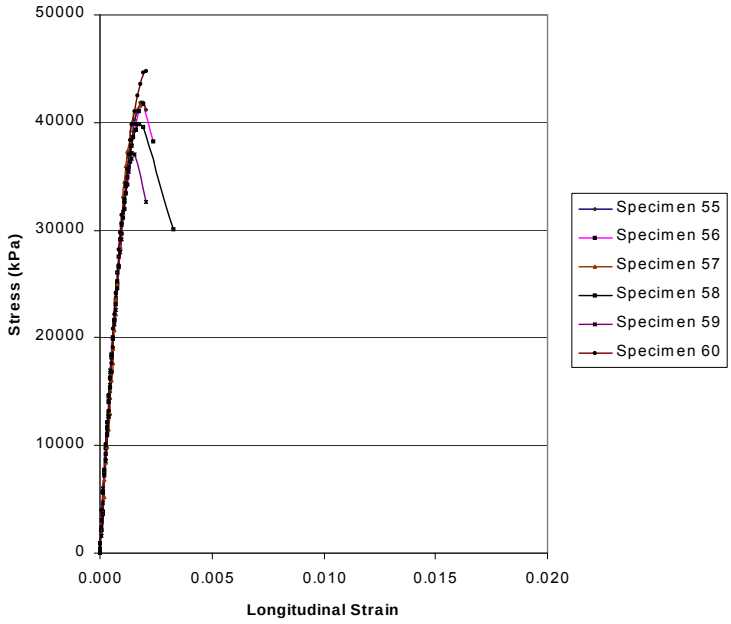

Fig. 3.21 Compressive stress-strain curves for plain, round, control specimens

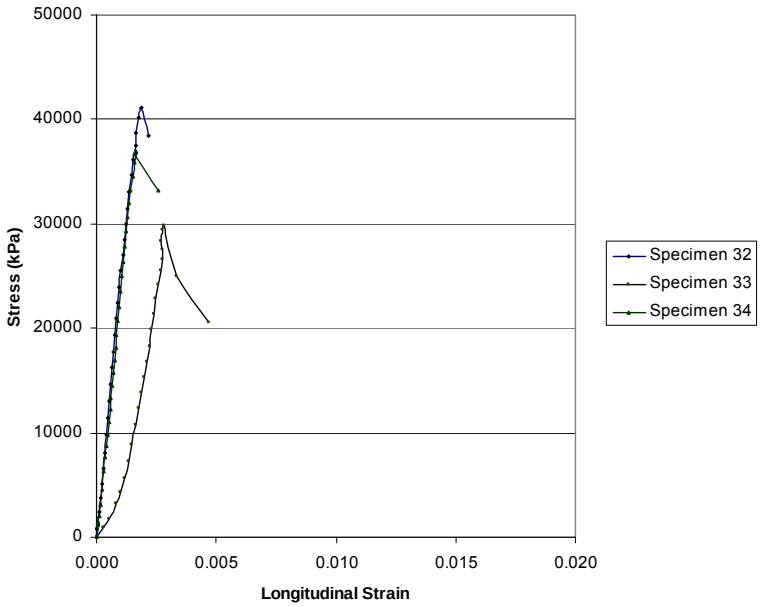

Fig. 3.22 Compressive stress-strain curves for plain, round specimens subjected to 150 freeze-thaw cycles

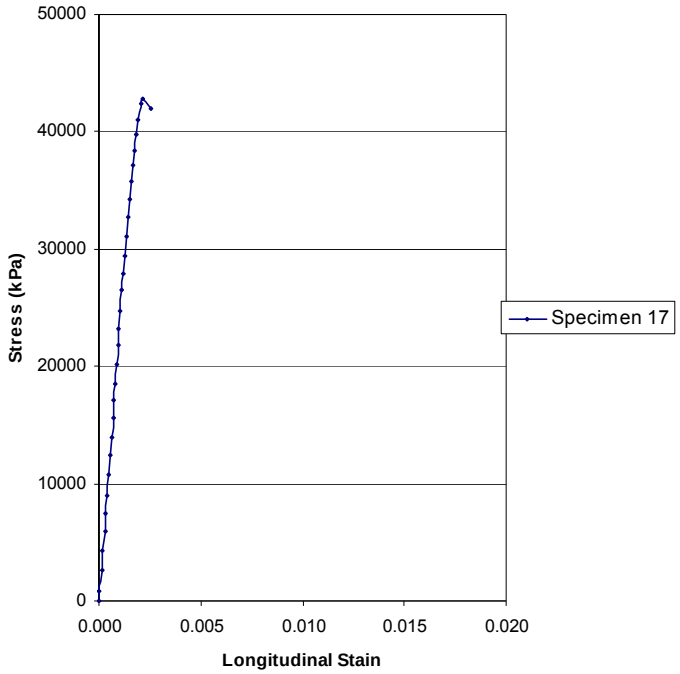

Fig. 3.23 Compressive stress-strain curves for plain, round specimens subjected to 300 freeze-thaw cycles

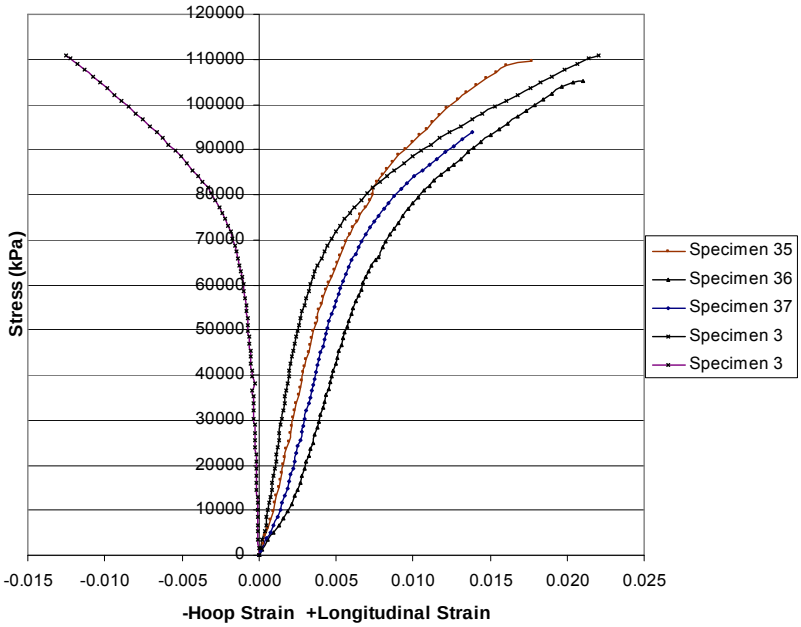

Fig. 3.24 Compressive stress-strain curves and tensile hoop strain for glass-wrapped, round, control specimens

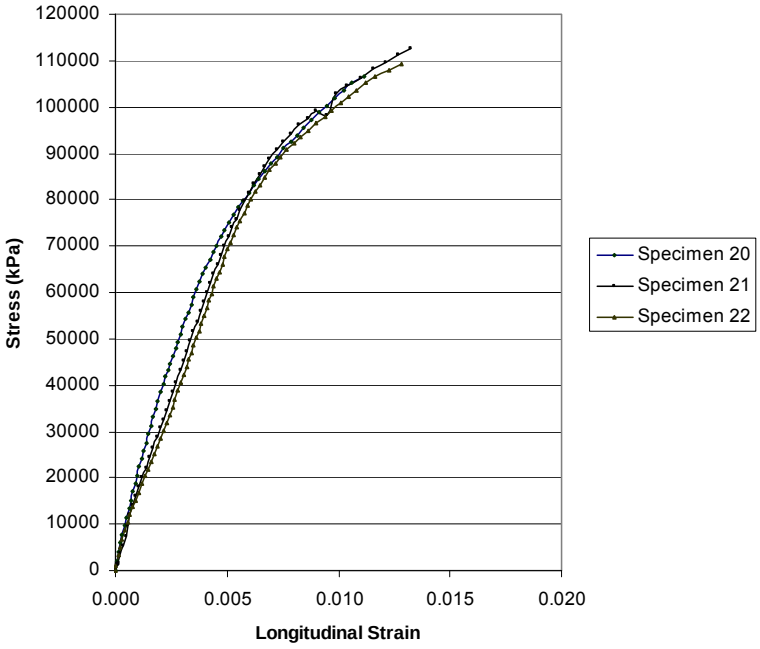

Fig. 3.25 Compressive stress-strain curves for glass-wrapped, round specimens subjected to 150 freeze-thaw cycles

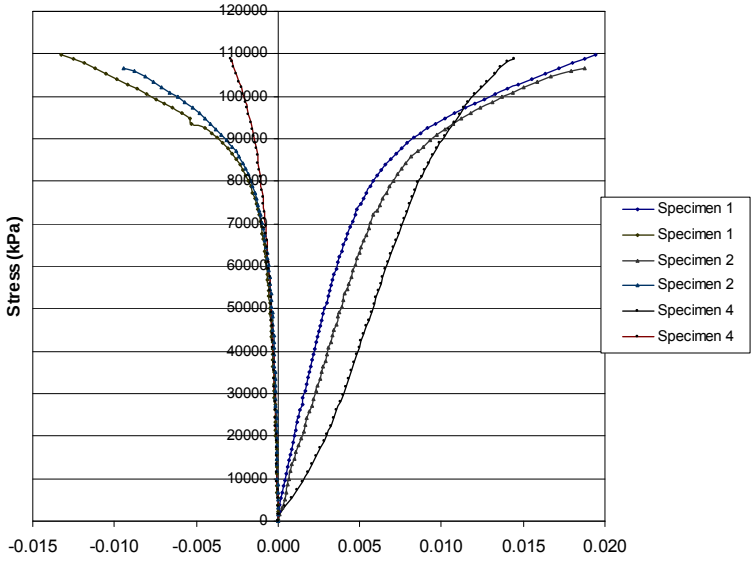

Fig. 3.26 Compressive stress-strain curves and tensile hoop strain for glass-wrapped, round specimens subjected to 300 freeze-thaw cycles

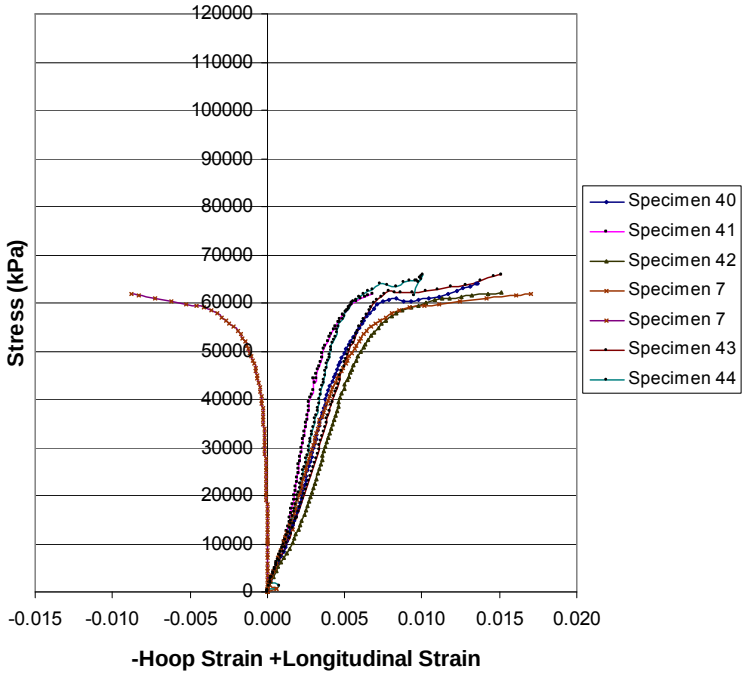

Fig. 3.27 Compressive stress-strain curves and tensile hoop strain for glass-wrapped, square, control specimens

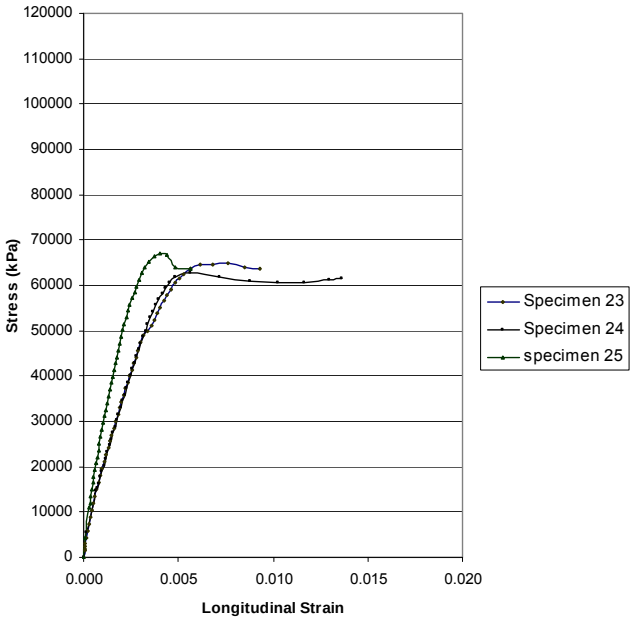

Fig. 3.28 Compressive stress-strain curves for glass-wrapped, square specimens subjected to 150 freeze-thaw cycles

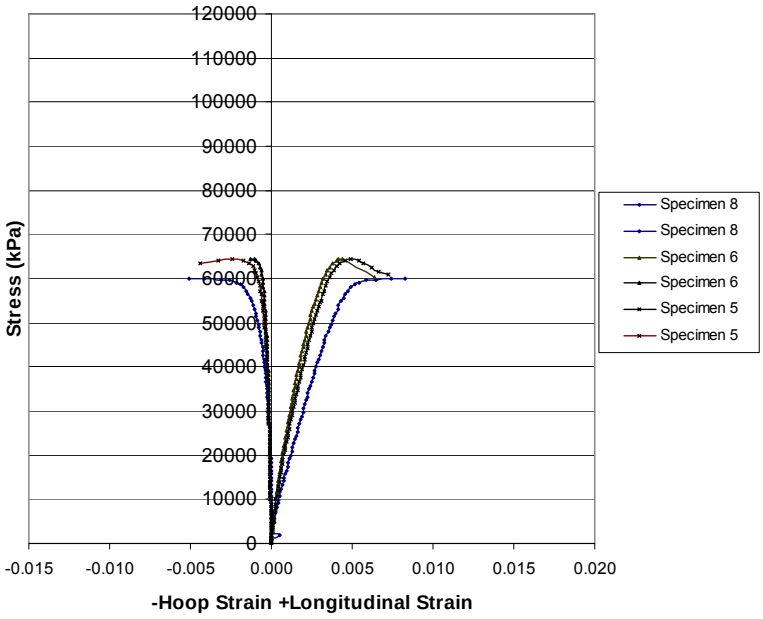

Fig. 3.29 Compressive stress-strain curves and tensile hoop strain for glass-wrapped, square specimens subjected to 300 freeze-thaw cycles

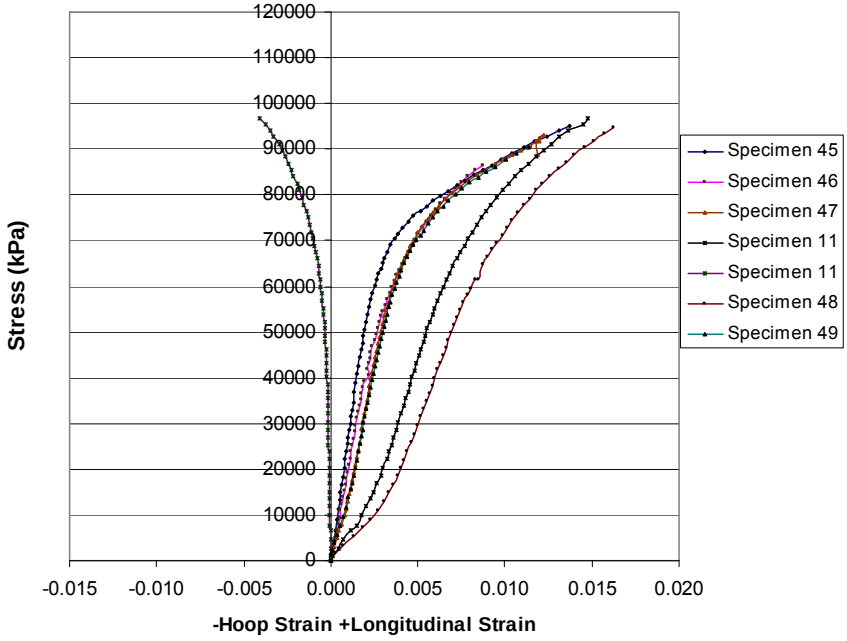

Fig. 3.30 Compressive stress-strain curves and tensile hoop strain for carbon-wrapped, round, control specimens

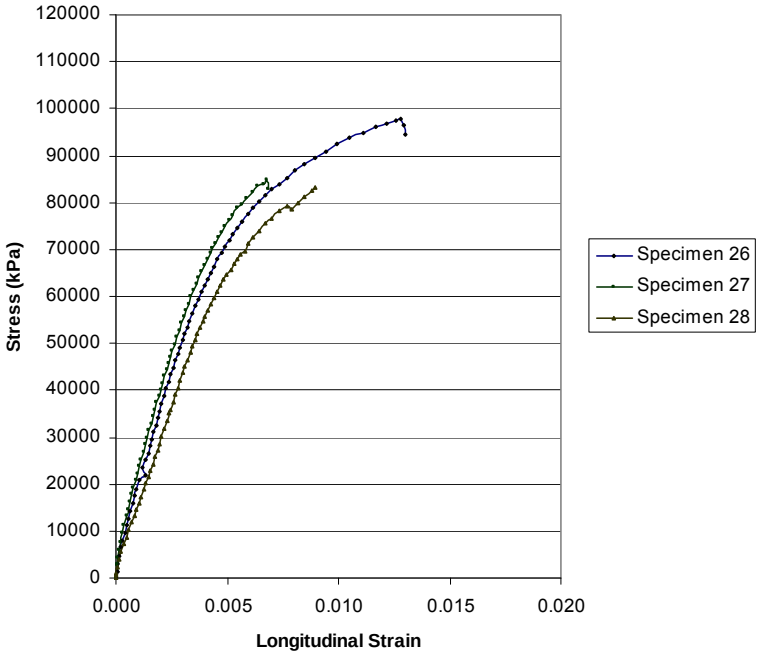

Fig. 3.31 Compressive stress-strain curves for carbon-wrapped, round specimens subjected to 150 freeze-thaw cycles

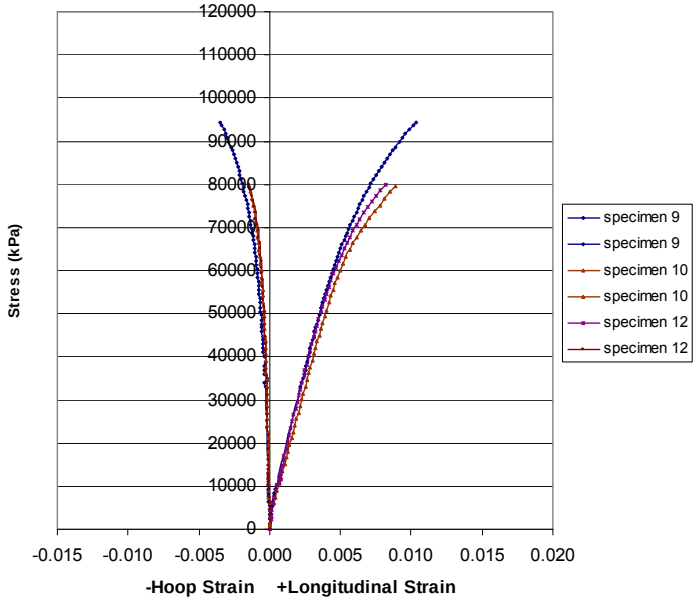

Fig. 3.32 Compressive stress-strain curves and tensile hoop strain for carbon-wrapped, round specimens subjected to 300 freeze-thaw cycles

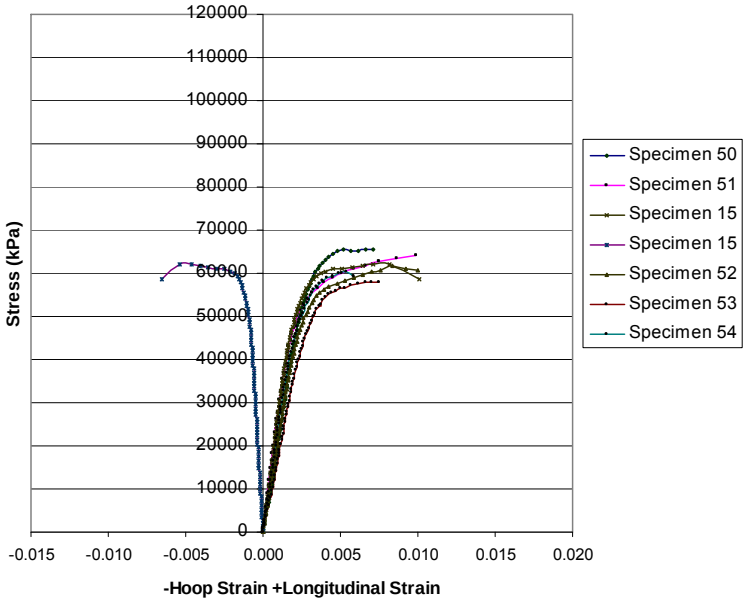

Fig. 3.33 Compressive stress-strain curves and tensile hoop strain for carbon-wrapped, square, control specimens

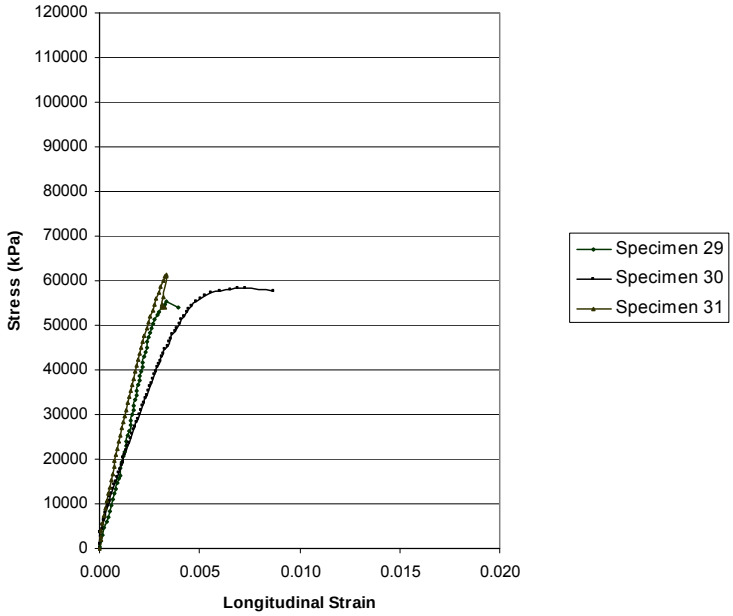

Fig. 3.34 Compressive stress-strain curves for carbon-wrapped, square specimens subjected to 150 freeze-thaw cycles

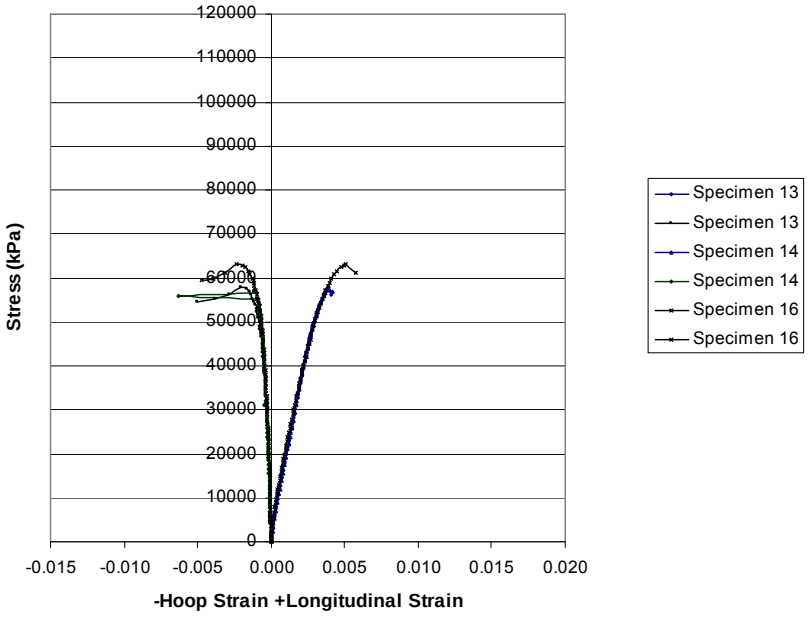

Fig. 3.35 Compressive stress-strain curves and tensile hoop strain for carbon-wrapped, square specimens subjected to 300 freeze-thaw cycles

Fig. 3.36 Failure modes for square specimens under compression testing

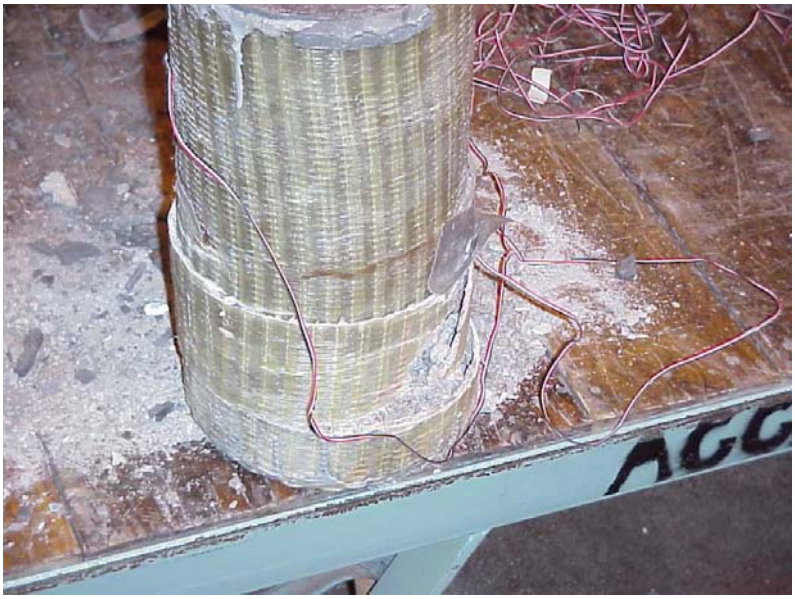

(a) Glass wrap

(b) Carbon wrap

Fig. 3.37 Failure modes for round specimens under compression testing

It was also noted that the square wrapped specimens demonstrated a sudden loss of strength after the peak stress was reached. However, the wraps were undamaged during this loss of strength. The loss of strength is most likely due to failure of the ineffectively confined regions of concrete. These regions do not experience capacity enhancement resulting from confinement.

A measure of ductility enhancement under compression is the ratio of the mean longitudinal failure strain of wrapped specimens ($\varepsilon_{u,\ wrapped}$) to the mean longitudinal failure strain of unwrapped specimens ($\varepsilon_{u,\ unwrapped}$).

The mean failure strains and strain ratios are given in Table 3.1. The ultimate strain for unwrapped specimens is difficult to determine accurately because of the rapid unloading near failure. Therefore, for unwrapped specimens, the strain at peak stress is used. As expected, ductility under compression is enhanced more for round specimens than for square specimens. In general freeze-thaw (F/T) conditioning reduces the ductility. Glass wrapped specimens are more ductile than the carbon wrapped specimens because the ultimate failure strain of glass is higher than that of carbon.

3.1.3 Statistical Analysis

Table 3.2 provides the ultimate compression strength, mean, standard deviation and 95% confidence margin for each category of specimens. The cross sectional area lost by the cavity containing Bristar was deducted when calculating the stresses. The 95% confidence margin is calculated as $t^* \frac{s}{\sqrt{n}}$, where s is the sample standard deviation, n is the sample size, and t^* is the value which a t-distributed random variable with $n - 1$ degrees of freedom will exceed with probability $(1 - 0.95)/2 = 0.025$ (Neter et al. 1992).

Table 3.1 Ductility enhancement under compression for wrapped specimens

Shape	Wrap	No. of F/T Cycles	Mean Longitudinal Failure Strain (%)	$\varepsilon_{u,\ wrapped}/\varepsilon_{u,\ unwrapped}$
Round	None	0	0.2	1.0
		150	0.2	1.0
		300	0.2	1.0
	Glass	0	1.8	9.0
		150	1.2	6.0
		300	1.7	8.5
	Carbon	0	1.3	6.5
		150	1.0	5.0
		300	0.9	4.5
Square	None	0	0.2*	1.0
		150	0.2*	1.0
		300	0.2*	1.0
	Glass	0	1.3	6.5
		150	1.2	6.0
		300	0.7	3.5
	Carbon	0	0.8	4.0
		150	0.5	2.5
		300	0.5	2.5

* Unwrapped square specimens were not used. It is assumed that the failure strain for unwrapped square specimens is approximately the same as that for unwrapped round specimens

The average compressive strength for the control, 150 freeze-thaw cycle, and 300 freeze-thaw cycle specimens is displayed in Figures 3.38-3.42. A 95% confidence interval is also provided. Due to the small sample sizes and unknown population variances, the t-distribution was used for all hypotheses tests in this report.

The null and alternate hypotheses are:

- Null hypothesis (H_o): There is no significant difference between the means of control and freeze-thaw specimens, i.e., $\mu_{control} = \mu_{F/T}$
- Alternate hypothesis (H_a): There is a significant difference in means of control and freeze-thaw specimens, i.e., $\mu_{control} \neq \mu_{F/T}$

Table 3.2 Freeze-thaw summary data

No. of F/T Cycles	Specimen Type		Ultimate Compressive Strength (kPa)			
	Shape	Wrap	Individual Specimens	Mean	Standard Deviation	95% Conf. Margin
300	Round	Glass	109801, 106451 108858	108370	1727	±4291
		Carbon	94459, 79721 79962	84714	8440	±20967
		Plain	42875, *, * [a]	42875	0	NA
	Square	Glass	62370, 64362 64551	63761	1208	±3002
		Carbon	57870, 57279 63004	59384	3149	±7822
150	Round	Glass	106575, 112621 109316	109504	3027	±7520
		Carbon	97675, 84705 83178	88519	7966	±19788
		Plain	41080, 29825 36926	35944	5691	±14138
	Square	Glass	64881, 61500 66988	64456	2769	±6877
		Carbon	55332, 58231 61421	58328	3046	±7566
0	Round	Glass	109504, 104977 114289, 110873 92200[b], 89000[b]	109911	3856	±6136
		Carbon	93254, 90494, 95130 86555, 93174, 96738	92558	3612	±3791
		Plain	41911, 41696, 40932 39973, 37114, 44818	41074	2531	±2656
	Square	Glass	65820, 65776, 64148 61856, 62216, 61792	63601	1907	±2002
		Carbon	61623, 58034, 60294 65542, 63967, 62082	61924	2652	±2783

[a] Specimens that did not survive 300 F/T cycles are denoted with *

[b] Data unreliable because specimens did not fail when tested at MSU and were retested at MDOT

Sample calculations

Comparing results for carbon wrapped, control, round specimens and carbon wrapped, 300 F/T cycle, round specimens, for the former

$\bar{x}_1 = 92558$ kPa, $S_1 = 3612$ kPa , $n_1 = 6$, and for the latter

$\bar{x}_2 = 84714$ kPa, S_2 =8440 kPa , $n_2 = 3$

where $\bar{x}$, *S*, and *n* are sample average, standard deviation, and size, respectively.

A conservative degree-of-freedom is (Neter at el. 1992)

d.o.f.= smaller of $n_1 - 1$ or $n_2 - 1 = 3 - 1 = 2 \Rightarrow t^* = 4.303$ (2 tail test)

The 95% confidence interval for $\mu_{control} - \mu_{F/T}$ (difference between the mean strength of control specimens not subjected to F/T and the mean strength of specimens subjected to F/T) is

$\mu_{control} - \mu_{F/T} = \bar{x}_1 - \bar{x}_2 \pm t^* \sqrt{\frac{s_1^2}{n_1} + \frac{s_2^2}{n_2}}$ where μ is population mean (Neter at el. 1992)

$= 7844 \pm 4.303\ (5091) = (-14063, 29751)$

According to statistical theory, when the confidence interval spans zero the means are not significantly different and H_o is not rejected.

The results of the hypothesis tests for the various comparisons are given in Table 3.3. The standard deviations and number of samples for each case are given in Table 3.2. The value of t* was 4.303 for all comparisons.

Table 3.3 Results of hypothesis tests (95%) on specimens exposed to freeze-thaw cycles

Shape	Wrap	No. of F/T Cycles	C.I. (kPa) for $\mu_{control} - \mu_{F/T}$	Outcome of Test
Round	Plain	150	(-9692, 19952)	Don't Reject H_o
		300	NA	
	Glass	150	(-10789, 11603)	Don't Reject H_o
		300	(-7799, 10881)	Don't Reject H_o
	Carbon	150	(-16745, 24821)	Don't Reject H_o
		300	(-14063, 29751)	Don't Reject H_o
Square	Glass	150	(-8506, 6796)	Don't Reject H_o
		300	(-4339, 4659)	Don't Reject H_o
	Carbon	150	(-5290, 12482)	Don't Reject H_o
		300	(-6565, 11645)	Don't Reject H_o

At the 95% confidence, means of the compressive strength of freeze thaw specimens are not significantly different from those of control specimens. Similarly, the freeze thaw cycles have no statistically significant effect on the compressive strength of round specimens.

At the 95% confidence level, means of the compressive strength of freeze thaw specimens are not significantly different from those of control specimens. Similarly, the freeze-thaw cycles have no statistically significant effect on the compressive strength of square specimens.

It should be noted that a reduction in mean compressive strength was observed for carbon-wrapped specimens after freeze-thaw conditioning. This difference is not statistically significant for the sample size used in this study.

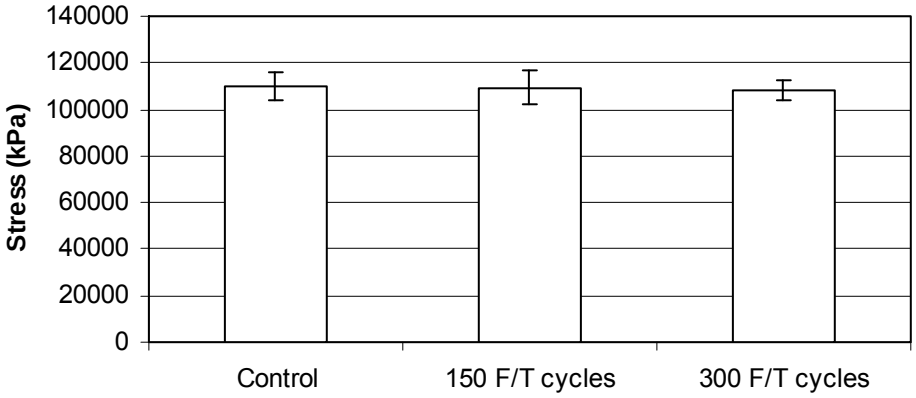

Fig 3.38 Average compressive strength of round glass-wrapped specimens

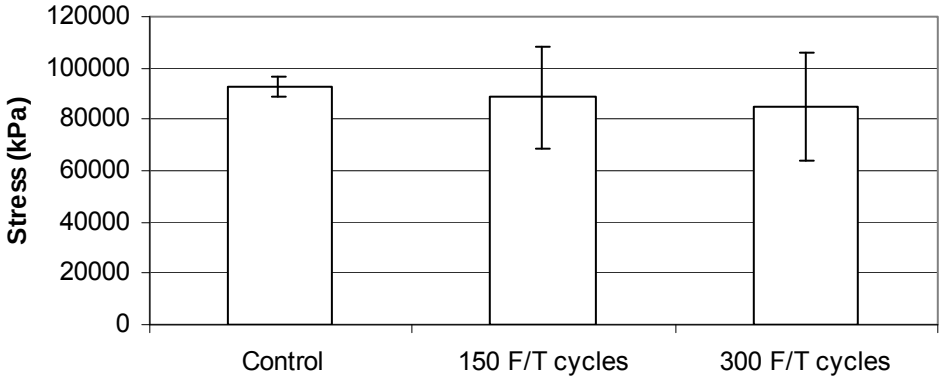

Fig 3.39 Average compressive strength of round carbon-wrapped specimens

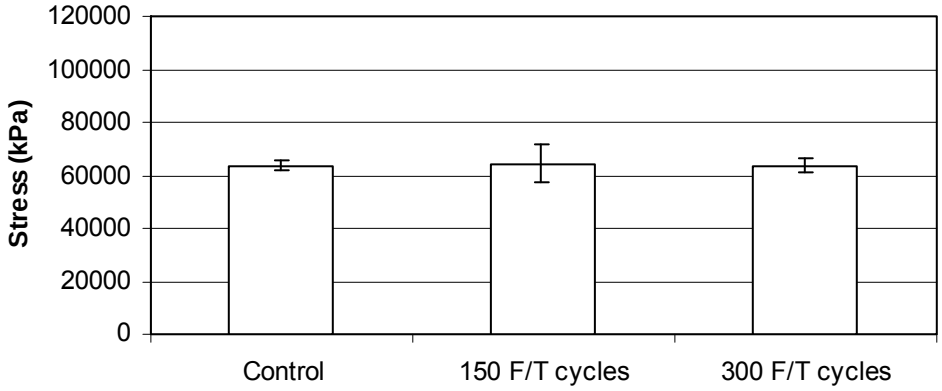

Fig 3.40 Average compressive strength of square glass-wrapped specimens

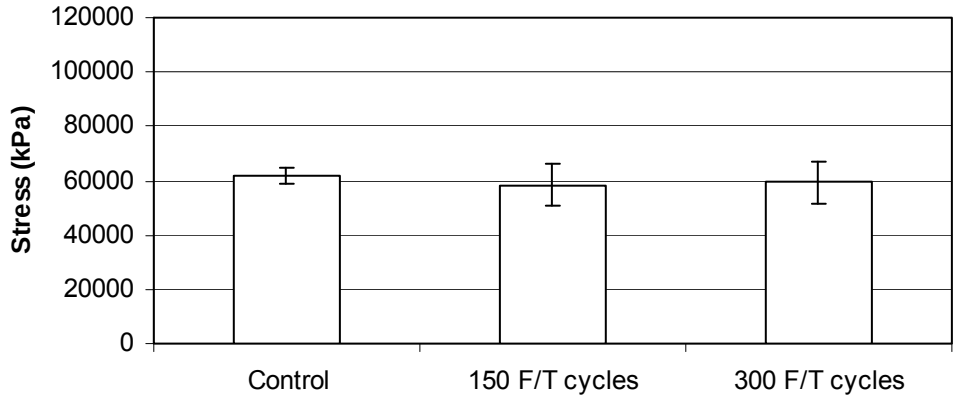

Fig 3.41 Average compressive strength of square carbon-wrapped specimens

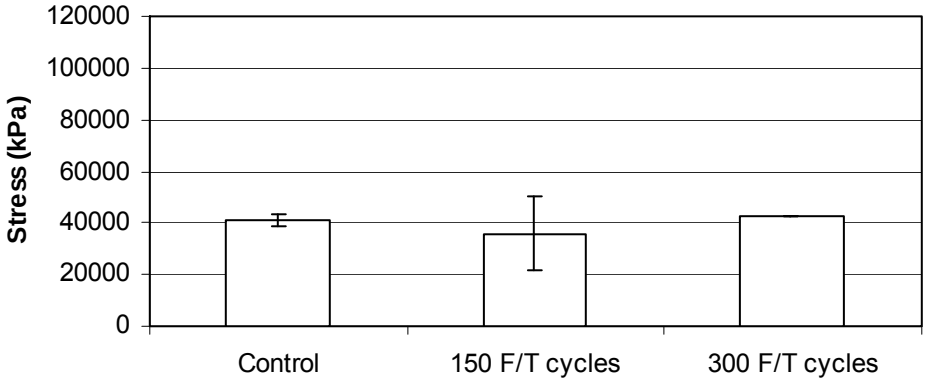

Fig 3.42 Average compressive strength of round plain specimens

3.1.4 Effect of Sustained Loads on Freeze-Thaw Durability of Wraps

Bristar was used in the wrapped specimens to investigate the durability of glass and carbon wraps under sustained load subjected to freeze-thaw cycling. The sustained load simulated the load generated in wrapped columns by corrosion products.

The compression strength of wrapped specimens subjected to freeze-thaw cycling was not significantly different than that of wrapped control specimens. This indicates that the wraps did not sustain any significant damage due to freeze-thaw cycling under sustained load.

3.1.5 Comparison of Measured and Predicted Confined Compression Strength

Equations for predicting the confined compression strength of wrapped circular and rectangular columns are outlined in Section 1.3.6. Here the confined compression strengths predicted by Eq. 1.1 and 1.5 are compared to the measured strengths. Measured FRP panel properties in Tables 2.1 and 3.1 were used in the predictions for unconditioned and conditioned specimens, respectively. The observed and predicted compression strengths are shown in Table 3.4. The table indicates that the Restrepol-DeVino model for rectangular sections over predicts the measured strengths of unconditioned specimens by about 38% and 9% for glass and carbon wrapped specimens, respectively. For unconditioned round glass and round carbon wrapped specimens, the Richart model over predicts the observed strength by about 16% and –2%, respectively. For conditioned specimens, the Restrepol-DeVino model for rectangular sections over predicts the measured strengths by about 21% and 9% for glass and carbon

wrapped specimens, respectively. For conditioned round glass and round carbon wrapped specimens, the predicted and the measured strength are almost the same.

Table 3.4 Comparison of measured and predicted confined compression strength

No. of F/T Cycles	Shape	Wrap Type	Predicted Strength (kPa)	Measured Strength (kPa)	Predicted/ Measured
0	Round	Glass	127,707	109,910	1.16
		Carbon	90,542	92,577	0.98
	Square	Glass	87,614	63,601	1.38
		Carbon	67,649	61,924	1.09
300	Round	Glass	108,224	108,370	1.00
		Carbon	85,131	84,714	1.00
	Square	Glass	77,147	63,761	1.21
		Carbon	64,742	59,384	1.09

3.2 Accelerated Corrosion

3.2.1 Mass Loss Results

Corrosion specimens were removed from the corrosion tank in two phases and measurements of corrosion-induced mass loss were determined. Mass loss data and corrosion depths for the first batch (exposed to 130 days of accelerated corrosion) and the second batch (exposed to 190 days of accelerated corrosion) are given in Tables 3.5 and 3.6, respectively. The standard deviation and 95% confidence margin for the corrosion depth also are provided. The 95% confidence margin was calculated in the same way as for the ultimate strength in Table 3.2. The corrosion depth for each individual bar varied significantly over the length of the bar. The depth reported in Tables 3.5 and 3.6 is the average depth calculated from the total mass loss for

each bar. The average corrosion depth over the entire bar can be calculated from the fractional mass loss (FML) of the bar.

$$FML = \frac{w_i - w_f}{w_i}$$

where

w_i = initial weight of bar

w_f = final weight of bar

Note that

$$FML = \frac{\rho\pi r_i^2 - \rho\pi r_f^2}{\rho\pi r_i^2} = \frac{r_i^2 - r_f^2}{r_i^2}$$

where ρ is the density.

$$\therefore \quad r_f = r_i\sqrt{1 - FML}$$

Average corrosion depth = $r_i - r_f$

$$= r_i\left(1 - \sqrt{1 - FML}\right)$$

The average corrosion depths for all categories and 95% confidence intervals are displayed in Fig. 3.43.

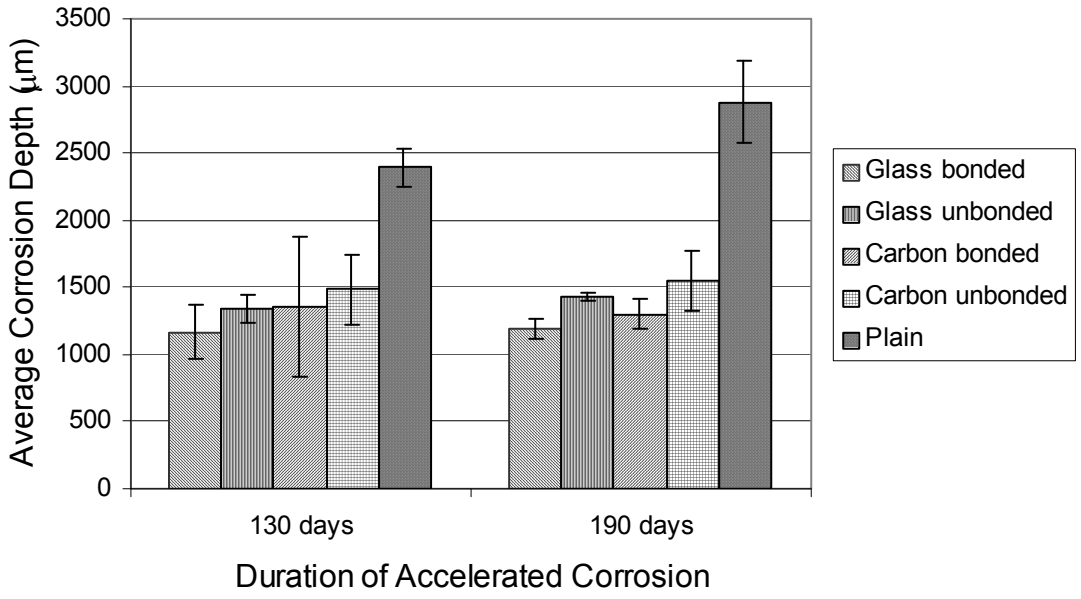

Fig. 3.43 Average corrosion depths due to accelerated corrosion

The following observations are made:

1. Corrosion depths for reinforcement in specimens with unbonded wraps were approximately 20% more than those in specimens with bonded wraps after 190 days of testing. This may be due to water seepage between the concrete and the plastic sheet used to create the unbonded condition.
2. Wrapping reduced the corrosion depth by 46% – 59% after 190 days of testing.

It should be noted that the specimens removed after 130 days had corrosion levels of "medium" to "severe" prior to wrapping. The specimens removed after 190 days, on the other hand, had a "low" corrosion level prior to wrapping. This accounts for the higher variability in the corrosion mass loss in the specimens removed after 130 days.

Table 3.5 Mass loss and average corrosion depth for specimens exposed to 130 days of accelerated corrosion

Specimen Type	Corrosion Level Before Wrapping	Bar No.	Original Mass (g)	Mass Loss (g)	Average Corrosion Depth (μm)			
					Individual Specimens	Mean	Standard Deviation	95% Conf. Margin
Glass bonded	Medium	9	289.0	82.5	982	1168	191	±200
		11	288.4	81.0	965			
	Low	86	281.0	93.0	1156			
		88	286.0	101.5	1250			
	Severe	45	289.5	119.5	1484			
		47	288.6	96.4	1168			
Glass unbonded	Severe	62	289.2	103.2	1257	1342	65	±104
		64	286.0	110.7	1378			
	Medium	50	288.7	108.0	1326			
		52	289.1	113.8	1405			
Carbon bonded	Medium	29	289.3	88.4	1058	1351	329	±524
		31	288.0	136.0	1737			
	Severe	70	288.6	121.1	1512			
		72	288.8	91.2	1097			
Carbon unbonded	Severe	54	288.8	121.5	1517	1482	161	±256
		56	288.9	120.7	1505			
	Medium	90	286.7	102.5	1260			
		92	281.4	127.0	1646			
Plain	Severe	66	286.0	187.0	2614	2397	169	±142
		68	289.0	175.5	2370			
	Low	38	289.0	176.0	2379			
		40	289.5	190.5	2637			
	Medium	2	290.3	181.5	2463			
		4	289.4	172.5	2314			
	Low	13	289.4	169.2	2258			
		15	289.3	162.3	2143			

Table 3.6 Mass loss and average corrosion depth for specimens exposed to 190 days of accelerated corrosion

Specimen Type	Corrosion Level Before Wrapping	Bar No.	Original Mass (g)	Mass Loss (g)	Average Corrosion Depth (μm)			
					Individual Specimens	Mean	Standard Deviation	95% Conf. Margin
Glass bonded	Low	17	289.7	95.9	1156	1191	73	±77
		19	288.7	98.5	1195			
	Low	57	289.5	101.3	1230			
		59	286.5	87.9	1063			
	Low	82	286.9	103.4	1271			
		84	280.9	98.2	1229			
Glass unbonded	Low	25	285.8	113.8	1424	1434	17	±27
		27	289.2	116.3	1439			
	Low	42	290.0	117.8	1456			
		44	288.6	114.5	1418			
Carbon bonded	Low	33	289.2	100.0	1214	1297	70	±112
		35	286.4	102.7	1265			
	Low	77	286.6	109.8	1362			
		79	285.9	108.6	1349			
Carbon unbonded	Low	22	289.9	115.2	1420	1550	140	±222
		24	288.7	116.3	1442			
	Low	93	280.4	125.8	1635			
		95	280.9	130.3	1701			
Plain	Low	5	288.7	187.7	2594	2880	193	±307
		7	285.8	204.0	2951			
	Low	73	288.4	208.8	3014			
		75	289.7	207.2	2961			

3.2.2 Statistical analysis

The following hypotheses are tested for the specimens exposed to 190 days of accelerated corrosion.

1. Null hypothesis (H_o): There is no significant difference between the mean corrosion depth for bonded and unbonded specimens with the same type of wrap.

   i.e., H_o: $\mu_{bonded} = \mu_{unbonded}$

   Alternate hypothesis (H_a): There is a significant difference between the mean corrosion depth for bonded and unbonded specimens with the same type of wrap.

   i.e., . H_a: $\mu_{bonded} \neq \mu_{unbonded}$

2. Null hypothesis (H_o): There is no significant difference between the mean corrosion depth for carbon bonded and glass bonded specimens or between carbon unbonded and glass unbonded specimens, i.e, H_o: $\mu_{carbon} = \mu_{glass}$

   Alternate hypothesis (H_a): There is a significant difference between the mean corrosion depth for carbon bonded and glass bonded specimens or carbon unbonded and glass unbonded specimens, i.e., H_a: $\mu_{carbon} \neq \mu_{glass}$

Sample calculations

Comparing results for carbon wrapped bonded specimens and carbon wrapped unbonded specimens, for the former

$\bar{x}_1 = 1297$ μm, $S_1 = 70$ μm, $n_1 = 4$, and for the latter

$\bar{x}_2 = 1550$ μm, $S_2 = 140$ μm, $n_2 = 4$

where $\bar{x}$, *S*, and *n* are sample average, standard deviation, and size, respectively.

A conservative degree-of-freedom is

d.o.f.= smaller of n_1 - 1 or $n_2 - 1 = 4\text{-}1=3 \Rightarrow t^* = 3.182$ (2 tail test)

The 95% confidence interval for $\mu_{\text{bonded}} - \mu_{\text{unbonded}}$, using a 2-sample t is

$\mu_{\text{bonded}} - \mu_{\text{unbonded}} = \bar{x}_1 - \bar{x}_2 \pm t^* \sqrt{\frac{s_1^2}{n_1} + \frac{s_2^2}{n_2}}$ where μ is population mean

$= -252 \pm 3.182\ (78) = (-500, -3.4)$

Since this confidence interval does not span zero, the means are significantly different and H_o is rejected.

The results of the hypothesis tests for the various comparisons are given in Table 3.7. The standard deviations and number of samples for each case are given in Table 3.6. The value of t* was 3.182 for all comparisons.

Table 3.7 Results of hypothesis tests (95%) on specimens exposed to accelerated corrosion

Wrap Type	C.I. for $\mu_{\text{bonded}} - \mu_{\text{unbonded}}$ (μm)	Outcome of Test
Glass	(-343, -144)	Reject H_o
Carbon	(-300, -3.4)	Reject H_o
FRP/Concrete Adhesion	C.I. for $\mu_{\text{carbon}} - \mu_{\text{glass}}$ (μm)	Outcome of Test
Bonded	(-41, 253)	Don't reject H_o
Unbonded	(-108, 340)	Don't reject H_o

The following observations are made:

- The mean corrosion depths for bonded and unbonded specimens are different at the 95% significance level. The bonded wrap is more effective in reducing the rate of corrosion than the unbonded wrap.

- The mean corrosion depths for specimens with glass and carbon wraps for either the bonded or unbonded conditions are not significantly different. Both wrap systems, glass and carbon, are equally effective in reducing the corrosion rate.

3.2.3 Strain Measurements

The wrapped corrosion specimens were fitted with strain gages. Two gages oriented in the circumferential direction were mounted at mid-height were mounted on each specimen. On some specimens, the strain gages were installed near the anodes, the site of corrosion and subsequent volume expansion. For others, strain gages were installed between the anode and cathode. The purpose of this arrangement was to investigate the variation in strain gage readings with respect to the site of corrosion. The observations below are for the specimens exposed to 190 days of accelerated corrosion:

- For glass bonded specimens (Figure 3.44), it is evident that the strain reading is considerably higher for specimen 7 (approximately 4200 micro strain) for which the gages are located at the anodes. For other specimens the gages (installed between the anodes and cathodes) are consistent at about 900 micro strain. Based on the average strains developed at gages not located at the anodes, the confining pressure is estimated to be about 950 kPa away from the anodes, but much higher near the anodes.
- For glass unbonded specimens (Figure 3.45), all strain gage readings are about 1500 micro strain regardless of the gage location. This yields a confining pressure of about 1600 kPa (scaled directly from Table 2.5 as 5644.9 x 1500/5310). The unbonded condition, created by a plastic sheet located between the wrap and the specimens, allows the wrap to expand more freely instead of concentrating the strains near the anode as in the bonded wraps.

- For carbon bonded specimens (Figure 3.46), the results are similar to those for the glass bonded specimens. The strains developed for specimen 13 (for which the gages are located at the anodes) are higher than the gage readings for the other specimens (for which gages are located between the anodes and the cathodes) and is approximately 1800 micro strain. The average strain value where gages are located between the anodes and the cathodes is about 1300 micro strain, and yields a confining pressure of about 1150 kPa.
- For carbon unbonded specimens (Figure 3.47), all strain gage readings are about the same regardless of the gage location and approximately 1300 micro strain. This yields a confining pressure of about 1150 kPa.

Figures 3.44 to 3.47 indicates that wrap strains for bonded specimens with both types of wraps tend to level off with time. One explanation could be that the stress concentration near the anodes in the bonded wraps is more effective in containing the corrosion-induced crack and reducing the corrosion rate. The slip of unbonded wraps and the resulting redistribution of strain along the entire wrap may be less effective at containing the large corrosion-induced crack near the anodes.

Figure 3.48 shows strains at gages placed on the anodes, and indicates the following:

- Even though the corrosion rate for the bonded specimens is lower than that for the unbonded specimens, hoop strains developed near the anodes for specimens with bonded wraps are higher than those developed with unbonded wraps. In the case of unbonded specimens, the entire wrap (to some degree) absorbs the volume expansion associated with corrosion of the reinforcement, while for bonded wraps the strain is localized near the corrosion-induced crack at the anode.

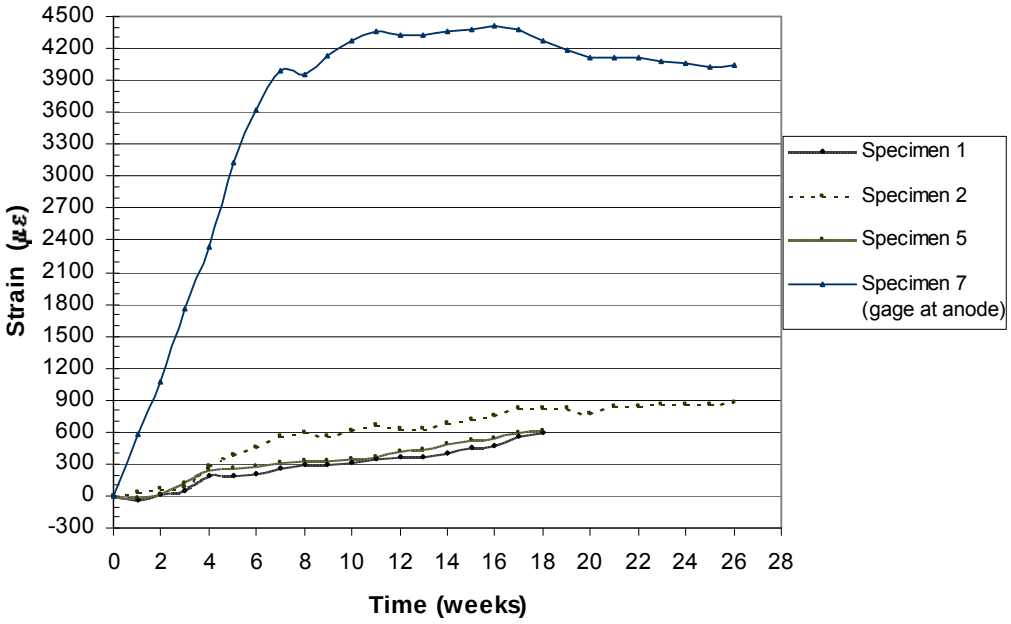

Fig. 3.44 Hoop strains in bonded, glass-wrapped specimens

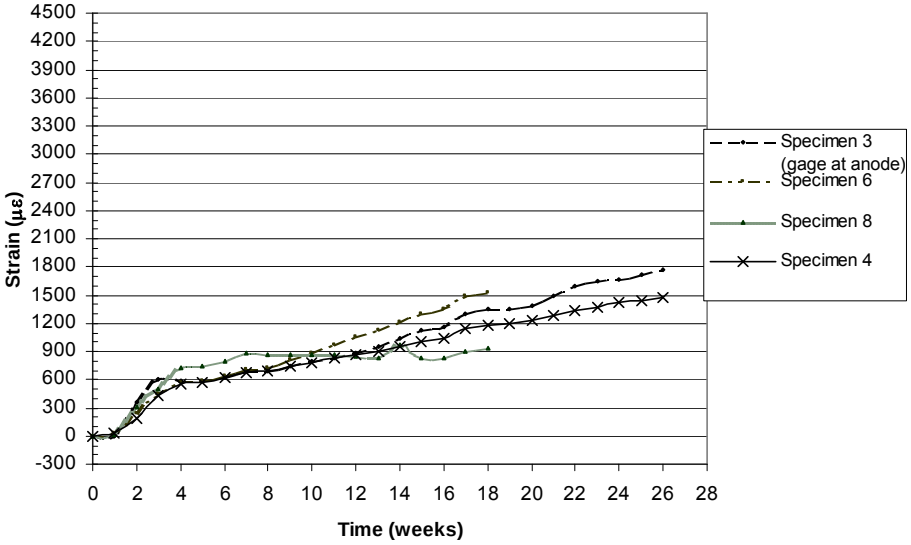

Fig. 3.45 Hoop strains in unbonded, glass-wrapped specimens

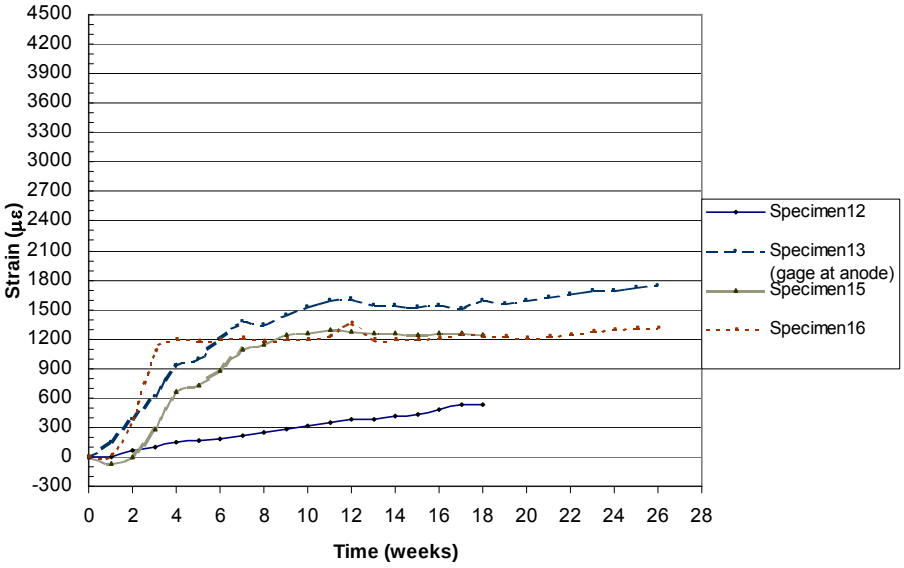

Fig. 3.46 Hoop strains in bonded, carbon-wrapped specimens

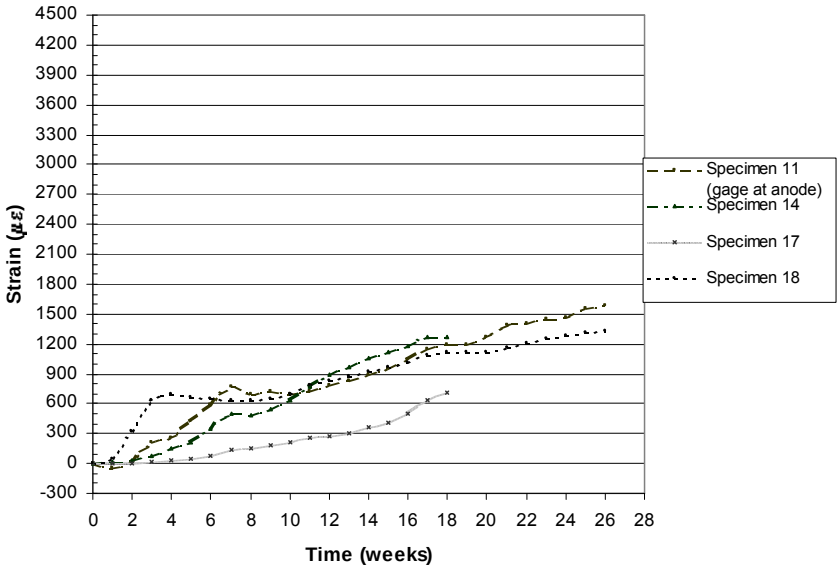

Fig. 3.47 Hoop strains in unbonded, carbon-wrapped specimens

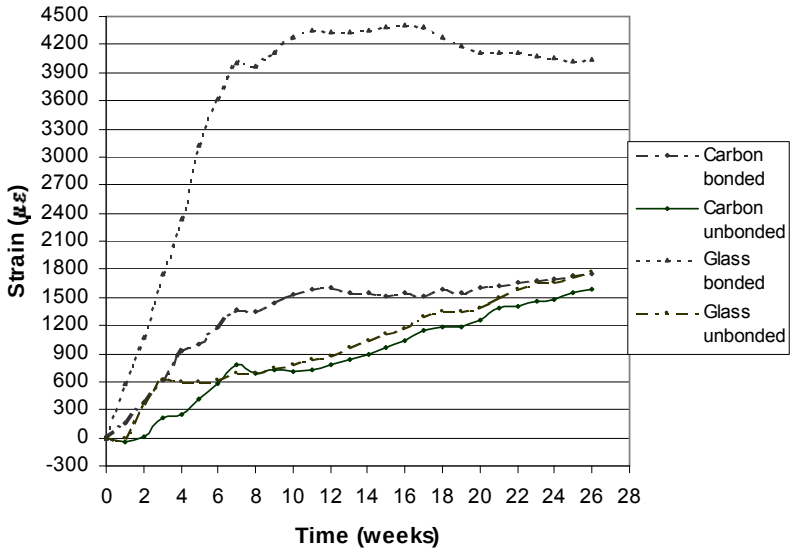

Fig. 3.48 Hoop strains in glass and carbon-wrapped specimens, gages at the anodes

- Corrosion of reinforcement seems to have a more direct effect on strain values generated in glass bonded wraps compared to those with carbon bonded wraps. The maximum strain for glass bonded wraps is approximately 4000 micro strain compared to 1800 micro strain for carbon bonded wraps. It should be noted that variations in strain readings also could be influenced by initial wrap tightness around the specimens and by crack width and direction. Although the wrap strain near the anode is large, there is no danger of stress rupture in the glass since the stress rupture limit (with a safety factor of 1.67) is about 0.2 ε_u = 4000 micro strain. Further, in real columns the strain near corroding bars will be significantly smaller because of the larger column diameter and concrete cover.

Note that the wrap strains measured in the accelerated corrosion test away from the anodes are lower than the wrap strains generated by Bristar in the freeze-thaw test. Thus the internal expansive force used in the freeze-thaw test was very conservative.

3.3 Effect of Freeze-Thaw and Wet-Dry Cycling on the Properties of FRP Panels

Table 3.8 provides the mean mechanical properties of FRP panels after 300 freeze-thaw cycles and 190 wet-dry cycles with 3% NaCl solution. The properties for unconditioned panels from Table 2.1 also are included in Table 3.8 to facilitate comparisons. Note that different sets of specimens were used for the unconditioned modulus and strength tests. Properties of individual specimens are given in Appendix B. It is difficult to control the thickness of panels fabricated using the wet lay-up process. This impacts the measured moduli because the volume fraction of fibers changes. For comparisons the effective stiffness (modulus × thickness) and ultimate strength per unit width per layer should be used since these are not sensitive to specimen thicknesses.

The following hypotheses are tested for the freeze-thaw and wet-dry conditioning:

- Null hypothesis (H_o): There is no significant difference between the mean property (effective stiffness, ultimate strength per unit width or ultimate strain) of the control specimen and the corresponding mean property of the conditioned specimen. i.e., H_o: $\mu_{control} = \mu_{conditioned}$
- Alternate hypothesis (H_a): There is a significant difference between the mean property of the control specimen and the corresponding mean property of the conditioned specimen.

  i.e., . H_a: $\mu_{control} \neq \mu_{conditioned}$

Table 3.8 Mean properties per layer for unconditioned and conditioned FRP panels

Wrap Type	Thickness (mm.)	Modulus (MPa)	Effective Stiffness (N/mm)	Ultimate Strength (MPa)	Ult. Str. Per Unit Width (N/mm)	Ultimate Strain
	Unconditioned					
Glass	1.227	22011	26967			
	1.275			421	536	0.019
Carbon	0.625	53061	33192			
	0.506			821	415	0.015
	300 Freeze-Thaw Cycles					
Glass	1.092	24148	26506	385	424	0.016
Carbon	0.508	79014	43171	820	448	0.010
	190 Wet-Dry Cycles					
Glass	0.914	29538	27467	469	439	0.016
Carbon	0.571	83765	46786	738	413	0.009

Table 3.9 Outcome of 95%-level significance tests for $\mu_{control} - \mu_{F/T}$

Wrap Type	Effective Stiffness	Ultimate Strength per Unit Width	Ultimate Strain
Glass	Do not reject H_o	Reject H_o	Reject H_o
Carbon	Reject H_o	Do not reject H_o	Reject H_o

Table 3.10 Outcome of 95%-level significance tests for $\mu_{control} - \mu_{wet\text{-}dry}$

Wrap Type	Effective Stiffness	Ultimate Strength per Unit Width	Ultimate Strain
Glass	Do not reject H_o	Reject H_o	Reject H_o
Carbon	Reject H_o	Do not reject H_o	Reject H_o

The 95% confidence intervals for the difference in the mean properties of control and conditioned panels, and the outcome of the significance tests, are given in Tables 3.9 and 3.10 for the freeze-thaw and wet-dry conditioning, respectively. The confidence intervals are computed as outlined in Section 3.2.2. By comparing these results to the unconditioned panels tested (see Table 2.1), the following observations are made:

- The freeze-thaw conditioning had little effect on the mean effective stiffness of glass panels while that of carbon panels appear to have been increased by 30%, the latter being significant

at the 95% level. The decrease of 21% in the mean ultimate strength per unit width of glass is significant at the 95% level, but the apparent increase in strength for carbon is not significant at the 95% level (because of the large variation for the unconditioned panels). The decrease of 20% and 28% in the mean ultimate strains of glass and carbon panels, respectively, is significant at the 95% confidence interval. It should be noted that many of the failures occurred at the grips and may have been premature. The ultimate strains of the unconditioned and conditioned specimens are significantly lower than the values reported by Aerospace Corporation (see Appendix A). It is likely that a better end fixture needs to be used for the tension testing of the FRP strips for obtaining accurate ultimate strengths and strains.

- The wet-dry conditioning had little effect on the mean effective stiffness of glass panels while that of carbon panels appear to have increased by 41%, the latter being significant at the 95% level. The decrease of 18% in the mean ultimate strength per unit width of glass is significant at the 95% level, but there is no significant change in strength for carbon. The decrease of 20% and 36% in the mean ultimate strains of glass and carbon panels, respectively, is significant at the 95% confidence interval.

The increase in effective stiffness for carbon FRP after conditioning is unexpected and has not been reported by other investigators. The carbon panels were extremely thin and many of the test specimen broke at the grips or split longitudinally. These failures may have been premature and contributed to the low ultimate strains for carbon.

In order to cross check the test results the following additional tests were performed:

- One carbon strip (Sample 6) left over near the edges of the panel exposed to freeze-thaw conditioning and from which the original samples were cut was tested.

- Two carbon specimens that broke at the grips and otherwise appeared undamaged were re-tested. One specimen had been subjected to freeze-thaw conditioning (Sample 4), and the other was subjected wet-dry conditioning (Sample 2).
- One glass sample that broke at the grip and otherwise appeared undamaged was re-tested. This specimen was subjected to 300 freeze-thaw cycles (Sample 5).

The results from these tests, shown in Table 3.11 and plotted in Figures 3.49, 3.50 and 3.51, indicate the following:

- The effective stiffness for the new carbon Sample 6 and the re-tested carbon Sample 4 (Figure 3.49) are very close to that of the mean value for unconditioned specimens, and are about 25% lower than the effective stiffness measured from the original test for Sample 4. The effective stiffness for the re-tested carbon Sample 2 (Figure 3.50) is 20% higher than the mean value for unconditioned specimens. The variation in the estimates is indicative of the difficulty in obtaining reliable measures for the very thin carbon specimens.
- The ultimate strengths per unit width are lower for the new and re-tested carbon specimens than for the original tests. This behavior is expected for the re-tested specimens, since some microcracks are likely to have developed during the first test causing premature failure during the re-test. The lower strength of the new specimen is most likely a reflection of the significant scatter in the strength results for carbon.
- The results for the re-tested glass specimen (Sample 5) are very close to the original test results, and indicate that the results for glass are much more reliable than those for carbon.

Table 3.11 Properties per layer of FRP panels from additional tests and re-tests

FRP Type (New or Retest)	Condi-tioning	Sample Number	Width (mm)	Thick. (mm)	Modulus (MPa)	Effective Stiffness (N/mm)	Ultimate Strength Per Unit Width (N/mm)	Ult. Strain
Carbon (new)	Freeze-thaw	Sample 6	10.69	1.092	63309	34547	347	0.010
Carbon (retest)	Freeze-thaw	Sample 4	12.53	1.161	57333	33468	418	0.009
Carbon (retest)	Wet-dry	Sample 2	13.20	1.346	56586	39946	374	0.009
Glass (retest)	Freeze-thaw	Sample 5	13.20	1.232	22879	24776	365	0.015

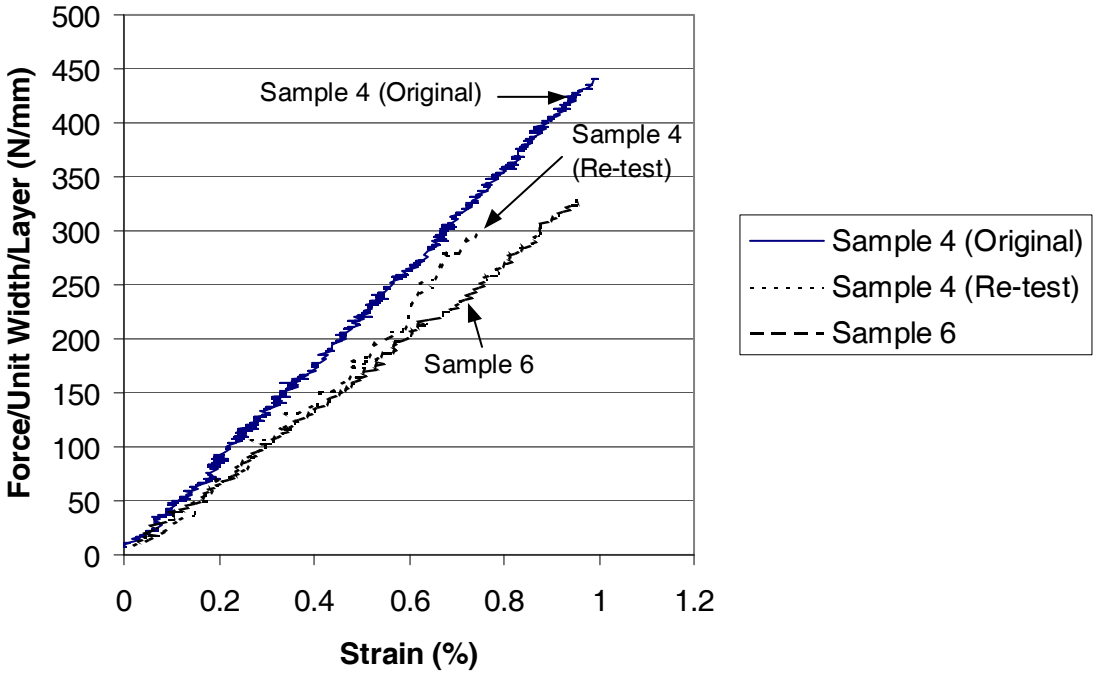

Fig. 3.49: New carbon sample and re-test of carbon sample subjected to freeze-thaw

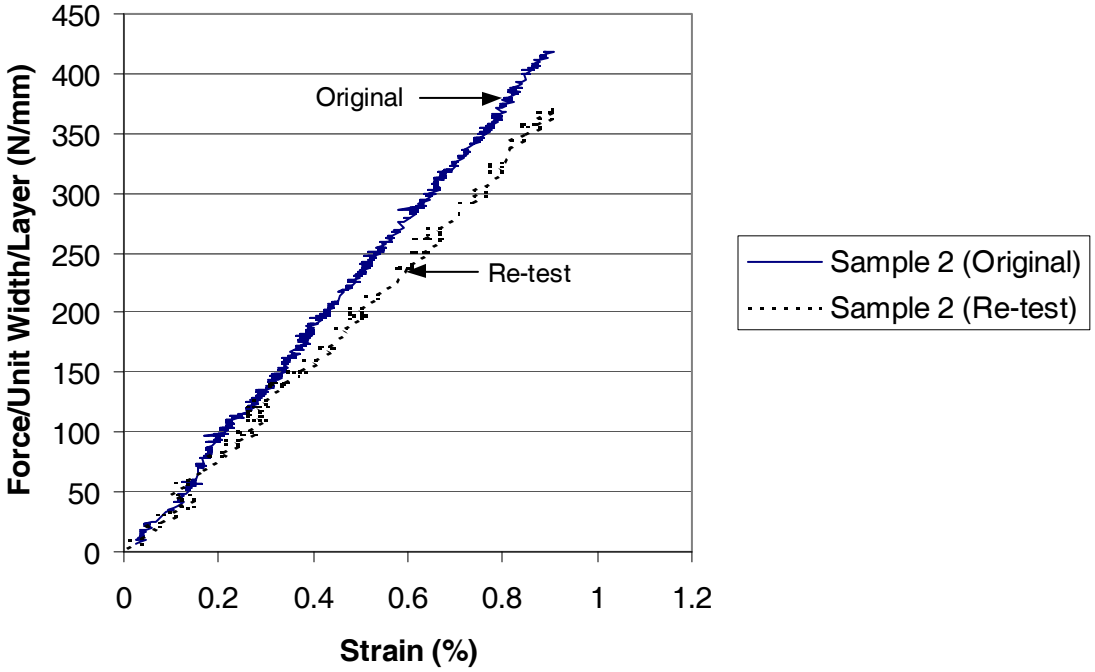

Fig. 3.50 New carbon sample and re-test of carbon sample exposed to wet-dry conditioning

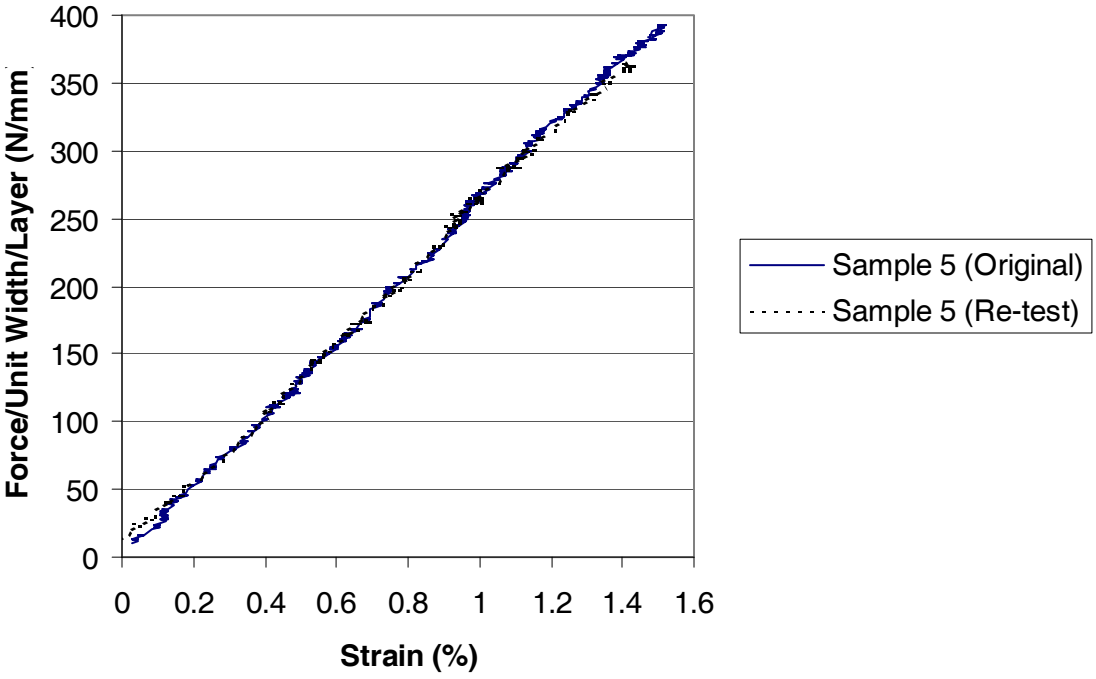

Fig. 3:51: Re-test of glass sample subjected to freeze-thaw

The unconditioned control panels and the conditioned panels were fabricated at different times and the epoxy mixes are likely to have been slightly different. Some of the observed differences in properties are likely to be due to fabrication variations. For more reliable comparisons control panels and panels to be conditioned for each FRP should be cut out of a single larger panel. Testing of the thin carbon panels also is problematic and better test fixtures and procedures may need to be implemented.

In general, the results from the panel tests are somewhat unreliable for carbon.

3.4 Impact Test

Both glass and carbon FRP panels did not display any significant damage due to the impact test. Minor interlaminar debonding was visible on the glass panels, which are somewhat transparent, at the point of impact. Interlaminar debonding could not be observed on the carbon panels because they are opaque. For column repair purposes, both types of FRP panels (glass and carbon) behaved in an acceptable manner. The wraps should therefore be able to sustain damage from vandalism or minor vehicle impact.

3.5 Behavior at Very High Temperature

At 100°C the wraps browned, at 150°C they charred and unraveled, and at 200°C the epoxy completely burned and evaporated. The discoloration was more pronounced for glass wrapped specimens due to the light color of the glass fibers. Thus, unless effective insulation is provided the wraps become ineffective at very high temperature and are not able to provide any confinement.

Chapter 4
Summary, Conclusions and Recommendations

Experiments were conducted to assess the effects of using glass and carbon FRP wraps in rehabilitating corrosion-damaged columns. Issues that were explored are: (1) freeze-thaw durability of concrete square and cylindrical specimens wrapped with glass and carbon FRP and subjected to an internal expansive force; (2) effect of wrapping on the rate of corrosion in an accelerated corrosion test; (3) effect of freeze-thaw and wet-dry cycles on the properties of FRP panels; and (4) the impact resistance of glass and carbon FRP; (5) effect of high temperature on FRP wraps.

4.1 Freeze-Thaw Test

Strength and durability tests were carried out on wrapped circular (diameter of 152 mm by 305 mm high) and square cylinders (152 mm by152 mm by 305 mm high). The primary purpose of the tests was to determine the endurance of the jackets under simulated cyclic environmental conditions. Creation of an internal bursting force similar to that produced by corroding steel was attempted. This was done by fabricating specimens with a hole in the longitudinal direction and filling it with an expanding cement known as Bristar (used for silent demolition). Chloride was impregnated into the cylinders during casting in order to simulate deteriorated concrete. Compression strength tests were carried out on plain and wrapped control cylinders as well as wrapped test specimens after 150 and 300 cycles of freeze-thaw conditioning. A total of sixty specimens were utilized in the freeze-thaw test. The strength of FRP panels subjected to 300 freeze-thaw cycles also was investigated.

Bristar was used in the wrapped specimens to investigate the durability of glass and carbon wraps under sustained load and subjected to freeze-thaw cycling. The sustained load simulated the load generated in wrapped columns by corrosion products. The means of the compressive strength of freeze-thaw specimens are not significantly different from those of control specimens at the 95% confidence level. This holds both for carbon and glass wraps, and for specimens with round and square cross sections. It should be noted that a reduction in mean compressive strength was observed for carbon-wrapped specimens after freeze-thaw conditioning. Based on our sample size and statistical analysis, this difference is not significant. The results indicate that the wraps did not sustain significant damage due to freeze-thaw cycling under sustained load.

The square wrapped specimens had lower compressive strength compared to the round specimens, even though the cross sectional area of the square prisms is higher than that of the round cylinders. This is due to the reduced confinement provided by the wraps for square cross sections and stress concentrations that develop at the corners. Wrapped square prisms always failed by rupture of the wrap at a corner. A reduction of approximately 30% to 40% in the failure strength was observed for the square wrapped specimens compared to the round wrapped specimens. This loss of strength due to reduced confinement in square specimens is reasonably accounted for by Restrepo and Devino's (1996) model of confinement. Richart's model of confinement (1928) predicts the strength of round wrapped specimens reasonably well.

Compression strength of wrapped specimens is 1.4 to 2.6 times larger than the strength of unwrapped specimens for square and round sections, respectively. Ductility of wrapped specimens under compression is 4 to 9 times larger than that of unwrapped specimens for square and round sections, respectively.

4.2 Accelerated Corrosion Test

Tests were conducted on twenty-four 152 mm x 305 mm concrete cylindrical specimens. A water/cement ratio of 0.6 and 2% Cl^- ion by weight of cement (intended to simulate chloride contaminated columns) were used in the mix. Initially all specimens were partially submerged in 3% NaCl solution and subjected to electrically induced corrosion until cracks were visible on the exterior surfaces. After the initial corrosion stage, specimens were wrapped with glass and carbon FRP. Specimens were then placed in a tub and soaked in 3% NaCl solution for one hour each day while the electrically induced accelerated corrosion continued for several weeks. Some specimens were removed after 130 days and others after 190 days. The merit of using unbonded wraps to minimize localized wrap strains near reinforcing bars was investigated. The ASTM G1 mass loss test was performed to determine the total corrosion of reinforcement in unwrapped and wrapped specimens. The strength of FRP panels exposed to 190 wet-dry cycles with salt water also was determined.

The mean corrosion depths for glass and carbon wraps are not significantly different for either the bonded or unbonded conditions. Both wrap systems, glass and carbon, are equally effective in reducing the corrosion rate. Wrapping reduced the corrosion depth by 46% – 59% after 190 days of testing.

The mean corrosion depths for bonded and unbonded specimens are significantly different after 190 days of accelerated corrosion. The bonded wrap is more effective in reducing the rate of corrosion than the unbonded wrap. Corrosion depths for reinforcement in specimens with unbonded wraps were approximately 20% more than those in specimens with bonded wraps after 190 days of testing. This may be due to water seepage between the concrete and the plastic sheet used to create the unbonded condition.

Wrap strains for bonded specimens with both types of wraps tend to level off with time. One explanation could be that the stress concentration near the anodes in the bonded wraps is more effective in containing the corrosion-induced crack and reducing the corrosion rate. The slip of unbonded wraps and the resulting redistribution of strain along the entire wrap may be less effective at containing the large corrosion-induced crack near the anodes.

4.3 Effect of Freeze-Thaw and Wet-Dry Cycles on FRP Panels

The tensile properties of glass and carbon FRP panels exposed to 300 freeze-thaw cycles and 190 wet-dry cycles with 3% NaCl solution were measured and compared to the properties of unconditioned panels. The effective stiffness (modulus × thickness) of glass FRP is not affected significantly by the freeze-thaw or wet-dry cycling. However, its ultimate strength per unit width decreased by 21% due to freeze-thaw cycling and 18% due to wet-dry cycling. The ultimate strain of glass FRP decreased by 20% due to both types of conditioning.

For carbon the test results indicated a 30% increase in the effective stiffness due to freeze-thaw cycling and a 41% increase due to wet-dry cycling. The ultimate strength per unit width was not significantly affected by either type of conditioning. The ultimate strain decreased by 28% due to freeze-thaw cycling and 36% due to wet-dry cycling. For carbon, the increase in stiffness after conditioning was surprising, and limited re-testing indicated that the results were not reliable for the thin carbon panels. Better grip fixtures are recommended for testing thin carbon FRP.

4.4 Behavior Under Impact and High Temperature

When supported on a concrete substrate, both glass and carbon FRP panels are not significantly damaged by 16.5 kg head with a 75 mm radius when dropped from a height of

0.79 m. Damage to wraps from vandalism or minor vehicle impact should therefore not be significant.

At temperature exceeding 150°C the epoxy in the wraps char and the wraps unravel. The wraps are therefore not effective at very high temperatures.

4.5 Recommendation for Field Installation

It is evident from the experimental study conducted that both carbon and glass wrap systems are equally resistant to freeze-thaw cycles and reduce the corrosion rate by about the same rate. Therefore, three layers of glass wrap or two layers of carbon wrap may be used to repair Michigan bridge columns. Reducing the number of layers may also be feasible, but it is not possible to provide any recommendation about this without additional studies.

The preferred wrap system will most likely depend on the material and installation cost rather than performance issues. However, it should be noted that many studies indicate strength degradation of glass FRP in an alkaline and/or humid environment under elevated temperature. Thus in regions with long periods of hot and humid conditions, carbon FRP may be preferable to glass FRP.

It is also recommended that a non-destructive technique or coring be used every ten years to monitor the condition of the concrete inside the wrap.

4.6 Repair Costs

The estimated cost for the conventional chip and patch repair technique that is currently used by the MDOT is approximately \$500-\$725/m^2 of repaired column surface. The estimated

cost of the glass and carbon wrap systems used in this research study as provided by the respective suppliers is provided in Table 4.1.

Table 4.1 Estimated material and installation cost for Tyfo-S glass and MBrace carbon wrap systems

Wrap Type	Material Cost /m^2/layer	Installation Cost /m^2/layer	No. of Layers	*Surface Prep./ m^2	Total Cost/ m^2
Glass	$54	$54	3	$101	$425
Carbon	$75	$54	2	$101	$360

* Estimated cost of surface preparation prior to wrap installation was provided by MDOT

The benefit of repairing corrosion-damaged columns with FRP wraps is dependent on the life of conventional chip and patch repair and that of FRP repaired columns. Because of the lack of long-term field experience with FRP wraps it is not possible to perform an effective cost-benefit analysis at this time.

Chapter 5
Field Installation and Future Studies

5.1 Corrosion Monitoring of Field Columns

Six corrosion probes were installed on six corrosion damaged field columns in the summer of 1999. These columns had considerable surface spalling and reinforcement was exposed at several locations. Each column was also fitted with two pre-weighed #13 reinforcing steel bars approximately 305 mm long to measure mass loss. The corrosion probes and the steel bars were located at the same level of the existing column reinforcement steel and about two meters above the roadway surface. The initial weights of the bars are given in Table 5.1. These columns are located on Lansing Road in Lansing, Michigan under the I-96 overpass (Bridge ID S09 and S10 of 23152)). Columns one through three are located on Pier 1 under the westbound overpass (S09), while columns four through six are located on Pier 1 under the eastbound overpass (S10). After superficially repairing the column surface spalls by patching (chloride was added to the patch to match existing chloride content of the column), two columns were wrapped with two layers of carbon fiber sheets, two were wrapped with three layers of glass fiber sheets and two were left unwrapped as control columns. Column wrapping was done in July 1999.

The corrosion probes manufactured by Rohrback Cosasco Systems, Inc. (Santa Fe Springs, California) are based on an electrical resistance measurement system. This system is simple to install, directly measures the total corrosion, does not need regular measurements, is smaller, easy to transport, and costs about $5,500 for six probes and the readout measurement device. The manufacturer's information for the probes are included in Appendix G.

Table 5.1 Initial weight of corrosion bars installed in field columns

Column No.	Column 1 Glass wrapped		Column 2 Carbon wrapped		Column 3 Control	
Bar No.	1	2	3	4	5	6
Bar Wt. (g)	252.09	276.14	270.70	263.80	263.58	271.13
Column No.	Column 4 Control		Column 5 Glass wrapped		Column 6 Carbon wrapped	
Bar No.	7	8	9	10	11	12
Bar Wt. (g)	270.76	270.70	275.87	270.26	270.23	275.85

Corrosion data was collected about twice a month. Due to the short duration since the corrosion probes were installed, the data is not significantly different from the initial readings. Corrosion monitoring is scheduled to continue for about 10 years. At that time, the reinforcing bars installed to monitor mass loss will be cleaned and mass loss analysis will be conducted.

Figures 5.1 and 5.2 show a column condition before and after minor surface repairs, respectively. Figure 5.3 shows a corrosion probe and pre-weighed reinforcing bars used for monitoring mass loss. Figures 5.4 and 5.5 show the field installation of glass and carbon wraps, respectively. Figure 5.6 shows columns after repairs were completed. The carbon wrapped column (in the foreground) is yet to be painted while the glass wrapped column (middle one) has been painted. Figures 5.7 and 5.8 show the finished installation.

Appendix H provides specifications for field installation as recommended by the wrap manufacturers – glass wrap system by Tyfo-S and carbon wrap system by Master Builders.

Figs. 5.1 Column condition before surface repairs

Figs. 5.2 Column condition after surface repairs

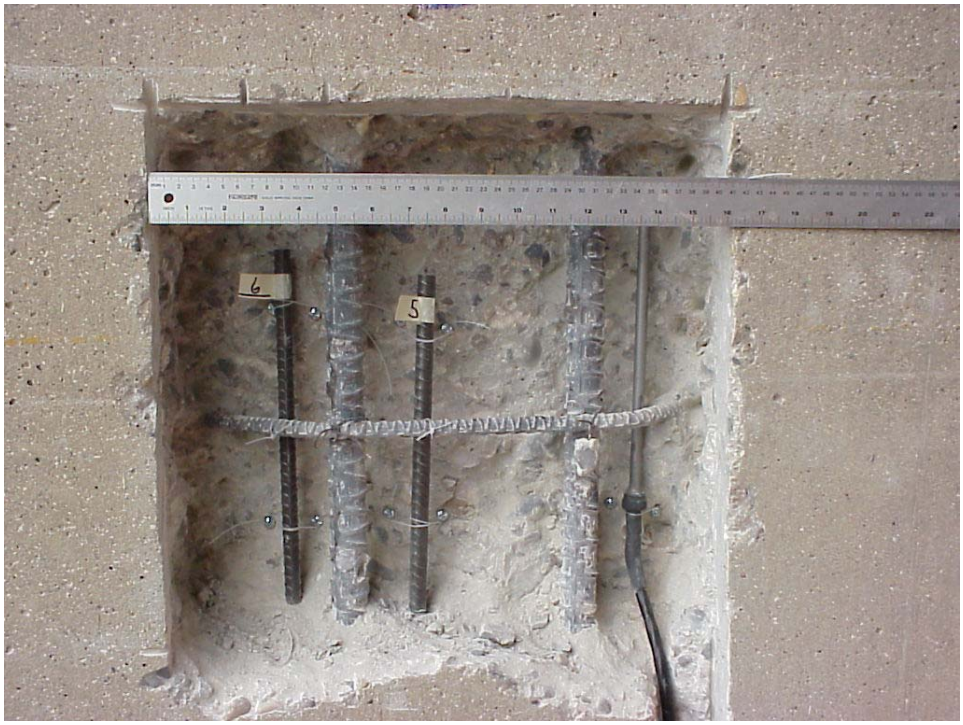

Fig. 5.3 Corrosion probe and reinforcing bars for monitoring mass loss

Fig. 5.4 Field installation of glass wrap to selected columns

Fig. 5.5 Field installation of carbon wrap to selected columns

Fig. 5.6 Completed installation of glass and carbon wraps (glass wrapped column in the background with top coat and final paint layers applied).

Fig. 5.7 Control (far left), carbon-wrapped (left) and glass-wrapped (right) columns under westbound overpass (S09)

Fig. 5.8 Control (far right), carbon-wrapped (right) and glass-wrapped (left) columns under eastbound overpass (S10)

5.2 Results of Field Monitoring

Wrapped and unwrapped columns in the field have been monitored for 10 months using corrosion probes. So far no significant corrosion activity has been detected.

Table 5.2 provides the reading collected from the corrosion probes using the portable monitoring instrument (Model Ck3 manufactured by Rohrback Cosasco Systems, Inc). It is apparent that some drift occurs in the readings. The accuracy of the readout appears to be ± 20.

Table 5.2 Dial readings for the corrosion probes installed in field columns

Date	Column 1 Glass Wrapped	Column 2 Carbon Wrapped	Column 3 Unwrapped	Column 4 Unwrapped	Column 5 Carbon Wrapped	Column 6 Glass Wrapped
7/12/99	222	222	252	246	212	222
8/20/99	228	215	234	245	223	223
9/26/99	231	215	232	*	214	219
10/10/99	231	225	232	*	225	220
11/7/99	240	232	239	*	226	229
12/13/99	242	236	248	251	232	232
1/28/00	255	246	248	*	242	**
2/15/00	251	**	248	*	239	**
5/20/00	242	239	240	*	230	229
6/25/00	222	220	228	*	210	215
7/10/00	222	218	224	238	210	212

* Probe not responding, ** keyhole to probe box was frozen and readout instrument could not be connected.

5.3 Calculation of Corrosion Rate

The corrosion rate for the concrete monitoring corrosion probes manufactured by Rohrback Cosasco is calculated as follows:

$$\text{Corrosion Rate (mils/year)} = \frac{\Delta\text{Dial Reading}}{\Delta\text{Time (Days)}} \text{ x } 0.365 \text{ x Span}$$

The corrosion probe used in the field columns (Model 650-0-T50) has a span of 25 mils.

Note: Intentionally left blank

References

ACI (2000). “Guide for the Design and Construction of Externally Bonded FRP Systems for Strengthening Concrete Structures.” *ACI Committee 440 R.*

Alampalli, S., O’Connor, J., and Yannotti, A. (1999). “Advancing Composites.” *Civil Engineering Magazine*, December A1-A7.

Allen, M. L. (1995). “Probability of Corrosion Induced Cracking in Concrete.” *Cement and Concrete Research*, Vol.25, No. 6, 1179-1190.

Almusallam, T. H., Al-Salloume, Y. A., and Alsayed, S. H. (2000). “Durability of Concrete Cylinders Wrapped with GFRP Sheets at Different Environmental Conditioning.” *Seventh Annual International Conference on Composites Engineering*, 27-28.

Arya C. and Sa'id-Shawqi, Q. (1996). " Factors Influencing Electrochemical Removal of Chloride from Concrete.” *Cement and Concrete Research*, Vol. 26, No. 6, 851-860.

ASTM, 1990. “Standard Practice for Preparing, Cleaning, and Evaluating Corrosion Test Specimens.” *ASTM Designation: G 1-90 (Reapproved 1994)*,
9-15.

Brockenbrough, R. L. and Gallagher, W. P. (1985). “Effect of Clamping Pressure and Joint Geometry on Corrosion Induced Bowing and Distortion of Bolted Joints in Weathering Steel.” *Journal of Construction Steel Research*, 213-238.

Chajes, Mertz, Thomson, and Farschman (1994). “Durability of Composite Material Reinforcement.” *Proceedings, Third Material Engineering Conference*, ASCE, 598-605.

De Wilde, W.P. (1988). *Proceedings of the International Conference on Computer Aided Design in Composite Material Technology*. Computational Mechanics Publication, Springer-Verlag Berlin Heidelberg.

Debaiky, A. and Green, G., and Hope, B., (1999). “FRP Rehabilitation of Corrosion-Damaged Concrete Structures.” *Proceedings of the 44th International SAMPE Symposium*, May 23-27.

Demers, M. et al. (1996). “The Strengthening of Structural Concrete with an Aramid Woven fiber/Epoxy Resin Composites”, *Proceedings of the 2nd* International Conference, ACMBS, Montreal, PQ, Canada, pp.435-442.

Detwiler, R., Kjellsen K., and Gjorv, O. (1991). “ Resistance to Chloride Intrusion of Concrete Cured at Different Temperatures.” *ACI Materials Journal*, Vol. 88, 19-24.

Fontana, M. G. (1986). *Corrosion Engineering*. McGraw-Hill, New York.

Fyfe Co. LLC (2000). "Tyfo SEH-51 Composite using Tyfo S Epoxy." San Diego, California.

Fyfe, E. R., Watson, R. J. and Watson, S. C. (1996). "Long-Term Durability of Composites Based on Field Performance and Laboratory Testing." *Proceedings of the ICCI'96 Conference*, Tucson, Arizona, 982-995.

Gomez, J., and Casto, B. (1996). "Freeze Thaw Durability of Composite Materials." *Proceedings of the ICCI'96 Conference*, Tucson, Arizona, 947-955.

Guttman, H. and Sereda, P.J. (1968). " Measurement of Atmospheric Factors Affecting the Corrosion of Metals." *Metal Corrosion in the Atmosphere*, ASTM STP 435, ASTM.

Halstead, O'Connor, Alampalli, and Minser. (2000). "Evaluating FRP Wrap with NDT Methods." *Proceedings of the NDT Conference*.

Hyun, A. (1995). "Fire Endurance and Hose Stream Tests of Three 48" high by 56" Wide Non-Symmetrical Walls." Technical Report, Inchape Testing Services of Warnock Hersey, Inc., Pittsburgh, CA.

Kenneth, W. N. and Labossiere, P. "Fiber Composite Sheets in Cold Climate Rehab." *Concrete International*, V. 20, No. 6, June 1998, pp. 22-24.

Kestner, Harries, Pessiki, Sause, and Ricles (1997). "Rehabilitation of Reinforced Concrete Columns using Fiber Reinforced Polymer Composite Jackets." Report No. 97-07. Advanced Technology for Large Structural Systems, Lehigh University, Bethlehem, PA.

Lee, C. (1998). "Accelerated Corrosion and Repair of Reinforced Concrete Columns Using CFRP Sheets", *M. Eng. Thesis*, Department of Civil Eng., University of Toronto, Toronto, ON, Canada, 106 p.

Lopez-Anido, R. (1993). "Influence of Temperature on the Service Life of Rebars." *Cement and Concrete Research*, Vol.23, No. 5, 1130-1190.

Malek, A. and Saadatmanesh H. (1996). "Physical and Mechanical Properties of Typical Fibers and Resins." *Proceedings of the ICCI'96* Conference, Tucson, Arizona, 68-79.

Mallick, P. K. (1993). *Fiber Reinforced Composites–Materials, Manufacturing and Design*. Second Edition, Marcel Dekker Inc., New York, 326-327.

Mander, J. B., Priestley, M. J. N., and Park R. (1988). "Theoretical Stress-Strain Model for Confined Concrete." *Journal of Structural Engineering*, ACSE, Vol. 114, No. 8, 1804-1826.

Martin, H. and Schieles, P. (1969). " The Influence of Time and Environmental Condition on Corrosion of Deformed Bars in Cracked Concrete." *Preliminary Report of RILEM International Symposium on Durability of Concrete*, Vol. II, Prague.

Martin, H. and Schieles, P. (1969). "The Influence of Cracks on Corrosion of Steel in Concrete." *Preliminary Report of RILEM International Symposium on Durability of Concrete*, Vol. II, Prague.

Master Builders, Inc. (1998). "MBrace Composite Strengthening System Engineering Design Guidelines." Second Edition, Cleveland, Ohio.

McCrum, R. (1994). MDOT office memorandum to Sonny Jadun, June 22.

Mehta, P., and Monteiro, J. (1993). *Concrete, structure, properties, and materials*. Second Edition, Prentice-Hall, Englewood Cliffs, 160-164.

Meier, U. (1996). "Composites for structural repair and retrofitting." *Proceedings, ICCI'96 Conference*, Tucson, Arizona, 1202-1216.

Michniewicz, J. (1996). "Repair and Rehabilitation of Reinforced Concrete Columns with Fiber-Reinforced Plastics", *M. Eng. Thesis*, Department of Civil Eng., University of Toronto, Toronto, ON, Canada, 97 p.

Murphy, K., Zhang, S., and Karbhari, V. M. (1999). "Effect of Concrete Based Alkaline Solutions on Short Term Response of Composites." *Proceeding of the 44th International SAMPE Symposium*, May 23-27.

Neter, J., Wasserman, W., and Whitmore, G.A. (1992). *Applied Statistics*, 4th Edition, Allyn and Bacon, Boston, MA.

Nilson A. and Winter G. (1991). *Design of Concrete Structures*. Eleventh Edition, McGraw-Hill, New York, New York.

Pantazopolou et al. (1996). "Repair of Corrosion-Damaged Concrete Using ACM", *Proceedings of the 2nd International Conference, ACMBE*, Montreal, PQ, Canada, pp.287-298.

Picher, F., Rochette, P., and Labossiere, P. (1996). "Confinement of Concrete Cylinders with CFRP." *Proceedings of the ICCI'96 Conference*, Tucson, Arizona, 829-841.

Pigeon, M. and Pleau, R.(1998). *Durability of Concrete in Cold Climates*. Modern Concrete Technology Series. E & FN Spon, London, UK, 1-5.

Restrepol, J. and DeVino, B. (1996). "Enhancement of the Axial Load Carrying Capacity of Reinforced Concrete Columns by means Fiberglass Epoxy-Jackets." *Proceedings of Advanced Composite Materials in Bridges and Structures II*, Montreal, August, 547-553.

Richart F. E., Brandtzaeg A, and Brown R. L. (1928). " A Study of the Failure of Concrete under Combined Compressive Stresses." University of ILL. Eng Exp. Stn. Bull 185.

Rivera, J. and Karbhari, V. (1999). Effects of Extended Freeze-Thaw exposure on Composite Wrapped Concrete Cylinders." *Proceedings of the 44th SAMPE Symposium*, May 23-27.

Rochette, P. and Labossiere, P. (1996). " A Plasticity Approach for Concrete Columns Confined with Composite Materials". *Proceedings of the 2nd International Conference, ACMBS*, Montreal, PQ, Canada, pp.359-366.

Sen, R., Mariscal, D., and Shahaway M. (1993). "Durability of Fiberglass Pretensioned Beams." *ACI Structural Journal*, Vol. 90, 525-533.

Sen, R., Mariscal, D., and Shahaway M. (1993). "Investigations of S_2 Glass Epoxy Strands in Concrete." *Proceedings of the FRP Components Structures, International Symposium*, 15-33.

Steckel, G. (2000). Personal Communication, The Aerospace Corporation, El Segundo, CA.

Tarricone P. (1995). "Composite Sketch." *Civil Engineering Magazine*, May, 52-55.

Toutanji, H. and Balaguru, P. (1998). "Durability Characteristics of Concrete Columns Wrapped with FRP Tow Sheets." *Journal of Materials in Civil Engineering*, February, 52-57.

Wrobel, P. (1994). "Laboratory Measurements of Corrosion Activity of Steel Reinforcement in Concrete using Simple Equipment." *Cement, Concrete, and Aggregates, CCAGPD*, Vol. 16, No. 2, Dec. 1994, 100-103.

Yamato, T., Emoto, Y., and Soeda, M. (1987). "Freezing and Thawing Resistance of Concrete Containing Chloride." *Concrete Durability*, ACI SP100-50, Vol. 1, 901-917.

Appendix A
Aerospace Corporation's FRP Panel Durability Data

Fyfe Company E-Glass/Epoxy
SEH 51/Tyfo S Epoxy

ENVIRONMENTAL EXPOSURE	YOUNG'S MODULUS, msi	TENSILE STRENGTH, ksi	FAILURE STRAIN, %	SHORT BEAM SHEAR STRENGTH, ksi	GLASS TRANSITION TEMP., °C	HARDNESS, SHORE D	WEIGHT CHANGE, %
CONTROL	3.96 ± 0.13	80.5 ± 5.1	2.10 ± 0.18	5.9 ± 0.5	65, 64, 68, 68	83 ± 3	
100% HUMIDITY/38°C							
1000 Hour	4.04 ± 0.13	71.6 ± 2.8	1.82 ± 0.08	6.0 ± 0.4	72	83 ± 2	0.56
3000 Hour	3.94 ± 0.10	67.9 ± 1.9	1.77 ± 0.05	5.8 ± 0.3	73	84 ± 2	0.82
10,000 Hour	3.93 ± 0.18	51.4 ± 2.1	1.31 ± 0.08	4.5 ± 0.3	73	82 ± 2	1.09
SALT WATER							
1000 Hour	4.03 ± 0.09	80.8 ± 2.2	2.07 ± 0.06	6.0 ± 0.9	65	85 ± 2	0.46
3000 Hour	4.02 ± 0.04	81.7 ± 1.2	2.09 ± 0.03	5.6 ± 0.2	63	84 ± 3	0.57
10,000 Hour	4.09 ± 0.07	66.0 ± 1.9	1.64 ± 0.04	4.6 ± 0.2	63	82 ± 2	0.91
pH 9.5 $CaCO_3$ SOLUTION							
1000 Hour	3.85 ± 0.03	83.2 ± 2.8	2.25 ± 0.11	5.9 ± 0.3	65	83 ± 2	0.36
3000 Hour	4.00 ± 0.13	80.8 ± 4.1	2.11 ± 0.11	6.0 ± 0.3	61	85 ± 2	0.53
10,000 Hour	3.88 ± 0.06	62.4 ± 2.5	1.63 ± 0.08	5.1 ± 0.3	64	84 ± 2	0.88
DRY HEAT AT 60°C							
1000 Hour	3.89 ± 0.06	82.0 ± 1.7	2.17 ± 0.08	6.4 ± 0.4	95	85 ± 2	-0.33
3000 Hour	4.05 ± 0.06	84.8 ± 2.4	2.16 ± 0.09	6.7 ± 0.8	87	85 ± 2	-0.44
20 FREEZE/THAW CYCLES	4.02 ± 0.06	78.0 ± 2.1	2.00 ± 0.06	5.2 ± 0.3	68	82 ± 3	0.59
UV/CONDENSATION, 100 CYCLES	4.03 ± 0.08	84.0 ± 3.1	2.18 ± 0.11	6.5 ± 0.2	86	83 ± 3	-0.42
DIESEL FUEL, 4 Hour	4.01 ± 0.06	83.4 ± 2.6	2.16 ± 0.06	5.9 ± 0.2	67	81 ± 2	

Master Builders "MBRACE" Carbon/Epoxy
CF-130/MBI Epoxy

ENVIRONMENTAL EXPOSURE	YOUNG'S MODULUS, msi	TENSILE STRENGTH, ksi	FAILURE STRAIN, %	SHORT BEAM SHEAR STRENGTH, ksi	GLASS TRANSITION TEMP., °C	HARDNESS, SHORE D	WEIGHT CHANGE, % (2 PLY/6 PLY)
CONTROL	**32.8 ± 1.8**	**636 ± 27**	**1.75 ± 0.09**	**7.8 ± 0.3**	**67, 67, 67, 70**	**92 ± 2**	
100% HUMIDITY/38°C							
1000 Hour	**34.0 ± 1.4**	**591 ± 25**	**1.59 ± 0.08**	**7.6 ± 0.1**	**75**	**91 ± 1**	**1.13/0.95**
3000 Hour	**33.2 ± 0.4**	**540 ± 17**	**1.51 ± 0.06**	**7.2 ± 0.1**	**74**	**92 ± 1**	**1.41/1.03**
10,000 Hour	**33.1 ± 0.8**	**596 ± 22**	**1.67 ± 0.07**	**6.9 ± 0.2**	**70**	**93 ± 2**	**1.51/1.46**
SALT WATER							
1000 Hour	**33.6 ± 0.5**	**619 ± 25**	**1.70 ± 0.05**	**7.5 ± 0.2**	**65**	**90 ± 3**	**1.14/0.65**
3000 Hour	**33.9 ± 1.1**	**623 ± 23**	**1.74 ± 0.07**	**7.6 ± 0.4**	**65**	**91 ± 2**	**1.24/0.88**
10,000 Hour	**32.1 ± 1.6**	**610 ± 23**	**1.75 ± 0.08**	**6.8 ± 0.1**	**63**	**91 ± 3**	**1.48/1.37**
pH 9.5 $CaCO_3$ SOLUTION							
1000 Hour	**32.9 ± 1.3**	**597 ± 27**	**1.70 ± 0.11**	**7.6 ± 0.1**	**65**	**92 ± 1**	**1.24/0.44**
3000 Hour	**31.8 ± 0.8**	**585 ± 35**	**1.70 ± 0.09**	**7.2 ± 0.6**	**67**	**91 ± 2**	**1.27/1.02**
10,000 Hour	**33.1 ± 1.5**	**615 ± 39**	**1.70 ± 0.12**	**6.7 ± 0.2**	**62**	**92 ± 1**	**1.31/0.78**
DRY HEAT AT 60°C							
1000 Hour	**33.4 ± 1.2**	**637 ± 23**	**1.73 ± 0.08**	**9.5 ± 0.2**	**84**	**94 ± 1**	**-0.47/-0.20**
3000 Hour	**32.6 ± 0.9**	**582 ± 12**	**1.67 ± 0.05**	**8.6 ± 0.4**	**85**	**93 ± 1**	**- /-0.33**
20 FREEZE/THAW CYCLES	**33.3 ± 1.7**	**561 ± 29**	**1.57 ± 0.06**	**7.5 ± 0.1**	**72**	**91 ± 1**	**1.32/0.97**
UV/CONDENSATION, 100 CYCLES	**33.6 ± 1.2**	**644 ± 37**	**1.76 ± 0.09**	**8.4 ± 0.3**	**79**	**91 ± 2**	**-0.63/-0.33**
DIESEL FUEL, 4 Hour	**34.1 ± 1.5**	**589 ± 9**	**1.61 ± 0.08**	**8.2 ± 0.1**	**66**	**93 ± 3**	**0.02/0.00**

Appendix B
Measured FRP Panel Properties

FRP panel properties were measured and reported by the Composite Materials and Structures Center at MSU. Carbon FRP panels were made of two layers. Unconditioned glass FRP panels were made of four layers, while conditioned glass FRP panels were made of three layers. Different sets of unconditioned specimens were tested for modulus and fracture properties.

Table B.1 Modulus of unconditioned FRP panels

Carbon Panels	Width (mm)	Thickness (mm)	Modulus (MPa)	Eff. Stiffness Per Layer (N/mm)
Sample 1	19.06	1.283	54993	35278
Sample 2	19.08	1.219	46644	28430
Sample 3	19.10	1.283	58995	37845
Sample 4	19.11	1.194	55407	33078
Sample 5	19.13	1.270	49335	31328
Average	19.10	1.250	53061	33192
Std. Dev.	0.025	0.041	4968	3612
Glass Panels	Width (mm)	Thickness (mm)	Modulus (MPa)	Eff. Stiffness Per Layer (N/mm)
Sample 1	19.06	4.788	22356	26760
Sample 2	19.10	5.055	19251	24328
Sample 3	19.13	4.877	27600	33651
Sample 4	19.11	4.953	24288	30075
Sample 5	19.16	4.788	19251	23043
Sample 6	19.09	4.826	23598	28471
Sample 7	19.15	5.042	17802	22439
Average	19.12	4.905	22011	26967
Std. Dev.	0.036	0.114	3450	4072

Table B.2 Fracture properties of unconditioned FRP panels

Carbon Panels	Width (mm)	Thickness (mm)	Ultimate Strength (MPa)	Ult. Str. Per Unit Width Per Layer (N/mm)	Ultimate Strain*
Sample 1	12.67	0.953	650.1	309.8	0.012
Sample 2	12.71	1.054	930.2	490.2	0.018
Sample 3	12.67	0.927	942.3	436.8	0.018
Sample 4	12.60	0.991	908.5	450.2	0.017
Sample 5	12.69	1.143	674.6	385.5	0.013
Average	12.67	1.013	821.1	414.5	0.015
Std. Dev.	0.043	0.086	145.7	69.5	0.0029
Glass Panels	Width (mm)	Thickness (mm)	Ultimate Strength (kPa)	Ult. Str. Per Unit Width Per Layer (N/mm)	Ultimate Strain*
Sample 1	12.67	5.080	407.4	517.4	0.019
Sample 2	12.71	5.144	430.3	553.4	0.020
Sample 3	12.61	5.138	432.1	555.0	0.020
Sample 4	12.62	5.126	414.9	531.7	0.019
Sample 5	12.56	5.011	418.3	524.0	0.019
Average	12.64	5.100	420.6	536.3	0.019
Std. Dev.	0.058	0.056	10.4	17.1	0.0005

* The ultimate strain was not measured directly. Since the stress-strain relationship is essentially linear, the ultimate strains are estimated using the ultimate strengths and the average modulus in Table B.1.

Table B.3 Properties of FRP panels subjected to 300 freeze-thaw cycles

Carbon Panels	Width (mm)	Thickness (mm)	Modulus (MPa)	Effective Stiffness Per Layer (N/mm)	Ult. Str. Per Unit Width Per Layer (N/mm)	Ultimate Strain
Sample 1	12.61	0.986	90500	44595	448.8	0.010
Sample 2	12.57	1.113	78094	43441	416.1	0.010
Sample 3	12.58	1.092	78481	42858	484.6	0.011
Sample 4	12.53	1.161	76431	44360	440.5	0.010
Sample 5	12.57	1.135	71567	40600	450.0	0.011
Average	12.57	1.097	79014	43171	448.0	0.010
Std. Dev.	0.03	0.067	6986	1598	24.6	0.0006
Glass Panels	Width (mm)	Thickness (mm)	Modulus (MPa)	Effective Stiffness Per Layer (N/mm)	Ult. Str. Per Unit Width Per Layer (N/mm)	Ultimate Strain
Sample 1	12.70	3.411	22818	25946	421.3	0.017
Sample 2	12.78	3.462	22101	25504	409.4	0.016
Sample 3	12.63	3.348	23764	26518	434.4	0.017
Sample 4	12.77	3.289	24930	27334	451.9	0.018
Sample 5	12.78	3.251	24164	26187	393.3	0.015
Sample 6	12.61	3.048	27110	27544	428.9	0.015
Average	12.71	3.302	24148	26506	423.6	0.016
Std. Dev.	0.08	0.146	1760	798	22.7	0.0012

Table B.4 Properties of FRP panels subjected to 190 wet-dry cycles

Carbon Panels	Width (mm)	Thickness (mm)	Modulus (MPa)	Effective Stiffness Per Layer (N/mm)	Ult. Str. Per Unit Width Per Layer (N/mm)	Ultimate Strain
Sample 1	13.30	1.003	103155	51748	410.0	0.008
Sample 2	13.20	1.346	69228	46597	417.9	0.009
Sample 3	13.20	1.232	78246	48196	433.3	0.009
Sample 4	13.21	1.181	76673	45279	369.4	0.008
Sample 5	12.97	1.176	78239	46005	436.7	0.010
Sample 6	12.34	0.884	97049	42892	406.3	0.009
Average	13.04	1.137	83765	46786	412.7	0.009
Std. Dev.	0.36	0.166	13229	2990	27.1	0.0007
Glass Panels	Width (mm)	Thickness (mm)	Modulus (MPa)	Effective Stiffness Per Layer (N/mm)	Ult. Str. Per Unit Width Per Layer (N/mm)	Ultimate Strain
Sample 1	12.53	2.888	28600	27533	426.6	0.014
Sample 2	12.62	2.710	29918	27028	463.4	0.017
Sample 3	12.53	2.908	28062	27205	457.7	0.017
Sample 4	12.71	2.743	32306	29540	411.6	0.014
Sample 5	12.61	2.739	30043	27428	427.8	0.016
Sample 6	12.58	2.764	28297	26066	432.7	0.016
Average	12.60	2.792	29538	27467	438.6	0.016
Std. Dev.	0.07	0.084	1591	1143	21.6	0.0012

Appendix C
Calculation Details

C.1 Strain in Column Wrap After 10 years

1. Geometric and Material Properties

Column diameter, D = 91.44 cm
Column area, A_c = 6563.60 cm^2
Initial volume of col. = A_c (100 cm) = 656360 cm^3
Core diameter = d_c = 80.01 cm
Longitudinal steel Ratio, ρ = 2%
Steel area, $A_s = \rho$ A_c = 131.27 cm^2
Tie steel diameter, d = 1.27 cm
Tie steel cross sectional area: $A_{sp} = \frac{\pi d^2}{4}$ = 1.266 cm^2
Tie Spacing = 30.48 cm
Volume of rust / volume of corroded steel = 6

2. Rust Volume

Corrosion rate for steel rebar (deformed) = 5%
Corroded steel area, $A_{crd\,s}$ = 0.05 A_s = 6.56 cm^2
Rust area, A_{rust} = 6 $A_{crd\,s}$ = 39.38 cm^2
Rust Volume, $V_{rust} = A_{rust}$ (100 cm) = 3938 cm^3
Corroded rate for ties (smooth steel) = 20%
Corroded tie steel area, $A_{crd,tie}$ = 0.2 A_{sp} = 0.2532 cm^2
Rust area spiral steel, $A_{rust,tie} = 6A_{crd,tie}$ = 6 (0.2532) = 1.519 cm^2
Rust volume tie steel, $V_{rust,tie} = A_{rust,tie}$ (length of tie) = 1.519 πd_c 100/30.48 = 1252.0 cm^3

3. Strain in Wrap

Change of volume in vertical steel: Chg. $V_{st} = \frac{5}{6}V_{rust} = \frac{5}{6}(3938) = 3281.66\,\text{cm}^3$

Change of volume in tie steel: Chg. $V_{sp} = \frac{5}{6}V_{rust-tie} = \frac{5}{6}(1252) = 1043.33\ \text{cm}^3$

Final column volume: Final V = Initial column volume +Chg. V_{st} +Chg.V_{sp}
= 656360 + 3281.66 + 1043.33 = 660684.99 cm^3

Final column diameter: $V_{final} = \frac{\pi (D_{final})^2}{4}100$

$D_{final} = 91.74$ cm

Strain generated in wrap: $Strain = \frac{D_{final} - D_{initial}}{D_{initial}} \approx .327\ \%$

C.2 Confining Pressure and Strain in Steel Jacket

Confining Pressure

From mechanics of thin walled cylinders, the confining pressure can be determined to be equal to:

$f_r = 2 (f_t\, t\, n) / D = 2 (E\, \varepsilon_t\, t\, n) / D$

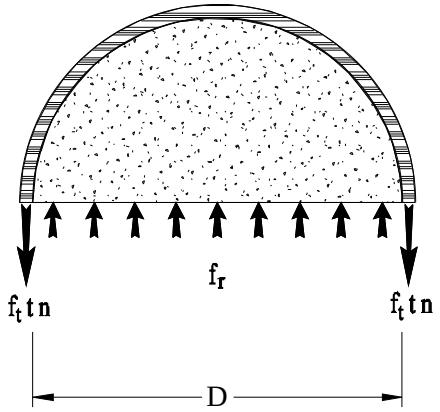

For glass FRP,

f_r = 2 (22011 x 0.00531 x 0.1227 x 3) / 15.24 = **5.645 MPa**

where:

t = the thickness of the wrap per layer = 0.1227 cm
f_t = the circumferential stress of wrap
n = number of wrap layers = 3
D = the dia. of the concrete cylindrical column = 15.24 cm
E = modulus of elasticity of the wrap (glass/epoxy) = 22011 MPa
ε_t = wrap strain = 0.531

Strain in Steel Jacket

$f_r\, D = 2\, f_{st}\, t_{st}$

$f_{st} = (f_r\, D) / (2\, t_{st})$

$\varepsilon_{st} = f_{st} / E_{st} = (f_r\, D) / (2\, t_{st}\, E_{st})$

= (5.645 x 15.24) / (2 x 0.477 x 200100) = **0.045%**

where

f_r = the confining pressure generating the strain in the jacket = 5.645 MPa
d = diameter of steel jacket = 15.24 cm
f_{st} = stress in steel jacket
E_{st} = modulus of elasticity of steel jacket = 200100 MPa
t_{st} = thickness of steel jacket =0.477 cm
ε_{st} = strain in steel jacket

Appendix D
Specimen, Bar and Gage Numbering

Table D.1 Specimen and gage numbering for freeze-thaw test

Freeze Thaw				
Specimen Type			Specimen Number	Gage Number
Shape	Wrap	Cycle		
Round	Glass	300	1	1
				2
		300	2	3
				4
		0	3	5
				6
		300	4	7
				8
Square		300	5	9
				10
		300	6	11
				12
		0	7	13
				14
		300	8	15
				16
Round	Carbon	300	9	17
				18
		300	10	19
				20
		0	11	21
				22
		300	12	23
				24
Square		300	13	25
				26
		300	14	27
				28
		0	15	29
				30
		300	16	31
				32
Round	Plain	300	17, 18, 19	-
Round	Glass	150	20, 21, 22	-
Square	Glass	150	23, 34, 25	-
Round	Carbon	150	26, 27, 28	-
Square	Carbon	150	29, 30, 31	-
Round	Plain	150	32, 33, 34	-
Round	Glass	0	3, 35, 36, 37, 38, 39	-
Square	Glass	0	7, 40, 41, 42, 43, 44	-
Round	Carbon	0	11, 45, 46, 47, 48, 49	-
Square	Carbon	0	15, 50, 51, 52, 53, 54	-
Round	Plain	0	55, 56, 57, 58, 59, 60	-

Table D.2 Specimen, bar and gage numbering for accelerated corrosion test

Specimen Type		Specimen Number	Bar Number†	Gage Number
Wrap	Bonded			
Glass	Yes	1	9	1
			11	2
	Yes	2	17	3
			19	4
	No	3	25	5*
			27	6*
	No	4	42	7
			44	8
	Yes	5	45	9
			47	10
	No	6	50	11
			52	12
	Yes	7	57	13*
			59	14*
	No	8	62	15
			64	16
	Yes	9	82	-
			84	-
	Yes	10	86	-
			88	-
Carbon	No	11	22	17*
			24	18*
	Yes	12	29	19
			31	20
	Yes	13	33	21*
			35	22*
	No	14	54	23
			56	24
	Yes	15	70	25
			72	26
	Yes	16	77	27
			79	28
	No	17	90	29
			92	30
	No	18	93	31
			95	32
Plain	-	19	2	-
			4	-
	-	20	5	-
			7	-
	-	21	13	-
			15	-
	-	22	38	-
			40	-
	-	23	66	-
			68	-
	-	24	73	-
			75	-

† Cathodes were also numbered

* Gage located on the anode-others are located between an anode and cathode

Appendix E
Concrete Mix Ratios and 28-Day Strength

Test	Material Weights (kg/m^3)				Pit No.		W/C Ratio	Average 28-Day Strength (MPa)
	Fine Agg. (Oven Dry)	Coarse Agg. (Oven Dry)	Water	NaCl	Fine Agg.	Coarse Agg.		
Freeze-Thaw	755.68	1111.54	161.0	11	19-46	95-5	0.4	37.70
Accel. Corrosion	607.16	1111.54	214.46	11	19-46	95-5	0.6	20.35

Appendix F
ASTM G1 Specifications

Designation: G 1 - 90 (Reapproved 1994)$^{\epsilon 1}$

Standard Practice for Preparing, Cleaning, and Evaluating Corrosion Test Specimens[1]

This standard is issued under the fixed designation G 1; the number immediately following the designation indicates the year of original adoption or, in the case of revision, the year of last revision. A number in parentheses indicates the year of last reapproval. A superscript epsilon (ε) indicates an editorial change since the last revision or reapproval.

$^{\epsilon 1}$ NOTE—Section 11 was added editorially in October 1994.

1. Scope

1.1 This practice covers suggested procedures for preparing bare, solid metal specimens for tests, for removing corrosion products after the test has been completed, and for evaluating the corrosion damage that has occurred. Emphasis is placed on procedures related to the evaluation of corrosion by mass loss and pitting measurements.

NOTE 1: Caution—In many cases the corrosion product on the reactive metals titanium and zirconium is a hard and tightly bonded oxide that defies removal by chemical or ordinary mechanical means. In many such cases, corrosion rates are established by mass gain rather than mass loss.

1.2 *This standard does not purport to address all of the safety concerns, if any, associated with its use. It is the responsibility of the user of this standard to establish appropriate safety and health practices and determine the applicability of regulatory limitations prior to use.* For specific precautionary statements, see Notes 1 and 6.

2. Referenced Documents

2.1 *ASTM Standards:*

A 262 Practices for Detecting Susceptibility to Intergranular Attack in Austenitic Stainless Steels[2]

D 1193 Specification for Reagent Water[3]

D 1384 Test Method for Corrosion Test for Engine Coolants in Glassware[4]

D 2776 Test Methods for Corrosivity of Water in the Absence of Heat Transfer (Electrical Methods)[5]

G 15 Terminology Relating to Corrosion and Corrosion Testing[6]

G 16 Guide for Applying Statistics to Analysis of Corrosion Data[6]

G 31 Practice for Laboratory Immersion Corrosion Testing of Metals[6]

G 33 Practice for Recording Data from Atmospheric Corrosion Tests of Metallic-Coated Steel Specimens[6]

G 46 Guide for Examination and Evaluation of Pitting Corrosion[6]

G 50 Practice for Conducting Atmospheric Corrosion Tests on Metals[6]

G 78 Guide for Crevice Corrosion Testing of Iron-Base and Nickel-Base Stainless Alloys in Seawater and Other Chloride-Containing Aqueous Environments[6]

3. Terminology

3.1 See Terminology G 15 for terms used in this practice.

4. Significance and Use

4.1 The procedures given are designed to remove corrosion products without significant removal of base metal. This allows an accurate determination of the mass loss of the metal or alloy which occurred during exposure to the corrosive environment.

4.2 These procedures, in some cases, may apply to metal coatings. However, possible effects from the substrate must be considered.

5. Reagents and Materials

5.1 *Purity of Reagents*—Reagent grade chemicals shall be used in all tests. Unless otherwise indicated, it is intended that all reagents conform to the specifications of the Committee on Analytical Reagents of the American Chemical Society where such specifications are available.[7] Other grades may be used, provided it is first ascertained that the reagent is of sufficiently high purity to permit its use without lessening the accuracy of the determination.

5.2 *Purity of Water*—Unless otherwise indicated, references to water shall be understood to mean reagent water as defined by Type IV of Specification D 1193.

6. Methods for Preparing Specimens for Test

6.1 For laboratory corrosion tests that simulate exposure to service environments, a commercial surface, closely resembling the one that would be used in service, will yield the most meaningful results.

6.2 It is desirable to mark specimens used in corrosion

[1] This practice is under the jurisdiction of ASTM Committee G-1 on Corrosion of Metals and is the direct responsibility of Subcommittee G01.05 on Laboratory Corrosion Tests.

Current edition approved March 30, 1990. Published May 1990. Originally published as G 1 - 67. Last previous edition G 1 - 88.

[2] *Annual Book of ASTM Standards*, Vol 01.03.

[3] *Annual Book of ASTM Standards*, Vol 11.01.

[4] *Annual Book of ASTM Standards*, Vol 15.05.

[5] *Discontinued*—Replaced by Guide G 96. See *1990 Annual Book of ASTM Standards*, Vol 03.02.

[6] *Annual Book of ASTM Standards*, Vol 03.02.

[7] *Reagent Chemicals, American Chemical Society Specifications*, American Chemical Society, Washington, DC. For suggestions on the testing of reagents not listed by the American Chemical Society, see *Analar Standards for Laboratory Chemicals*, BDH Ltd., Poole, Dorset, U.K., and the *United States Pharmacopeia and National Formulary*, U.S. Pharmaceutical Convention, Inc. (USPC), Rockville, MD.

tests with a unique designation during preparation. Several techniques may be used depending on the type of specimen and test.

6.2.1 *Stencil or Stamp*—Most metallic specimens may be marked by stenciling, that is, imprinting the designation code into the metal surface using hardened steel stencil stamps hit with a hammer. The resulting imprint will be visible even after substantial corrosion has occurred. However, this procedure introduces localized strained regions and the possibility of superficial iron contamination in the marked area.

6.2.2 Electric engraving by means of a vibratory marking tool may be used in situations where the extent of corrosion damage is known to be small. However, this approach to marking is much more susceptible to having the marks lost as a result of corrosion damage during testing.

6.2.3 Edge notching is especially applicable in cases where extensive corrosion and accumulation of corrosion products is anticipated. Long term atmospheric tests and sea water immersion tests on steel alloys are examples where this approach is applicable. It is necessary to develop a code system when using edge notches.

6.2.4 Drilled holes may also be used to identify specimens where extensive metal loss, accumulation of corrosion products, or heavy scaling is anticipated. Drilled holes may be simpler and less costly than edge notching. A code system must be developed when using drilled holes. Punched holes should not be used as they introduce residual strain.

6.2.5 In cases where it is undesirable to deform the surface of specimens after preparation procedures, for example, when testing coated surfaces, tags may be used for specimen identification. A metal or plastic wire can be used to attach the tag to the specimen and the specimen identification can be stamped on the tag. It is important to assure that neither the tag nor the wire will corrode or degrade in the test environment. It is also important to be sure that there are no galvanic interactions between the tag, wire, and specimen.

6.3 For more searching tests of either the metal or the environment, standard surface finishes may be preferred. A suitable procedure might be:

6.3.1 Degrease in an organic solvent or hot alkaline cleaner. (See also Practice G 31.)

NOTE 2—Hot alkalies and chlorinated solvents may attack some metals.

NOTE 3—Ultrasonic cleaning may be beneficial in both pre-test and post-test cleaning procedures.

6.3.2 Pickle in an appropriate solution if oxides or tarnish are present. In some cases the chemical cleaners described in Section 6 will suffice.

NOTE 4—Pickling may cause localized corrosion on some materials.

6.3.3 Abrade with a slurry of an appropriate abrasive or with an abrasive paper (see Practices A 262 and Test Method D 1384). The edges as well as the faces of the specimens should be abraded to remove burrs.

6.3.4 Rinse thoroughly, hot air dry, and store in desiccator.

6.4 When specimen preparation changes the metallurgical condition of the metal, other methods should be chosen or the metallurgical condition must be corrected by subsequent treatment. For example, shearing a specimen to size will cold work and may possibly fracture the edges. Edges should be machined.

6.5 The clean, dry specimens should be measured and weighed. Dimensions determined to the third significant figure and mass determined to the fifth significant figure are suggested. When more significant figures are available on the measuring instruments, they should be recorded.

7. Methods for Cleaning After Testing

7.1 Corrosion product removal procedures can be divided into three general categories: mechanical, chemical, and electrolytic.

7.1.1 An ideal procedure should remove only corrosion products and not result in removal of any base metal. To determine the mass loss of the base metal when removing corrosion products, replicate uncorroded control specimens should be cleaned by the same procedure being used on the test specimen. By weighing the control specimen before and after cleaning, the extent of metal loss resulting from cleaning can be utilized to correct the corrosion mass loss.

NOTE 5—It is desirable to scrape samples of corrosion products before using any chemical techniques to remove them. These scrapings can then be subjected to various forms of analyses, including perhaps x-ray diffraction to determine crystal forms, as well as chemical analyses to look for specific corrodants, such as chlorides. All of the chemical techniques that are discussed in Section 6 tend to destroy the corrosion products and thereby lose the information contained in these corrosion products. Care may be required so that uncorroded metal is not removed with the corrosion products.

7.1.2 The procedure given in 6.1.1 may not be reliable for cases where heavily corroded specimens are to be cleaned. The application of replicate cleaning procedures to specimens with corroded surfaces will often, even in the absence of corrosion products, result in continuing mass losses. This is because a corroded surface, particularly of a multiphase alloy, is often more susceptible than a freshly machined or polished surface to corrosion by the cleaning procedure. In such cases, the following method of determining the mass loss due to the cleaning procedure is preferred.

7.1.2.1 The cleaning procedure should be repeated on specimens several times. The mass loss should be determined after each cleaning by weighing the specimen.

7.1.2.2 The mass loss should be graphed as a function of the number of equal cleaning cycles as shown in Fig. 1. Two lines will be obtained: AB and BC. The latter will correspond to corrosion of the metal after removal of corrosion products. The mass loss due to corrosion will correspond approximately to point B.

7.1.2.3 To minimize uncertainty associated with corrosion of the metal by the cleaning method, a method should be chosen to provide the lowest slope (near to horizontal) of line BC.

7.1.3 Repeated treatment may be required for complete removal of corrosion products. Removal can often be confirmed by examination with a low power microscope (for example, 7× to 30×). This is particularly useful with pitted surfaces when corrosion products may accumulate in pits. This repeated treatment may also be necessary because of the requirements of 6.1.2.1. Following the final treatment, the specimens should be thoroughly rinsed and immediately dried.

7.1.4 All cleaning solutions shall be prepared with water and reagent grade chemicals.

7.2 Chemical procedures involve immersion of the corrosion test specimen in a specific solution that is designed to remove the corrosion products with minimal dissolution of any base metal. Several procedures are listed in Annex A1. The choice of chemical procedure to be used is partly a matter of trial and error to establish the most effective method for a specific metal and type of corrosion product scale.

NOTE 6: Caution—These methods may be hazardous to personnel.

7.2.1 Chemical cleaning is often preceded by light brushing (non metallic bristle) or ultrasonic cleaning of the test specimen to remove loose, bulky corrosion products.

7.2.2 Intermittent removal of specimens from the cleaning solution for light brushing or ultrasonic cleaning can often facilitate the removal of tightly adherent corrosion products.

7.2.3 Chemical cleaning is often followed by light brushing or ultrasonic cleaning in reagent water to remove loose products.

7.3 Electrolytic cleaning can also be utilized for removal of corrosion products. Several useful methods for corrosion test specimens of iron, cast iron, or steel are given in Annex A2.

7.3.1 Electrolytic cleaning should be preceded by brushing or ultrasonic cleaning of the test specimen to remove loose, bulky corrosion products. Brushing or ultrasonic cleaning should also follow the electrolytic cleaning to remove any loose slime or deposits. This will help to minimize any redeposition of metal from reducible corrosion products that would reduce the apparent mass loss.

7.4 Mechanical procedures can include scraping, scrubbing, brushing, ultrasonic cleaning, mechanical shocking, and impact blasting (for example, grit blasting, water-jet blasting, etc.). These methods are often utilized to remove heavily encrusted corrosion products. Scrubbing with a nonmetallic bristle brush and a mild abrasive-distilled water slurry can also be used to remove corrosion products.

7.4.1 Vigorous mechanical cleaning may result in the removal of some base metal, therefore care should be exercised. These should be used only when other methods fail to provide adequate removal of corrosion products. As with other methods, correction for metal loss due to the cleaning method is recommended. The mechanical forces used in cleaning should be held as nearly constant as possible.

8. Assessment of Corrosion Damage

8.1 The initial total surface area of the specimen (making corrections for the areas associated with mounting holes) and the mass lost during the test are determined. The average corrosion rate may then be obtained as follows:

$$\text{Corrosion Rate} = (K \times W)/(A \times T \times D)$$

where:

K = a constant (see 7.1.2),
T = time of exposure in hours,
A = area in cm^2,
W = mass loss in grams, and
D = density in g/cm^3 (see Appendix X1).

8.1.1 Corrosion rates are not necessarily constant with time of exposure. See Practice G 31 for further guidance.

8.1.2 Many different units are used to express corrosion rates. Using the units in 7.1 for T, A, W, and D the corrosion rate can be calculated in a variety of units with the following appropriate value of K:

Corrosion Rate Units Desired	Constant (K) in Corrosion Rate Equation
mils per year (mpy)	3.45×10^6
inches per year (ipy)	3.45×10^3
inches per month (ipm)	2.87×10^2
millimeters per year (mm/y)	8.76×10^4
micrometers per year (um/y)	8.76×10^7
picometers per second (pm/s)	2.78×10^6
grams per square meter per hour ($g/m^2 \cdot h$)	$1.00 \times 10^4 \times D$
milligrams per square decimeter per day (mdd)	$2.40 \times 10^6 \times D$
micrograms per square meter per second ($\mu g/m^2 \cdot s$)	$2.78 \times 10^6 \times D$

NOTE 7—If desired, these constants may also be used to convert corrosion rates from one set of units to another. To convert a corrosion rate in units X to a rate in units Y, multiply by K_Y/K_X; for example:

$$15 \text{ mpy} = 15 \times (2.78 \times 10^6)/(3.45 \times 10^6) \text{ pm/s}$$

8.2 Corrosion rates calculated from mass losses can be misleading when deterioration is highly localized, as in pitting or crevice corrosion. If corrosion is in the form of pitting, it may be measured with a depth gage or micrometer calipers with pointed anvils (see Guide G 46). Microscopical methods will determine pit depth by focusing from top to bottom of the pit, when it is viewed from above (using a calibrated focusing knob) or by examining a section that has been mounted and metallographically polished. The pitting factor is the ratio of the deepest metal penetration to the average metal penetration (as measured by mass loss).

NOTE 8—See Guide G 46 for guidance in evaluating depths of pitting.

NOTE 9—See Guide G 78 for guidance in evaluating crevice corrosion.

8.3 Other methods of assessing corrosion damage are:

8.3.1 *Appearance*—The degradation of appearance by rusting, tarnishing, or oxidation. (See Practice G 33.)

8.3.2 *Mechanical Properties*—An apparent loss in tensile strength will result if the cross-sectional area of the specimen (measured before exposure to the corrosive environment) is reduced by corrosion. (See Practice G 50.) Loss in tensile strength will result if a compositional change, such as dealloying taking place. Loss in tensile strength and elongation will result from localized attack, such as cracking or intergranular corrosion.

8.3.3 *Electrical Properties*—Loss in electrical conductivity can be measured when metal loss results from uniform corrosion. (See Test Methods D 2776.)

8.3.4 *Microscopical Examination*—Dealloying, exfoliation, cracking, or intergranular attack may be detected by metallographic examination of suitably prepared sections.

9. Report

9.1 The report should include the compositions and sizes of specimens, their metallurgical conditions, surface preparations, and cleaning methods, as well as measures of corrosion damage such as corrosion rates (calculated from mass losses), maximum depths of pitting, or losses in mechanical properties.

10. Precision and Bias

10.1 The factors that can produce errors in mass loss measurement include improper balance calibration and standardization. Generally, modern analytical balances can determine mass values to ±0.2 mg with ease and balances are available that can obtain mass values to ±0.02 mg. In general, mass measurements are not the limiting factor. However, inadequate corrosion product removal or overcleaning will affect precision.

10.2 The determination of specimen area is usually the least precise step in corrosion rate determinations. The precision of calipers and other length measuring devices can vary widely. However, it generally is not necessary to achieve better than ±1 % for area measurements for corrosion rate purposes.

10.3 The exposure time can usually be controlled to better than ±1 % in most laboratory procedures. However, in field exposures, corrosive conditions can vary significantly and the estimation of how long corrosive conditions existed can present significant opportunities for error. Furthermore, corrosion processes are not necessarily linear with time, so that rate values may not be predictive of the future deterioration, but only are indications of the past exposure.

10.4 Regression analysis on results such as are shown in Fig. 1 can be used to obtain specific information on precision. See Guide G 16 for more information on statistical analysis.

10.5 Bias can result from inadequate corrosion product removal or metal removal caused by overcleaning. The use of repetitive cleaning steps, as shown in Fig. 1, can minimize both of these errors.

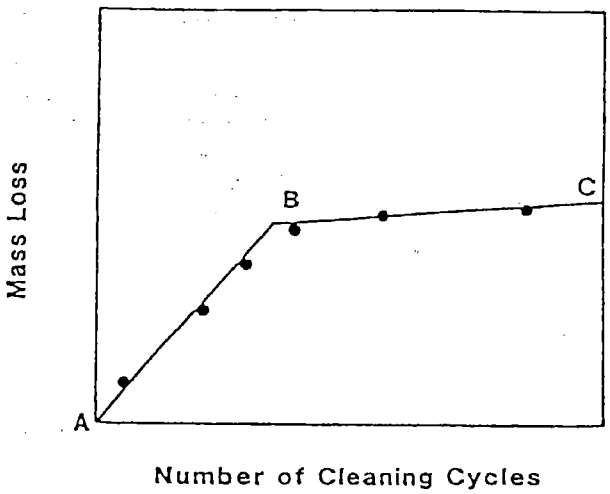

FIG. 1 Mass Loss of Corroded Specimens Resulting from Repetitive Cleaning Cycles

10.5.1 Corrosion penetration estimations based on mass loss can seriously underestimate the corrosion penetration caused by localized processes, such as pitting, cracking, crevice corrosion, etc.

11. Keywords

11.1 cleaning; corrosion product removal; evaluation; mass loss; metals; preparation; specimens

ANNEXES

(Mandatory Information)

TABLE A1 CHEMICAL CLEANING PROCEDURES FOR REMOVAL OF CORROSION PRODUCTS

Designation	Material	Solution	Time	Temperature	Remarks
C.1.1	Aluminum and Aluminum Alloys	50 mL phosphoric acid (H_3PO_4, sp gr 1.69) 20 g chromium trioxide (CrO_3) Reagent water to make 1000 mL	5 to 10 min	90°C to Boiling	If corrosion product films remain, rinse, then follow with nitric acid procedure (C.1.2).
C.1.2		Nitric acid (HNO_3, sp gr 1.42)	1 to 5 min	20 to 25°C	Remove extraneous deposits and bulky corrosion products to avoid reactions that may result in excessive removal of base metal.
C.2.1	Copper and Copper Alloys	500 mL hydrochloric acid (HCl, sp gr 1.19) Reagent water to make 1000 mL	1 to 3 min	20 to 25°C	Deaeration of solution with purified nitrogen will minimize base metal removal.
C.2.2		4.9 g sodium cyanide (NaCN) Reagent water to make 1000 mL	1 to 3 min	20 to 25°C	Removes copper sulfide corrosion products that may not be removed by hydrochloric acid treatment (C.2.1).
C.2.3		100 mL sulfuric acid (H_2SO_4, sp gr 1.84) Reagent water to make 1000 mL	1 to 3 min	20 to 25°C	Remove bulky corrosion products before treatment to minimize copper redeposition on specimen surface.
C.2.4		120 mL sulfuric acid (H_2SO_4, sp gr 1.84) 30 g sodium dichromate ($Na_2Cr_2O_7 \cdot 2H_2O$) Reagent water to make 1000 mL	5 to 10 s	20 to 25°C	Removes redeposited copper resulting from sulfuric acid treatment.
C.2.5		54 mL sulfuric acid (H_2SO_4, sp gr 1.84) Reagent water to make 1000 mL	30 to 60 min	40 to 50°C	Deaerate solution with nitrogen. Brushing of test specimens to remove corrosion products followed by re-immersion for 3 to 4 s is recommended.
C.3.1	Iron and Steel	1000 mL hydrochloric acid (HCl, sp gr 1.19) 20 g antimony trioxide (Sb_2O_3) 50 g stannous chloride ($SnCl_2$)	1 to 25 min	20 to 25°C	Solution should be vigorously stirred or specimen should be brushed. Longer times may be required in certain instances.
C.3.2		50 g sodium hydroxide (NaOH) 200 g granulated zinc or zinc chips Reagent water to make 1000 mL	30 to 40 min	80 to 90°C	Caution should be exercised in the use of any zinc dust since spontaneous ignition upon exposure to air can occur.

TABLE A1 *Continued*

Designation	Material	Solution	Time	Temperature	Remarks
C.3.3		200 g sodium hydroxide (NaOH) 20 g granulated zinc or zinc chips Reagent water to make 1000 mL	30 to 40 min	80 to 90°C	Caution should be exercised in the use of any zinc dust since spontaneous ignition upon exposure to air can occur.
C.3.4		200 g diammonium citrate ($(NH_4)_2HC_6H_5O_7$) Reagent water to make 1000 mL	20 min	75 to 90°C	Depending upon the composition of the corrosion product, attack of base metal may occur.
C.3.5		500 mL hydrochloric acid (HCl, sp gr 1.19) 3.5 g hexamethylene tetramine Reagent water to make 1000 mL	10 min	20 to 25°C	Longer times may be required in certain instances.
C.3.6		Molten caustic soda (NaOH) with 1.5–2.0 % sodium hydride (NaH)	1 to 20 min	370°C	For details refer to Technical Information Bulletin SP29-370, "DuPont Sodium Hydride Descaling Process Operating Instructions."
C.4.1	Lead and Lead Alloys	10 mL acetic acid (CH_3COOH) Reagent water to make 1000 mL	5 min	Boiling	...
C.4.2		50 g ammonium acetate (CH_3COONH_4) Reagent water to make 1000 mL	10 min	60 to 70°C	...
C.4.3		250 g ammonium acetate (CH_3COONH_4) Reagent water to make 1000 mL	5 min	60 to 70°C	...
C.5.1	Magnesium and Magnesium Alloys	150 g chromium trioxide (CrO_3) 10 g silver chromate (Ag_2CrO_4) Reagent water to make 1000 mL	1 min	Boiling	The silver salt is present to precipitate chloride.
C.5.2		200 g chromium trioxide (CrO_3) 10 g silver nitrate ($AgNO_3$) 20 g barium nitrate ($Ba(NO_3)_2$) Reagent water to make 1000 mL	1 min	20 to 25°C	The barium salt is present to precipitate sulfate.
C.6.1	Nickel and Nickel Alloys	150 mL hydrochloric acid (HCl, sp gr 1.19) Reagent water to make 1000 mL	1 to 3 min	20 to 25°C	...
C.6.2		100 mL sulfuric acid (H_2SO_4, sp gr 1.84) Reagent water to make 1000 mL	1 to 3 min	20 to 25°C	...
C.7.1	Stainless Steels	100 mL nitric acid (HNO_3, sp gr 1.42) Reagent water to make 1000 mL	20 min	60°C	...
C.7.2		150 g diammonium citrate ($(NH_4)_2HC_6H_5O_7$) Reagent water to make 1000 mL	10 to 60 min	70°C	...
C.7.3		100 g citric acid ($C_6H_8O_7$) 50 mL sulfuric acid (H_2SO_4, sp gr 1.84) 2 g inhibitor (diorthotolyl thiourea or quinoline ethyliodide or betanaphthol quinoline) Reagent water to make 1000 mL	5 min	60°C	...
C.7.4		200 g sodium hydroxide (NaOH) 30 g potassium permanganate ($KMnO_4$) Reagent water to make 1000 mL *followed by* 100 g diammonium citrate ($(NH_4)_2HC_6H_5O_7$) Reagent water to make 1000 mL	5 min	Boiling	...
C.7.5		100 mL nitric acid (HNO_3, sp gr 1.42) 20 mL hydrofluoric acid (HF, sp gr 1.198–48 %) Reagent water to make 1000 mL	5 to 20 min	20 to 25°C	...
C.7.6		200 g sodium hydroxide (NaOH) 50 g zinc powder Reagent water to make 1000 mL	20 min	Boiling	Caution should be exercised in the use of any zinc dust since spontaneous ignition upon exposure to air can occur.
C.8.1	Tin and Tin Alloys	150 g trisodium phosphate ($Na_3PO_4 \cdot 12H_2O$) Reagent water to make 1000 mL	10 min	Boiling	...
C.8.2		50 mL hydrochloric acid (HCl, sp gr 1.19) Reagent water to make 1000 mL	10 min	20°C	...
C.9.1	Zinc and Zinc Alloys	150 mL ammonium hydroxide (NH_4OH, sp gr 0.90) Reagent water to make 1000 mL *followed by* 50 g chromium trioxide (CrO_3) 10 g silver nitrate ($AgNO_3$) Reagent water to make 1000 mL	5 min 15 to 20 s	20 to 25°C Boiling	... The silver nitrate should be dissolved in water and added to the boiling chromic acid to prevent excessive crystallization of silver chromate. The chromic acid must be sulfate free to avoid attack of the zinc base metal.
C.9.2		100 g ammonium chloride (NH_4Cl) Reagent water to make 1000 mL	2 to 5 min	70°C	...

APPENDIX

(Nonmandatory Information)

TABLE X1 DENSITIES FOR A VARIETY OF METALS AND ALLOYS

NOTE X1.1—All UNS numbers that include the letter X indicate a series of numbers under one category.

NOTE X1.2—An asterisk indicates that a UNS number not available.

UNS Number	Alloy	Density g/cm³
	Aluminum Alloys	
A91100	1100	2.71
A91199	1199	2.70
A92024	2024	2.78
A92219	2219	2.84
A93003	3003	2.73
A93004	3004	2.72
A95005	5005	2.70
A95050	5050	2.69
A95052	5052	2.68
A95083	5083	2.66
A95086	5086	2.66
A95154	5154	2.66
A95357	5357	2.69
A95454	5454	2.69
A95456	5456	2.66
A96061	6061	2.70
*	6062	2.70
A96070	6070	2.71
A96101	6101	2.70
A97075	7075	2.81
A97079	7079	2.75
A97178	7178	2.83
	Stainless Steels	
S20100	Type 201	7.94
S20200	Type 202	7.94
S30200	Type 302	7.94
S30400	Type 304	7.94
S30403	Type 304L	7.94
S30900	Type 309	7.98
S31000	Type 310	7.98
S31100	Type 311	7.98
S31600	Type 316	7.98
S31603	Type 316L	7.98
S31700	Type 317	7.98
S32100	Type 321	7.94
S32900	Type 329	7.98
N08330	Type 330	7.98
S34700	Type 347	8.03
S41000	Type 410	7.70
S43000	Type 430	7.72
S44600	Type 446	7.65
S50200	Type 502	7.82
	Other Ferrous Metals	
F1XXXX	Gray cast iron	7.20
GXXXXX–KXXXXX	Carbon steel	7.86
*	Silicon Iron	7.00
KXXXXX	Low alloy steels	7.85

TABLE X1 *Continued*

UNS Number	Alloy	Density g/cm³
	Aluminum Alloys	
	Copper Alloys	
C38600	Copper	8.94
C23000	Red brass 230	8.75
C26000	Cartridge brass 260	8.52
C28000	Muntz metal 280	8.39
*	Admiralty 442	8.52
C44300	Admiralty 443	8.52
C44400	Admiralty 444	8.52
C44500	Admiralty 445	8.52
C68700	Aluminum brass 687	8.33
C22000	Commercial bronze 220	8.80
C60800	Aluminum bronze, 5 % 608	8.16
*	Aluminum bronze, 8 % 612	7.78
*	Composition M	8.45
*	Composition G	8.77
C51000	Phosphor bronze, 5 % 510	8.86
C52400	Phosphor bronze, 10 % 524	8.77
*	85-5-5-5	8.80
C65500	Silicon bronze 655	8.52
C70600	Copper nickel 706	8.94
C71000	Copper nickel 710	8.94
C71500	Copper nickel 715	8.94
C75200	Nickel silver 752	8.75
	Lead	
L53305–53405	Antimonial	10.80
L5XXXX	Chemical	11.33
	Nickel Alloys	
N02200	Nickel 200	8.89
N04400	Nickel copper 400	8.84
N06600	Nickel chromium iron alloy 600	8.51
N06625	Nickel chromium molybdenum alloy 625	8.14
N08825	Iron nickel chromium alloy 825	8.14
N08020	Iron nickel chromium alloy 20 Cb-3	8.08
*	Iron nickel chromium cast alloy 20	8.02
N10665	Nickel molybdenum alloy B2	9.2
N10276	Nickel chromium molybdenum alloy C-276	8.8
N06985	Nickel chromium molybdenum alloy G-3	8.3
	Other Metals	
M1XXXX	Magnesium	1.74
R03600	Molybdenum	10.22
P04980	Platinum	21.45
P07016	Silver	10.49
R05200	Tantalum	16.60
L13002	Tin	7.30
R50250	Titanium	4.54
Z13001	Zinc	7.13
R60001	Zirconium	6.53

Appendix G
Corrosion Probe Manufacturer's Data Sheets

Model CK-3
CORROSOMETER® Instrument

Features:
- *Intrinsically Safe*
- *Portable*
- *For All Process Systems*

The Model CK-3 CORROSOMETER® Instrument is the industry standard for portable monitoring of CORROSOMETER® probes. It has a reputation for rugged reliability earned throughout the world in vastly diverse applications. This intrinsically-safe instrument is suitable for monitoring the full range of CORROSOMETER® probes which measure metal loss in virtually any environment.

The Model CK-3 Instrument determines the metal loss that has occurred on a CORROSOMETER® probe since installation of the probe. As corrosion and/or erosion occurs on the probe, successive readings taken with the instrument at suitable intervals enable a metal loss against time graph to be generated, from which corrosion rates may be determined.

This easy-to-operate and sensitive portable unit provides a low capital cost entry in the field of corrosion monitoring where continuous measurement is not essential for corrosion management.

The instrument incorporates a battery test and includes a test probe for verification of instrument and probe extension cable integrity. The instrument is easily carried to the CORROSOMETER® probes where the simple readings may be taken in less than a minute.

The Model CK-3 Instrument is certified intrinsically safe by both Underwriter's Laboratory in the U.S.A. and BASEEFA in the United Kingdom.

Specifications are subject to change without notice.

a Corrpro company

Specifications:

- **Corrosion Resolution:**
  1 division (0.1% of Probe Span).
- **Measurement Repeatability:**
  ± 1 dial division.
- **Power Source:**
  Four 4.5 Volts Eveready #523 Alkaline, Panasonic PX21, or Mallory PX21 Power Cells
- **Average Battery Life:**
  6 months with normal usage.
- **Operation Temperature Range:**
  -10° C to +65° C.
- **Probe Cable:**
  5 ft. (1.5 m) coiled cord.
- **Weight:**
  4.5 lbs. (2.0 kg.)
- **Shipping Weight:**
  7 lbs. (3.2 kg.)
- **Safety Rating:** Tested and listed by Underwriters Laboratory, for use in Class 1, Division 1, Group A & B areas. T2A
  BASEEFA CK-3 System
  Certificate No. Ex 832132
  CODED EEx ib IIC T4

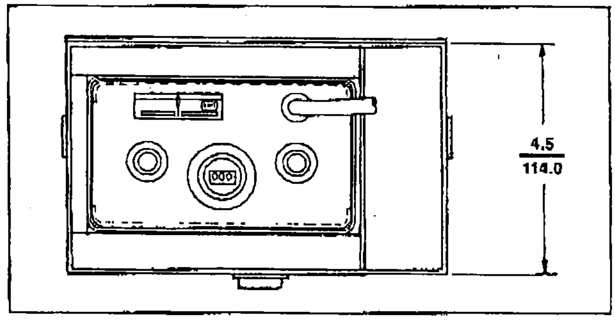

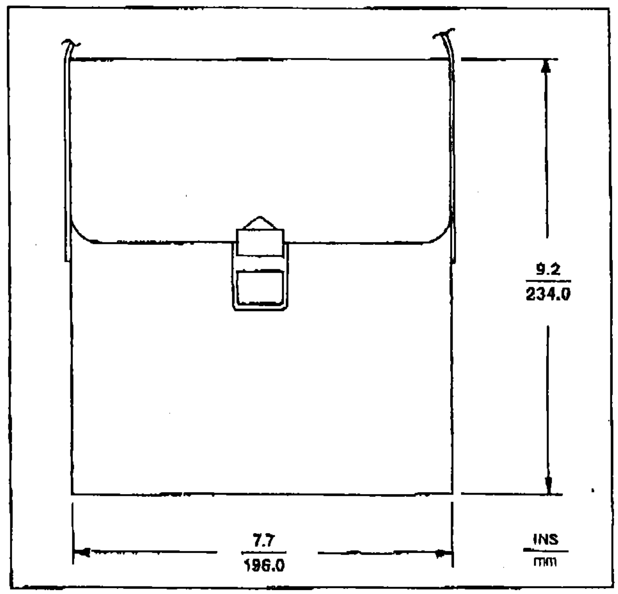

Ordering Information:

MODEL	DESCRIPTION
CK-3	PORTABLE CORROSOMETER® INSTRUMENT

CODE	SOFTWARE
0	NONE
1	WITH BASIC CORRDATA® P.C. SOFTWARE PACKAGE
2	WITH CORRDATA® PLUS WINDOWS® P.C. SOFTWARE PACKAGE

CK-3 —— 2 ◄—— TYPICAL ORDER NUMBER

• Each Model CK-3 is provided with carrying case, 4 batteries; P/N 094062, Instrument Test Probe: P/N 044012-5, and one Operation and Maintenance Manual.

SPARE BATTERIES:
P/N 094062 (4 required)

REPRESENTATIVE:

ROHRBACK COSASCO SYSTEMS, INC.
11841 East Smith Avenue
Santa Fe Springs, CA 90670
U.S.A.
Tel. (562) 949-0123
(800) 635-6898 (U.S. toll free)
Fax (562) 949-3065

ISO 9001

Certificate No. FM 10694

Rohrback Cosasco Systems corrosion monitoring equipment is manufactured and sold under one or more of the following U.S. patents: 4138878, 4230290, 4338563, 4514681, 4537071, 4587479, 4605626, 4525567, 4755744, 4630580, 4641787, 4882537, 5243297

CORROSOMETER®
Probe Selection Guide

GENERAL APPLICATIONS

CORROSOMETER® probes and instruments determine metal loss from corrosion or erosion by the electrical resistance method. This method may be used in virtually any environment except liquid metals or some conductive molten salts.

CORROSOMETER® instruments directly measure the **metal loss** on CORROSOMETER® probes. Plotting **metal loss** as a function of time permits **corrosion rate** to be determined. The slope of the curve represents the average **corrosion rate** over the selected interval.

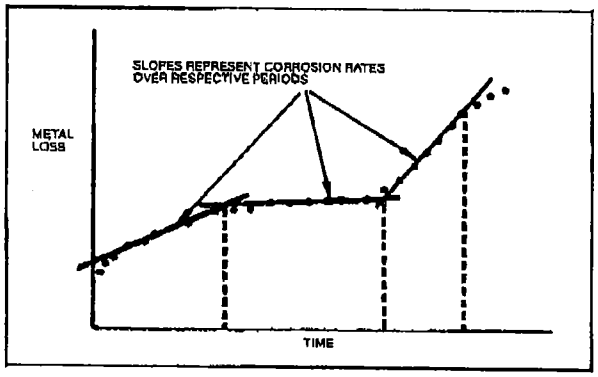

PRINCIPLE OF OPERATION

The electrical resistance of a section of electrically conductive material such as a metal may be expressed by the formula.

$$R = \rho \frac{L}{A}$$

where: ρ is the intrinsic electrical resistivity of the material
L is the length of the section
A is the cross-sectional area of the section

The intrinsic resistivity, ρ , varies from alloy to alloy and is temperature dependent.

For a given alloy at constant temperature, the electrical resistance of a fixed-length specimen increases as the cross-sectional area decreases. Consequently, the measurement of electrical resistance may be used to determine metal loss.

Compensation for change of resistivity ρ with temperature is achieved by the use of a reference element protected from the corrosion process. As the electrical resistance of the measurement element increases with temperature, so does the electrical resistance of the reference element. However, the resistance ratio of the two elements remains unchanged, thereby providing automatic compensation for temperature changes.

Since CORROSOMETER® probes have a lower electrical resistance than the connecting cables and connectors, separate electrical current and voltage monitoring wires must be used. By energizing the probe elements with the same electrical current, the resistance ratio of the elements is determined by measuring the voltage ratio of the elements.

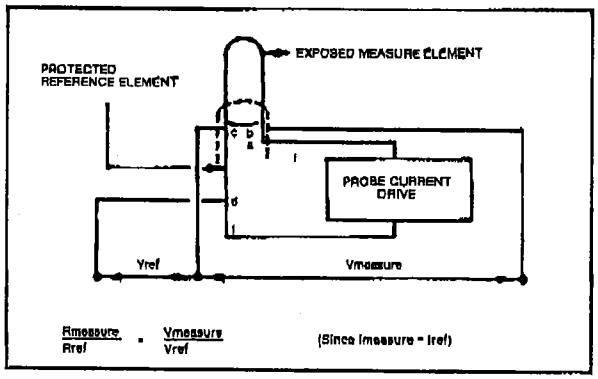

PROBE MOUNTING CONFIGURATIONS

There are a wide variety of CORROSOMETER® probes to match various applications. The major probe categories are as follows.

1. Internal process monitoring probes
   a. Removable under system pressure
   b. Non-removable under system pressure
2. Laboratory probes
3. External and structural monitoring probes
4. Environmental monitoring probes

In general the CORROSOMETER® probes have sensing elements made of the metal or alloy for which corrosion data is required. The probe bodies may be of the same alloy, but thicker, or of a higher, less corrosive alloy. Details are given on the data sheet for each model probe.

Internal Process Monitoring Probes Removable Under System Pressure

Probes that are removable under system pressure are particularly useful to enable inspection or change out of probes without shutting down or isolating the system.

Two systems are available depending on the pressure.

a. RETRACTABLE SYSTEM for pressures up to 1,500 psi.
b. RETRIEVABLE SYSTEM for pressures up to 3,600 psi and 6,000 psi.

RETRACTABLE process probes are introduced into the system through a stuffing box mounted external to a valve. A specially-designed retracting device is available for insertion or removal of probes at pressures too high to permit safe operation by hand (above 150 psi requires over 50 lb. insertion force).

RETRIEVABLE process probes are sealed into the system in a COSASCO® access fitting. A separate COSASCO® service valve and retriever is used for insertion and removal of the probes under system pressures.

Internal Process Monitoring Probes Fixed Type (Non-removable under system pressure)

Probes which are not removable under system pressure are sometimes used for reasons of economy or special process limitations. These may be mounted with a flange or NPT threaded connection. NPT connections are available with fixed or adjustable length.

CORROSION MEASUREMENT ELEMENTS

Several CORROSOMETER® element forms are available.

Selection of the most suitable element form and especially the correct probe sensitivity is important to obtaining good quality corrosion data.

Elements are available in a wide variety of alloys; consult the probe data sheets for those available in each type.

Strip, Tube & Wire Loop Elements

These elements are generally more economical and available in a wider range of alloys than for other element forms. Two forms of element seals are available to protect the reference element within the probe body.

Glass-to-metal seals provide the highest seal integrity and are generally suitable for process fluid in the range of 0-9 pH and temperatures up to 500 degrees F. They are not suitable for fluids containing fluoride ions which attack glass, ceramics and epoxies.

Teflon® coating and ceramic fill provide the alternative seal of the reference element in loop elements.

Cylindrical Elements

These probes have the element directly welded to the probe body to provide the highest integrity seal for aggressive environments. They provide a large surface area for measurement, have the fastest dynamic response to temperature transients, and are the least susceptible to the effect of any conductive deposits (such as Iron Sulfide) where present. The construction enables these probes to be used in environments in pH range 0-14, at temperatures up to 500 degrees F (260 degrees C). A high temperature model is also available for temperatures above 500 degrees F.

The body of the cylindrical element probe is normally supplied in the same alloy as the element to prevent the effects of possible galvanic corrosion between the probe body and probe element.

Flush Elements

Flush element probes are available where it is particularly necessary to monitor localized wall effects, or where protrusion into the line would cause damage to the probe; for example, during pigging operations.

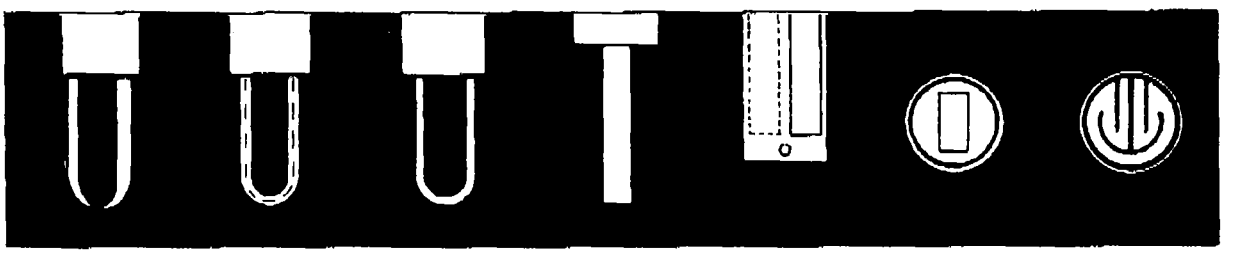

S4, S8	T4, T8	W40, W80	T10, T20, T50	S4,* S8*	S8*	S10,* S20,* S40*
STRIP LOOP	TUBE LOOP	WIRE LOOP	CYLINDRICAL	ATMOSPHERIC	FLUSH END VIEW	FLUSH END VIEW

* CORROSION ON ONE SIDE ONLY

PROBE MATERIALS

Care should be taken to check that the wetted probe components are compatible with the process fluid. Pressure ratings are specified on this basis. CORROSOMETER® probes are designed with pressure retaining capability beyond the probe element. However, the pressure rating may be impaired if the probe is not removed within a reasonable period of time after expiration of the probe element.

Probe Body and Wetted Parts

For loop element and flush element probes, the standard body materials are 304 and 316 stainless steel. Cylindrical element probes generally have wetted parts of the same alloy as the probe element.

Probe Element Seals

Teflon® is rated to 500 degrees F (260 degrees C) maximum. Glass seals are rated to 500 degrees F (260 degrees C) maximum in a pH range of less than 9. For standard cylindrical probes, the process operating temperature is limited to 500 degrees F (260 degrees C) by internal Teflon® insulators. For high temperature cylindrical element probes, internal insulation is ceramic.

Probe Fill Material

Standard probe fill materials are ceramic or epoxy. In non-glass sealed loop element probes, this material may be wetted by process fluid. In glass sealed loop probes and cylindrical element probes, this fill material will only be wetted on penetration of the corrosion element.

PRESSURE CONTAINMENT

All CORROSOMETER® process probes incorporate a hermetically sealed electrical connector designed to hold full rated pressure. This connector should be considered as the primary seal. CORROSOMETER® probe elements are designed for maximum operational integrity but by their very nature these elements are sacrificial. For this reason, element seals are not considered in terms of process containment. Specialized probe designs are available which incorporate 100% Teflon® seals (for hydrofluoric acid applications, for example) and additional secondary seals are available for the most severe duty.

PROBE SPAN SELECTION CHART

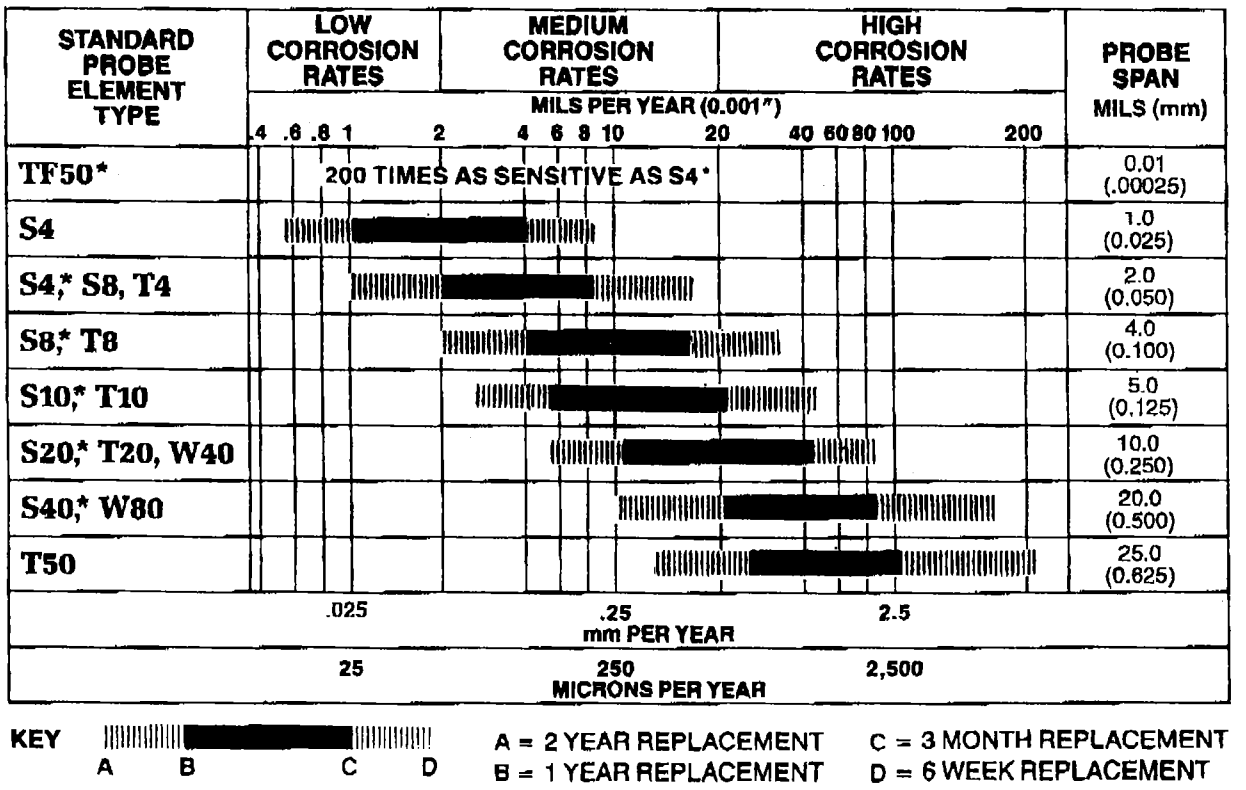

* CORROSION ON ONE SIDE ONLY

* Teflon is a registered trademark of Dupont.

PROBE SENSITIVITY SELECTION

Selecting the correct probe sensitivity is the key to getting the best results from your corrosion monitoring program in the most cost-effective manner possible. A sensitive probe will respond more quickly to process upsets than one with a greater span, but the element will corrode away and require replacement more quickly. Sensitive elements (T4, for example) are the best choice when anticipated general corrosion rates are low or when it is desired to obtain rapid response to changes, such as in a short-term test. Less sensitive, longer life elements are recommended when corrosion rates are medium to high and the objective of the program is to ensure that corrosion stays within acceptable limits rather than to rapidly detect process upsets. In general we recommend that elements be selected to be replaced every 9-12 months to give the optimum combination of sensitivity and responsiveness. When responsiveness is the primary consideration consult the PROBE RESPONSE TIME CHART. As an example, if a response within a maximum of 12 hours is required to a corrosion rate of 25 mpy, a T4 (or more sensitive) element must be used. A T8 element would respond in approximately 18 hours. This chart is based upon the practical level of detection for a CORROSOMETER® probe; 1% of probe life or 10 divisions out of the entire 1000 division probe span.

PROBE RESPONSE TIME CHART

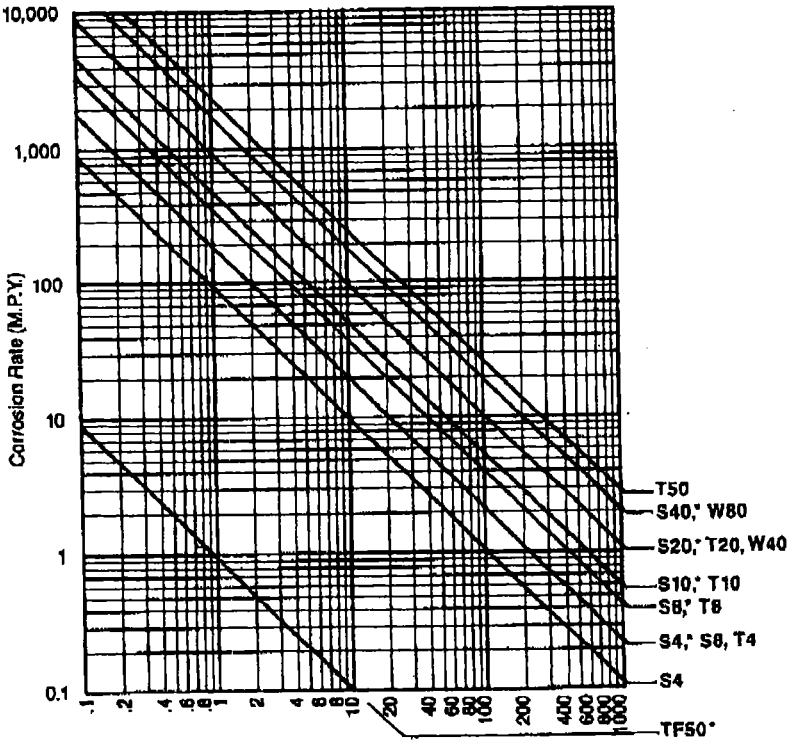

Response Time – Hours
(Based on 1% Probe Life or 10 Divisions)

REPRESENTATIVE:

ROHRBACK COSASCO SYSTEMS, INC.
11841 East Smith Avenue
Santa Fe Springs, CA 90670
U.S.A.
Tel. (562) 949-0123
(800) 635-8698 (U.S. toll free)
Fax (562) 949-3065

ISO 9001
BSI REGISTERED FIRM
NATIONAL ACCREDITATION OF CERTIFICATION BODIES
Certificate No. FM 10694

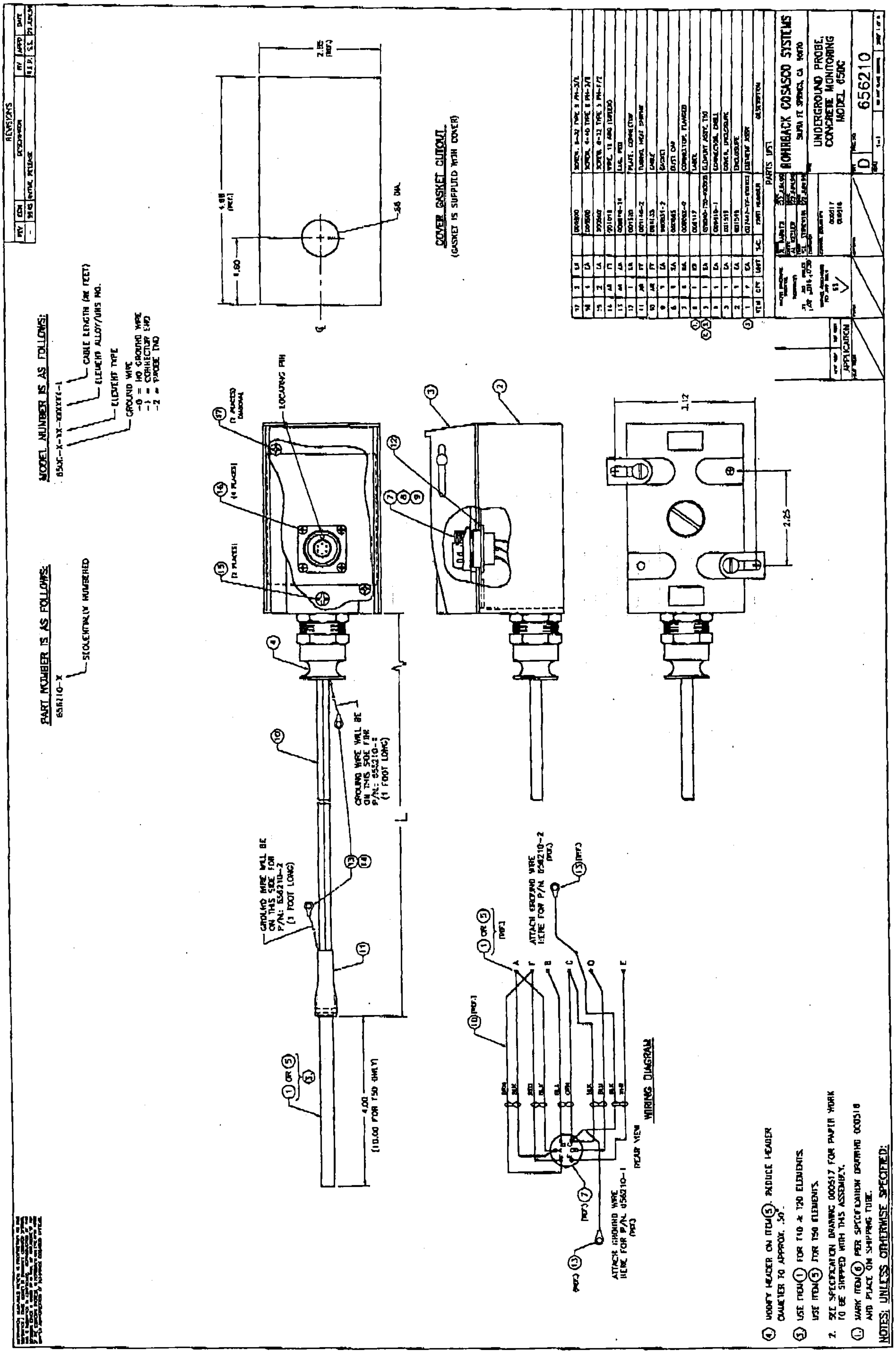
REVISIONS
PART NUMBER IS AS FOLLOWS:
MODEL NUMBER IS AS FOLLOWS:
COVER GASKET CUTOUT
(GASKET IS SUPPLIED WITH COVER)
WIRING DIAGRAM
REAR VIEW
PARTS LIST
ROHRBACK COSASCO SYSTEMS
UNDERGROUND PROBE, CONCRETE MONITORING MODEL 650C
656210
NOTES: UNLESS OTHERWISE SPECIFIED:

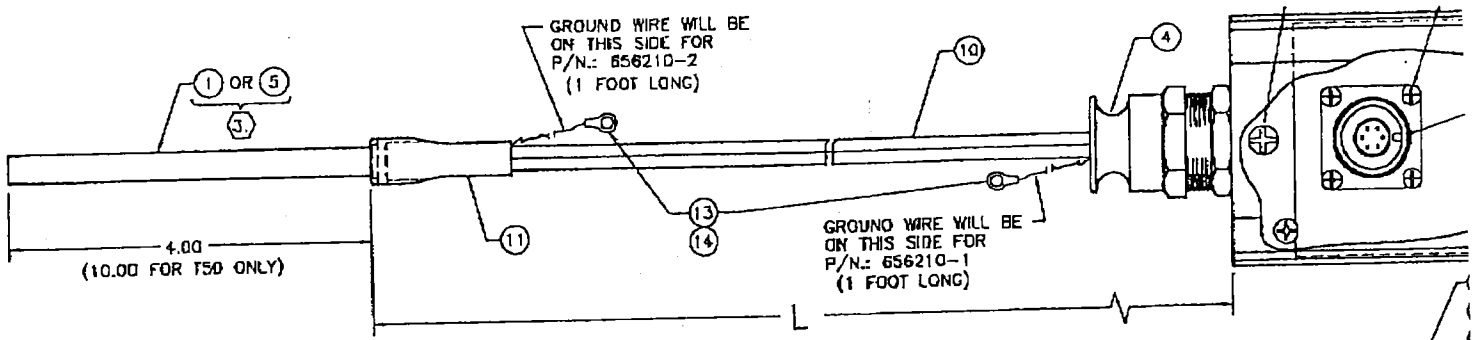

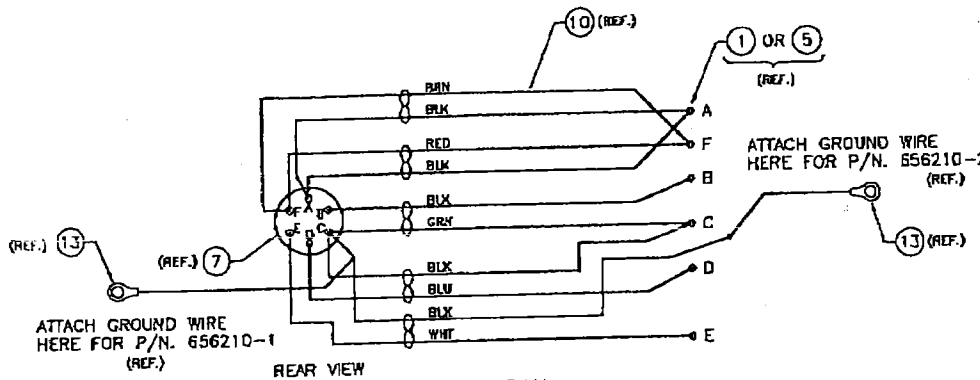

WIRING DIAGRAM

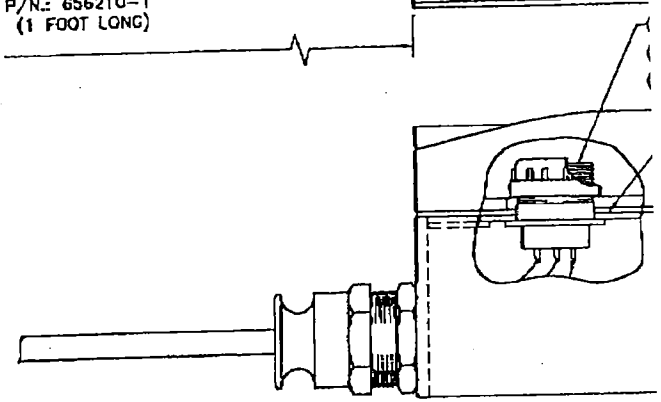

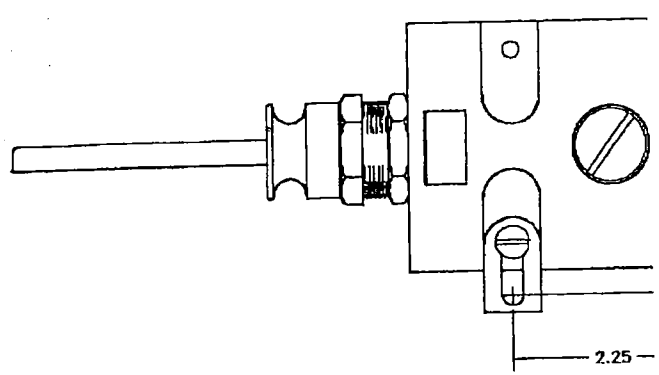

4. MODIFY HEADER ON ITEM 5. REDUCE HEADER DIAMETER TO APPROX. .50".

3. USE ITEM 1 FOR T10 & T20 ELEMENTS.
USE ITEM 5 FOR T50 ELEMENTS.

2. SEE SPECIFICATION DRAWING 000517 FOR PAPER WORK TO BE SHIPPED WITH THIS ASSEMBLY.

1. MARK ITEM 6 PER SPECIFICATION DRAWING 000518 AND PLACE ON SHIPPING TUBE.

NOTES: UNLESS OTHERWISE SPECIFIED:

Appendix H
Field Installation of Fiber Reinforced Plastic (FRP) Wraps on Concrete Columns

Materials.-The following is a list of material required for each type of composite system:

1. TYFO SHE-51 composite system (glass):
   Vendor: FYFE Co.
   6044 Cornerstone Court West, Suite C
   San Diego, CA 92121-4730
   Tel: 619-642-0694

   Local Rep.: Kurt Baron
   Tel: 847-706-9230

Fabric:	Tyfo SEH-51
Epoxy:	Tyfo-S, parts A & B
Top coat:	Tyfo-WS, parts A&B
Paint:	Tyfo A (acrylic), or Tyfo U (polyurethane). Color: Concrete gray

2. MBrace composite system (carbon):
   Vendor: Master Builders, Inc.
   23700 Chagrin Boulevard
   Cleveland, OH 44122
   Tel: 800-MBT-9990

   Local Rep.: Brad Costello
   Tel: 248-683-3554

Fabric:	MBrace CF130
Primer:	MBrace Primer, parts A&B
Saturant:	Mbrace Saturant, parts A&B
Filler:	Mbrace Putty, parts A&B
Top Coat:	Mbrace Top Coat. Color: Concrete gray

Construction Methods.-

Do not apply when ambient temperatures are lower than 4°C.
Do not apply to wet surface or when rainfall is anticipated.
Do not apply when dew point is within 3°C of the concrete surface temperature.
Do not apply when humidity is 90% or higher.
Manufacturer's representative shall be on site for initial placement.
Directions of the manufacturer's representative shall be followed.

1. TYFO SEH composite system:

A. Remove loose concrete from the column surface and fill all voids to a smooth surface using Type S-F or Type S-M patching mixture, depending on the depth of the patch. The area of the patch shall be blown out with oil-free compressed air. The cleaned area for patching shall be flushed out with clean water under pressure immediately prior to application of the patching mixture. Forming methods used to retain the patching mixture shall not leave holes in the concrete surface. The patch shall cure for at least three days prior to application of wrap. Uneven surfaces, protrusions, and sharp edges shall be ground smooth. Dust from surface grinding shall be removed by using an oil-free air blower or other suitable means.

B. Pre-cut desired number of layers of fabric to a length exceeding the column perimeter by at least 150 mm. Off site labor shall be used where possible. An overlap of 150 mm shall be provided in the fiber direction when terminating the wrap.

C. Round or bevel corners by grinding to a radius of at least 20 mm.

D. The concrete surface shall be free of any moisture at the time of application.

E. Mix parts A and B of Tyfo-S epoxy at a ratio of 100:42 by volume (or 100:34.5 by weight) with a tolerance of 10%. Stir with a mechanical mixer, typically 5 minutes at 400 to 600 rpm until uniformly blended. Pot life is 3 hours at 20°C and 45 minutes at 38°C.

F. Apply one coat of Tyfo-S epoxy by brush or roller to prime the surface. Volume to be applied may vary depending on the porosity of the concrete surface. Wait 2 to 4 hours and then apply wrap (as described below) while primer is still tacky.

G. Tyfo-S epoxy shall be applied to TYFO fabric as follows:
   (1) Place dry fabric sheets in a saturation bath and add epoxy. Work epoxy into fabric using gloved hands, a paint roller, or similar tool. Alternatively, an automatic saturating machine may be used.
   (2) After the fabric has been completely saturated (both sides), remove excess epoxy by squeegying it out with a plastic trowel or by blotting the excess resin with the next dry fabric to be saturated.
   (3) Use a PVC pipe to spool the saturated fabric prior to wrapping column.

H. The fabric shall be placed on the column entirely by hand assuring a smooth, uniform, mat finish. The (white) glass fibers shall be oriented horizontally. The (yellow) Kevlar fibers will then be oriented vertically. Pull the layer so that it is taut and free of bubbles. A lap length of at least 150 mm is required in the fiber longitudinal direction when terminating the layer.

I. Apply additional layers while the wrapped column surface is still tacky to the touch, ensuring that overlaps are staggered.

J. Mix parts A and B of Tyfo-WS epoxy at ratio of 100:42 by volume (or 100:34.5 by weight) with a tolerance of 10%.

K. Apply final coat of Tyfo-WS top coat with a minimum thickness of 0.4 mm. Epoxy shall be tacky to touch before final coat is applied.

L. The system shall be protected from damage, debris, and moisture during the initial curing period of 24 hours. Final curing is completed in 72 hours.

M. Apply finish of two coats of Tyfo A or Tyfo U paint with a minimum thickness of 0.1 mm per coat.

2. MBrace composite system

A. Remove loose concrete from the column surface and fill all voids to a smooth surface using Type S-F or Type S-M patching mixture, depending on the depth of the patch. The area of the patch shall be blown out with oil-free compressed air. The cleaned area for patching shall be flushed out with clean water under pressure immediately prior to application of the patching mixture. Forming methods used to retain the patching mixture shall not leave holes in the concrete surface. Uneven surfaces to receive FRP shall be filled with Type S-F mixture or other approved material. Surface irregularities must be rounded and smoothed to less than 1 mm using a grinder. Dust from surface grinding shall be removed by using an oil free air blower or other suitable means.

B. Pre-cut desired number of layers of fabric to a length exceeding the column perimeter by at least 100 mm. Off site labor shall be used where possible. An overlap of 100 mm shall be provided in the fiber direction when terminating the wrap. The length of the carbon sheet should preferably be less than 3 m for manageability.

C. Round or bevel corners by grinding to a radius of at least 13 mm.

D. The concrete surface shall be free of any moisture at the time of application.

E. Mix parts A and B of the primer at a ratio of 3:1 by volume (or 100:30 by weight). Stir with a mechanical mixer for at least 3 minutes at 400 to 600 rpm until uniformly blended. Pot life of the epoxy is approximately one-half to one hour after mixing.

F. Prime the concrete surface with the primer using a brush or a roller at a rate of 0.25 to 0.4 kg/m^2. Volume to be applied may vary depending on the porosity of the concrete surface.

G. Mix parts A and B of the filler at a ratio of 3:1 by volume (or 100:30 by weight).

H. Apply filler to primed surface preferably within 1 or 2 days of, and no more than one week after, applying the primer. The filler may be applied immediately after applying the primer.

Applying the filler is optional.

I. Wait 2 to 4 hours before mixing and applying the saturant. The surface must be tacky to touch when applying the saturant, otherwise it must be roughened using sandpaper. If sandpaper is used, then the surface shall be cleaned using an air blower before applying the saturant.

J. Mix parts A and B of the saturant at a ratio of 3:1 by volume (or 100:34 by weight). Pot life of the saturant is approximately one-half to one hour.

K. Apply one coat of the saturant to primed surface using a medium nap (9.5 mm) roller at a rate of 0.25 to 0.4 kg/m^2.

L. Place carbon sheet on a flat horizontal surface so that the backing paper is on top, smooth down by hand and peel away backing paper, and then wrap the sheet around the column. The surface that originally contained the backing paper shall be placed against the column and the fibers shall be oriented horizontally (i.e., the corners containing the obtuse angles of the diamond stitch pattern shall be aligned horizontally).

M. Squeeze the surface of adhered carbon sheet in the fiber direction in order to impregnate the saturant into the sheet. Remove excess epoxy by squeegying it out with a plastic trowel (without sharp edges) and roll out bubbles.

N. Apply additional saturant over the bonded carbon sheet at the overlap.

O. Wait a minimum of 30 minutes and then roll on an overcoat of saturant. (This is done for each layer.)

P. Repeat saturant mixing and rolling for consecutive carbon sheets, waiting 1 to 2 hours after applying each layer. Apply while previous coat of saturant is tacky to touch and stagger wrap overlaps for each layer.

Q. The system shall be protected from damage, debris, and moisture during the curing period of not less than 24 hours.

R. Apply finish of two coats of Mbrace Top Coat using a 10 mm nap roller at a rate of 4.9 m^2/liter per coat.